Characterisation of silicalite and post synthesis modified silicalite using adsorption.

Michael David Halhead

Submitted in fulfillment of the requirements for the degree of

Master of Science in Engineering

Deparment of Chemical Engineering
University of Cape Town
Cape Town, South Africa

Supervisor: Dr. K. P. Möller

September 2001

Synopsis

The study of adsorption on microporous materials such as zeolites is of tremendous scientific and industrial interest. The effective development and design of both equipment and processes is reliant on the availability of accurate information on the processes of adsorption in these materials. Zeolites, of the type studied in this thesis, are becoming increasingly important in a wide range of fields such as ion-exchange, purification, separations particularly of close boiling compounds and catalytic processes.

The work presented had two primary objectives. The first was the design and construction of a reliable apparatus for the measurement of adsorption isotherms. This adsorption apparatus was based upon the gravimetric technique due to the reliability, high sensitivity and the widespread use of this type of technique. The system constructed was a flow system as opposed to the more commonly used vacuum system. The choice of a flow gravimetric system introduces a number of advantages:

- The effect of the heat of adsorption is reduced
- The system is better able to replicate industrial conditions
- The gravimetric technique is simple to use

The adsorption microbalance facilitated the measurement of the adsorption isotherms of linear (n-hexane) and branched (3-methyl pentane and 2,3 dimethyl butane) light paraffins on silicalite-1. Silicalite was chosen as it represents a well studied adsorbent that has potential industrial applications in the adsorption separation field. The study of the adsorption of these light paraffins was extended to the characterisation of the effects of post synthesis modification; de-alumination and silanisation.

The parent silicalite-1 adsorbent had a Si/Al ratio of 200. The Henry constant for the adsorption of n-hexane at $373K$ was found to be $1.85 \times 10^{-2} mol \cdot kg^{-1} \cdot Pa^{-1}$ which compared well with Henry constants published in literature. The Henry constant for the de-aluminated silicalite was significantly higher ($2.49 \times 10^{-2} mol \cdot kg^{-1} \cdot Pa^{-1}$) than that of the parent. Silanisation appeared to reduce the Henry constant, in comparison to the parent adsorbent, however the decrease was within the limits

of the experimental error. The degree of silanisation had little effect on the Henry constants. For all the adsorbents the degree of branching showed the expected trend, the Henry constant decreased as the degree of branching increased.

The heat of adsorption for the adsorption of n-hexane on the parent silicalite-1 ($68.2kJ \cdot mol^{-1}$) again gave a good comparison to literature. The acid washed silicalite yielding a higher heat of adsorption of $109.40kJ \cdot mol^{-1}$, whereas the silanisation appeared to reduce the heat of adsorption in comparison to the parent, with the degree of silanisation having little or no effect on the heat of adsorption. The heat of adsorption for the 10 cycles silanised silicalite ($58.19kJ \cdot mol^{-1}$) was virtually identical to that of the 15 cycle silanised silicalite ($60.43kJ \cdot mol^{-1}$).

The repeatability of the adsorption isotherms measured using the microbalance was shown to be extremely good. Successive isotherm measurements were shown to be repeatable, well within the limits of the experimental error. It was found that the microbalance could accurately and repeatably measure the mass to within $30\mu g$. The average error in the loading was only 2%. However, the error in the partial pressure was more significant with an average of 10%, although it was shown that the theoretical error in the low loading region could be as high as 35%. The performance testing of the saturator showed a more reasonable error of less than 2%. The implication of the partial pressure error is that the microbalance would benefit from a reliable means of measuring the partial pressure, whereas the present system relies on a calculated partial pressure. Regardless of this, the microbalance system still produced results that compared well with literature.

The adsorption at $373K$ and $393K$ of n-hexane, 3 methyl pentane, and 2,3 dimethyl butane on the parent silicalite adsorbent produced adsorption parameters that were reconcilable with literature results for the adsorption of these compounds on silicalite-1. The measurement of the adsorption isotherms at lower temperatures proved difficult as there was not sufficient low loading data for the adsorption isotherms at the lower temperatures. The high temperature isotherms provided sufficient information for the adsorption energy profiles to be determined.

The pelletisation of the silicalite was shown to have no observable effect on the adsorption of either the linear or branched compounds, allowing the comparisons between the powdered parent adsorbent and the pelleted post synthesis modified adsorbents.

Contrary to expectations the silicalite-1 parent exhibited non-energetically homogeneous traits. It was shown that the isosteric heat of adsorption for the adsorption of n-hexane on the parent adsorbent was not constant with loading. The examination of the entropy ($-\Delta S$) of adsorption highlighted a change in the adsorption. Increases in the adsorption entropy have been observed in literature in connection with the re-arrangement of the n-hexane into the sinusoidal channels. The entropy increase presented here occurred at a significantly lower loading than the 4 molecules/u.c. that is often quoted, indicating two stage adsorption process occurred.

The de-alumination of the parent silicalite resulted in an adsorbent that showed similar adsorption traits to those of the parent adsorbent. No satisfactory explanations were found for the significant differences in the heat of adsorption; although the heterogeneity of the adsorbent appears to have been exacerbated, with the initial adsorption stage being the most severely effected.

The acid leaching process appears to have altered the external surface of the zeolite. This is confirmed by the silanised de-alumination adsorbents which yielded adsorption parameters that compared better with the parent adsorbent than the de-aluminated adsorbent.

The heterogeneous nature of the adsorbent was still observed on the silanised adsorbents where the isosteric heat and entropy of adsorption followed the same trend as the de-aluminated adsorbent. This leads to the conclusion that the heterogeneous nature of the adsorbent was located on the internal surface of the adsorbent. It was also observed that an increase in the degree of silanisation shifted both the isosteric heat of adsorption and the entropy of adsorption energies, indicating that more energy is required for the adsorbate to access the internal surface of the adsorbent.

Table of Contents

List of Figures

List of Tables

Nomenclature

A	Constant dependent on the zeolite type and pore size	
A	Helmholtz free energy	$J \cdot mol^{-1}$
$\mathcal{A}$	Surface area	m^2
A_i	Virial adsorption isotherm model constants	
ADC	Analog to digital convert counters	
B	Constant dependent on the zeolite type and pore size	
b	Langmuir equilibrium constant	Pa^{-1}
C	Calibration factor	mg/ADC
c	Fowler-Guggenheim lateral interaction parameter	
$\bar{C}_{ads}$	Intraparticle concentration of adsorbate	$mol \cdot dm^{-3}$
C_D	Coefficient of drag	
C_{ads}	Adsorbate adsorbed phase concentration	$mol \cdot g^{-1}$
C_{gas}	Adsorbate gas phase concentration	$mol \cdot dm^{-3}$
D	Drag force	N
F	Flow rate	$ml \cdot min^{-1}$
G	Gibbs free energy	$J \cdot mol^{-1}$
g	Gravitational acceleration	$m \cdot s^{-2}$
ΔG	Standard free energy	$J \cdot mol^{-1}$
H	Enthalpy	$J \cdot mol^{-1}$
ΔH	Limiting heat of adsorption	$kJ \cdot mol^{-1}$

j_g	Internal partition function in the gas phase	
j_s	Internal and vibrational partition function of an adsorbed molecule	
K	Dimensionless Henry adsorption constant , see equation (2.21)	
k	Henry adsorption constant	Pa^{-1}
$\mathtt{K}$	Adsorption equilibrium constant	$cm^3 \cdot g^{-1}$
$\mathtt{k}_{ads}$	First order adsorption rate constant	$cm^3 \cdot g^{-1} \cdot s^{-1}$
k_B	Boltzmann constant $k_B = 1.38 \times 10^{-23}\ J \cdot K^{-1}$	$J \cdot K^{-1}$
k'	Henry's adsorption constant	$mol \cdot kg^{-1} \cdot Pa^{-1}$
K_0	Dimensionless van't Hoff pre-exponential factor	
k_0	van't Hoff pre-exponential factor	Pa^{-1}
$K_{i,exp}$	Experimental adsorption equilibrium constant	$mol \cdot kg^{-1} \cdot Pa^{-1}$
L	Bed length	m
M	Molar mass	$g \cdot gmol^{-1}$
m	Mass	mg
N	Total number of data points	
n	Number of sites occupied per adsorbed molecule in Nitta isotherm	
n_a	Number of thermodynamically inert moles of adsorbent	mol
n_i	Noise	mg
n_s	Number of moles adsorbed	mol
P	Partial pressure	Pa
P°	Standard pressure $P^\circ = 101.32\ KPa$	Pa
q	Adsorbed concentration/loading	$mol \cdot kg^{-1}$
q^{st}	Isosteric heat of adsorption	$kJ \cdot mol^{-1}$
q_m	Mass loading	mg/mg_{cat}
q_s	Saturated adsorbed concentration	$mol \cdot kg^{-1}$

R	Universal gas constant $R = 8.314\ J \cdot mol^{-1} \cdot K^{-1}$	
S	Entropy	$J \cdot mol^{-1} \cdot K^{-1}$
s	Standard deviation of a sample	
ΔS	Entropy change on adsorption	$J \cdot mol^{-1}$
t	Time	s
t	t-distribution for small samples	
T_x	Temperature. Where x is the location	°C
U	Internal energy	$J \cdot mol^{-1}$
u	Adsorbate-adsorbate interaction parameter	J
V	Percentage of total flow rate (directly proportional to the MFC voltage output)	
V_s	Volume of the sample assembly	m^3
W	Weight	N
$\bar{x}$	Sample mean	

Greek Symbols

α	Regression constant	
β	Regression constant	
Λ	Thermal de Broglie wavelength	m
μ	Peak retention time	s
μ	Population mean	
μ_1'	First absolute moment	s
Φ	Surface potential	$J \cdot mol^{-1}$
π	Spreading pressure	$J \cdot m^{-3}$
ρ	Density	$kg \cdot m^{-3}$
ρ_p	Particle density	$g \cdot cm^{-3}$
σ	Standard deviation of a population	

σ^2	Variance of the population	
θ	Degree of coverage (q/q_s)	
θ_{true}	True mass	mg
$\mathcal{E}$	Calibration variance or offset	mg
ε	Desorption energy per molecule	J
ε_b	Bed porosity	
ε_p	Particle porosity	
ε_{LJ}	Energy constant for Lennard-Jones potential	J

Subscripts

a	Actual value
ads	Adsorbed phase
C	Configurational contribution to the entropy
cal	Calibration
$calc$	Calculated value
exp	Experimental value
gas	Gas phase
m	Measured value
T	Translational contribution to the entropy
$T2D$	Translation entropy with 2 degrees of freedom
$T3D$	Translation entropy with 3 degrees of freedom
th	Thermal contribution to the entropy
ads	Adsorbent
bal	Balance
dil	Diluentant
sat	Saturator

Abbreviations

SEM Scanning electron microscopy

23DMB 2,3 Dimethyl butane

3MP 3 Methyl pentane

ADC Analog to digital converter.

BCD Binary coded decimal.

BET Brunauer, Emmett, and Teller

CSTR Continuous stirred tank reactor

CVD Chemical Vapour Deposition

FID Flame ionisation detector

HPLC High Pressure Liquid Chromatography

IUPAC International Union of Pure and Applied Chemistry

MFC Mass flow controller

nC_6 n-Hexane

PFR Plug flow reactor

TEOS Tetraethoxysilane

u.c. Unit cell

WHSV Weight hourly space velocity h^{-1}

wt% Weight percent

XRD X-ray diffraction

ZLC Zero length column

Blob Binary Large Object

I/O Input/output

PSU Power supply unit

SSR Solid state relay

Chapter 1

Introduction

Adsorption has been used over a long period as a physical-chemical process. However, it has only found major industrial application comparatively recently, within the last four decades. The use of adsorption as a means of separation is becoming increasingly important as it can result in large energy savings, especially for the separation of close boiling compounds. In the United Kingdom, for example, the distillation related energy consumption accounts for 13% of the total energy used by the process industry (Lestak and Collins, 1997).

Detailed information on adsorption is required in order to effectively design adsorption processes and equipment. This increase in industrial interest is driving the research into adsorption processes and the development of adsorbents.

1.1 Objectives

The proposed work had two primary objectives:

- The design and construction of an apparatus capable of make accurate, and repeatable adsorption measurement.
- Characterise the adsorption of light paraffins on silicalite-1, de-aluminated silicalite-1, and finally silanised silicalite-1.

1.1.1 Adsorption measurement apparatus

A key objective of this work was the design and construction of an apparatus to measure adsorption isotherms. The aim was to build an apparatus that was capable of accurately measuring adsorption

isotherms, particularly of hydrocarbons on zeolites or other similar microporous materials. Zeolites are of particular interest as they play a significant role in many separation and catalytic processes.

Due to the previous acquisition of a *C. I. Electronics MkII* microbalance the decision was made that the adsorption apparatus should be designed around this piece of equipment. In order for the apparatus to be of practical use it had to fulfil the following requirements:

- It was essential that it was simple to use
- It was naturally required to produce accurate results that were comparable to literature
- It needed to produce repeatable results
- It had to be versatile, in other words the system should be able to handle a wide variety of conditions and experimental profiles
- It had to be affordable, as severe cost constraints were imposed on the project.

A requirement for the construction of any apparatus is that the performance and limits need to be known in order for the apparatus to be used appropriately, therefore one of the primary aims of this work was that the adsorption apparatus needed to be fully characterised.

1.1.2 Characterisation of adsorption of light paraffins on silicalite-1

The secondary objective of this work was to use the adsorption apparatus to characterise the adsorption of linear and branched light paraffins on silicalite-1 and post synthesis modified silicalite-1. The experimental work on silicalite-1 was intended to have the dual purpose of providing a well documented base by which the performance of the adsorption microbalance could be measured. The adsorption of light paraffins on silicalite-1 was also intended to provide a base line to compare the adsorption of the same paraffins on a number of post synthesis modified silicalites.

Due to the increased use of adsorption as a means to separate close boiling hydrocarbons the fine tuning of adsorbents using various post synthesis modification techniques has become of great interest to the petro-chemical industry. These techniques include de-alumination and the use of a CVD silanisation technique to control pore openings. It was therefore deemed appropriate to examine the effects of these post synthesis modification techniques on the adsorption of light paraffins.

1.2 Thesis overview

Chapter 2 - Adsorption: A review

This chapter presents a review of the current literature addressing the adsorption of hydrocarbon on zeolites providing a theoretical basis for the work performed. First a detailed review of the common adsorption measurement technique is presented. This is followed by a review of the isotherm models currently in use. Finally the parameters used to describe adsorption are presented. Included in this chapter are results presented in literature describing the adsorption of n-hexane, 3 methyl pentane, and 2,3 dimethyl butane on MFI type adsorbents.

Chapter 3 - Adsorption microbalance design and construction

The design and construction of the adsorption microbalance is described in detail in this chapter, including a detailed description of the control software written specifically for this project. All the assumptions and compromises made in the design of the adsorption microbalance are presented and discussed.

Chapter 4 - Experimental methods

The experimental methods used in the measurement of the adsorption isotherms are presented, including the techniques used in the post synthesis modification; the pelletisation, acid leaching (dealumination) and finally the silanisation techniques are described.

Chapter 5 - Characterisation of the adsorption microbalance

As the adsorption microbalance was a new apparatus, it was essential that the performance and limits of the apparatus were known. The results presented in this chapter provide a basis for the analysis of the adsorption results. This chapter includes the limitations of the microbalance system, an examination of the major error sources and finally an error analysis is performed.

Chapter 6 - Results and discussion

Adsorption was shown to be a powerful characterisation tool. This chapter presents the adsorption characteristics for the silicalite-1 adsorbent and the post synthesis modified silicalite-1 adsorbents. The focus is on the adsorption of n-hexane and particularly the adsorption energies of n-hexane, with a brief look at the effect of the degree of branching in the adsorbate on the adsorption.

Chapter 7 - Conclusions

Conclusions were drawn based on the findings in the previous chapters and they are discussed in this chapter.

Appendix A - Materials

A detailed list of the materials used in the experimental work is presented.

Appendix B - Error analysis

The analysis of the error in the experimental results required the derivation of a statistical model to account for the multiple sources of uncertainty. This appendix presents a detailed description of the statistical model developed.

Appendix C - Model fitting

The methods used to fit the experimental data to the adsorption isotherm models are covered in this appendix. Included is a list of the parameters determined for the experimental data and, where available, an estimate of the error in the parameters is presented.

Appendix D - Experimental data

The CD-ROM accompanying this thesis contains all the experimental data. This appendix presents the layout of the CD-ROM. It also includes information on not only the experimental data but also the programs and files written for this work.

Chapter 2

Adsorption: A review

It is estimated the 40% of the cost of a chemical process lies in the separation processes required (Jasra and Bhat, 1988). As a direct consequence, developments in separation technology have parallelled the growth in the chemical industry. Adsorption processes are widely used in the chemical, biochemical and petroleum industries, for both purification (removal of trace quantities of impurities) and for bulk separations (Ruthven, 1988). Adsorption purification systems have been in use for a number of years in very diverse fields such as air and water purification and sugar decolourisation. More recently, within the past two decades, bulk separation processes have become more popular with the advent of adsorbents of increased capacity and selectivity.

Adsorption systems are not limited to industrial processes, as many applications in the laboratory have been found. Probably the most used laboratory adsorption system is the N_2 BET (Brunauer, Emmett and Teller) surface area and pore distribution analysis. This process uses the adsorption of nitrogen to determine the surface area and pore size distribute of solids (Do, 1998). The laboratory use of adsorption is by no means limited to the ubiquitous BET, the characterisation of solids using adsorption of a range of compounds is gaining significant favour (Abrams and Corbin, 1995). Adsorption characterisation has the ability of extracting data, such as surface heterogeneity, that would otherwise be very difficult, if not impossible, to obtain.

Adsorbents have seen a considerable amount of development in the past two decades and the list of available adsorbents is increasing (Do, 1998). Zeolites have been used in industrial processes for number of year, faujasite is a prime example, but the interest in zeolites is increasing particularly due to their rather unique properties (Ruthven, 1988). Zeolites have well defined pore openings, channels and cages which are only dependent on the zeolite type, making them ideally suited to applications that require molecular sieving (Meier and Olson, 1978). Silicalite-1 is of particular interest in the field of separations as it has the same medium size pore opening as ZSM-5, in fact their structures are virtually identical, without the aluminium (or at least significantly less aluminium) and therefore

without the catalytic activity of ZSM-5, thus allowing the use of this adsorbent at high temperature with a significantly reduced possibility of undesirable reactions occurring (Choudhary and Mayadevi, 1996).

The development of these adsorption processes requires a considerable amount of information. This data can be obtained by a number of means, from experimental measurements (using the appropriate technique), to the modelling of experimental results using one of the myriad of available models. Adsorption is an enormous field of ongoing research and it would be unreasonable to try and review the entire state of the art. Therefore, a small subset of relevant available literature has been reviewed in the hope of developing an understanding of the science involved in the adsorption processes on zeolites.

2.1 Adsorption measurement techniques

The most convenient independent variables for single component gas adsorption are temperature and pressure. The key dependent variables are the adsorbed amount (q) and the enthalpy (H) of the adsorbed molecules (Myers and Siperstein, 2001). The aim of adsorption measurement is to measure all the extensive variables (q, H, S, etc.). Conceptually the measurement of these variables is trivial, however there are significant experimental difficulties is determining the adsorbed phase (Zhu et al., 1998). This review will focus only on the adsorption measurement techniques that are commonly found in literature such as the gravimetric, volumetric, or chromatographic methods (Zhu et al., 1998; Post et al., 1991; Ruthven, 1984). There are numerous other techniques available such as the use of NMR (Hunger and Horvath, 1997) however it is beyond the scope of this review to examine all available techniques. Do (1998) presents a fuller review of adsorption measurement techniques.

Each adsorption measurement technique has its own advantage and all of them have inherent deficiencies. Table 2.1 highlights the more popular techniques found in literature, along with their advantages and disadvantages. The requirement of a good adsorption measurement method is that the results obtained are independent of the method used. Sun et al. (1998) compares the results obtained using the volumetric method with those obtained via the gravimetric method. Although there were discrepancies, the results were close enough to assume that the results were independent of the measurement technique. Ruthven and Kumar (1980) and Schneider and Smith (1968) have shown similar observations for the chromatographic method.

2.1.1 Gravimetric adsorption measurement techniques

The gravimetric method is by no means a new technique, indeed the first literature citing it, for humidity measurements, was published in the early 1400's by the german Cardinal Nicolaus Cusanus

Table 2.1: Strengths and deficiencies of the adsorption measurement techniques reviewed.

Method	Strength	Deficiencies
Gravimetric	• Quick data collection. • Adsorbed amount measured directly.	• Flow rate is limited due to the instability of the balance at high flow rates. • Only practical for single component adsorption. • Potentially non-isotherms if the adsorbate is strongly adsorbed.
Volumetric	• Simple to use.	• Potential non-isothermal due to vacuum. • Accumulation of errors.
Chromatographic	• Easy to set up. • Simple to use. • Extends to multi-component measurements. • Allows quick measurement of the Henry's constant.	• Data analysis is cumbersome. • Non-isothermal operation.

(1401-1463) (Robens, 1995), yet this method is still is among the most commonly used techniques presented in literature (Eigenmann et al., 2000; Hershkowitz and Madiara, 1993; Gélin et al., 1995; Ruthven, 1984). This probably due to the fact that the gravimetric technique is highly sensitive, experimentally simple to use and the only available technique that directly measures the adsorbed phase (Brown, 1988; Gélin et al., 1995), as a mass increase due to the adsorption of the adsorbate.

The basis for the gravimetric method is the ability to measure the mass of the adsorbed phase. This is done by placing the adsorbent on a balance, commonly referred to as a microbalance due to their low loading and high sensitivity (some of the available microbalances can resolve masses in the microgram range), and then weighing both the mass of the adsorbent and the adsorbed phase at a known partial pressure of the adsorbate. Thus the mass of the adsorbed phase can be determined with a high degree of accuracy, limited only by the accuracy of the apparatus (Zhu et al., 1998; Brown, 1988).

As already discussed, at it simplest the gravimetric method is just the weighing of the adsorbent after it has equilibrated with the adsorbate. To do this numerous of types of experimental apparatus' have been developed to overcome the difficulties of weighing a adsorbent in a controlled atmosphere. Three types of adsorption apparatus', based on the gravimetric technique, commonly found in literature will be presented and discussed.

2.1.1.1 Vacuum gravimetric adsorption apparatus

The vacuum gravimetric adsorption apparatus refers to an apparatus in which the adsorption is done in a done in a vacuum, with an initial pressure of less than 10^{-5}Torr (Cavalcante and Ruthven, 1995; Gélin et al., 1995).

A vacuum balance system typically consists of a microbalance (such as those produced by *Cahn-Ventron Corporation*, *C.I. Electronics*, *Mettler*, or a host of others) which is connected to a vacuum system, and an adsorbate dosing system. The adsorbate is introduced into the evacuated adsorber where it quickly fills the space. The pressure can be measured using a suitable pressure transducer, thus all the necessary independent variables (T, P_i, and in this case q) have been measured directly (Gélin et al., 1995; Cavalcante and Ruthven, 1995; Eder and Lercher, 1997; Ruthven and Loughlin, 1971).

There are numerous reasons for using the vacuum system (Gélin et al., 1995):

1. The buoyancy and drag do not affect the microbalance measurement of the mass, and therefore no corrections are need.
2. The effects of flow patterns in the reactor are negated.
3. The partial pressure of the adsorbate can be directly measured, using a sufficiently sensitive pressure transducer or gauge.
4. The effect of competitive adsorption is negated. Competitive adsorption should not be significant for most gas phase adsorption, the carrier gas can generally be considered inert (non-adsorbing) (Abrams and Corbin, 1995). However, this is not the case in liquid phase adsorption.

Unfortunately a vacuum system has some inherent faults that one should be aware of prior to the use of such a system:

1. Vacuum systems are expensive.
2. They are notoriously difficult to use, the smallest defect in the fittings makes it nearly impossible to draw the required vacuum and low pressure transducers require careful calibration.
3. The thermal conductivity of the gas phase is low, due to the low pressures, therefore the thermal effects due to the heat of adsorption can lead to misleading results (Gélin et al., 1995; Chihara et al., 1976). This is particularly problematic for large changes in the partial pressure, as the adsorbents temperature will increase due to the lower energy transfer (Gélin et al., 1995).

4. The adsorption process tends to be done as a series of step changes in the adsorbate partial pressure. The time required for the sample to reach equilibrium at each step can be fairly long, on some systems the equilibrium time can be in the order of hours or even days (Abrams and Corbin, 1995). This requires that only a limited number of partial pressure steps be performed, resulting in the isotherm being constructed from only a small number of equilibrium points. The concern is that due to this lower resolution it is entirely possible that important information could be lost (Gélin et al., 1995). This failing is not unique to the vacuum system.

Gélin et al. (1995) presented a variation on the vacuum systems that aimed to address the last two failings presented above. Their system is simply a standard vacuum system into which the adsorbate is continuously dosed into the system at a very slow rate ($5 \times 10^{-5} - 2 \times 10^{-3}$Torr.s^{-1}). The intention was that if the adsorbate pressure could be increased at a sufficiently slow rate, then the adsorbed phase would remain in equilibrium with the adsorbate gas. This means that it would be possible to measure an almost continuous isotherm. Extreme care would need to be taken to ensure that the adsorbed phase remains in equilibrium with the gas phase, otherwise the results would be misleading.

2.1.1.2 Flow gravimetric adsorption apparatus

Silva and Rodrigues (1997) describes the use of a "flow" gravimetric system for the measurement of adsorption isotherms. This type of gravimetric apparatus differs from the vacuum system described above in that the adsorbate is introduced into the system in a gas stream, comprising an inert carrier gas (nitrogen, or helium) and the adsorbate.

The motivation for using a flow system is that it overcomes some of the difficulties inherent to a vacuum system, by reducing the expense and the experimental difficulties of vacuum systems and most importantly, the thermal effects, due to heat of adsorption, should prove less significant (the adsorbent bed should remain isothermal due to the improve energy transfer parameters of the gas stream) (Yang et al., 1996; Silva and Rodrigues, 1997; Hershkowitz and Madiara, 1993).

The use of a flow system does however introduce its own set of complications, the most significant of which is probably the effect of the flowing gas. The effects of buoyancy and drag can become a significant factor in this type of system (Brown, 1988; Yang et al., 1996). Care also needs to be taken with the arrangement of the adsorbent on the sample holder and the sample holder in relation to the gas flow in order to reduce the effects of the flow patterns on the adsorption (Eigenmann et al., 2000).

The effects of buoyancy/drag can significantly alter the results, especially when the adsorption is measured at higher pressures or when the flow rate of the gas is varied (Sun et al., 1998). One potential solution is to determine a correction factor, for the buoyancy effects, by performing a set of experiments on a "blank" absorbent (i.e. an adsorbent on which no adsorption actually occurs)

(Yang et al., 1996; Zhu et al., 1998). However, this a cumbersome process which could be prone to errors. Alternative a simple expression such as equation 2.1 can be used to correct for the effects of buoyancy (Sun et al., 1998).

$$W_a = W_m + V_s \rho_{gas} g \tag{2.1}$$

The sample assembly volume (V_s) can be determined by measuring the weight change that occurs when helium is used at low pressures. It may be assumed that helium is non-adsorbing on silicalite-1 (Sun et al., 1998).

2.1.1.3 Tapered element oscillating microbalance (TEOM)

Recently there has been an exciting development in the gravimetric measurement of adsorption with the introduction of the so called *inertial* microbalance, commonly referred to as a tapered element oscillating microbalance (TEOM), (Hershkowitz and Madiara, 1993; Zhu et al., 1998) although the use of an *inertial* microbalance was reported by Patashnick et al. (1980), for the measurement of the quantity of dust suspended in a gas.

The main feature of this apparatus is an oscillating element in which the adsorbent bed in placed. The gas can flow through the bed at a high flow rate without disturbing the measurements. As the measurements are based on inertial forces, instead of weight, as the mass changes so does the frequency of oscillation and so via calibration the mass can be determined quite accurately (Zhu et al., 1998). The TEOM apparatus has a number of advantages for the measurement of adsorption isotherms (Zhu et al., 1998; Hershkowitz and Madiara, 1993):

1. A well-defined gas phase due to the high gas flow rates through the adsorbent.
2. Improved heat and mass transfer as a direct result of the high gas flow rates.
3. Faster response to changes in the gas phase due to the improved mass transfer.
4. A high mass resolution across the entire range, a low system standard deviation and a stable baseline.
5. Highly reproducible results, as the apparatus is hardly influenced by changes in the experimental conditions, although the spring constant is a weak function of temperature (Halliday and Resnick, 1988).
6. Experimental conditions can be varied over a wide range of pressures and temperatures.

The biggest limitation of the TEOM apparatus is that it cannot distinguish between the mass of vapour between the particles and the mass that is adsorbed on the catalysts (Hershkowitz and Madiara, 1993). A unique limitation of the TEOM it that the apparatus will "weigh" the mass of the vapour in the reactor, therefore there is a need to ensure that the "dead" volume in the reactor is as small as possible (Hershkowitz and Madiara, 1993).

2.1.2 Barometric/Volumetric adsorption isotherm measurement technique

The volumetric method features prominently in literature for measuring adsorption isotherms (Loos, 1997; Cerro and Smith, 1969; Berlier et al., 1995). The principle of the volumetric method consists of successive expansions of the gas from a buffer tank to the adsorber (Berlier et al., 1995). From the known volume of the tanks, the adsorbed amount can be calculated using an appropriate equation of state, in conjunction with the relevant pressure-volume and temperature measurements (Loos, 1997).

As with all adsorption measurement techniques the volumetric method has its deficiencies. In the case of the volumetric method, because the adsorbed amount is determined via a series of calculations and measurements, there is an accumulation of errors (Zhu et al., 1998). Loos (1997) has shown that with careful experimentation these errors can be controlled to within approximately 5% of the adsorbed amount.

2.1.3 Chromatographic adsorption measurement technique

The chromatographic method is a common alternative to the volumetric or gravimetric methods for the measurement of adsorption isotherms (Sakuth et al., 1995; Ruthven and Kumar, 1980). Traditionally this method has been limited to the measurement of adsorption isotherms in the Henry's "region", the lower adsorbate concentration region when the adsorbed phase has a linear relation to the gas phase (Ruthven and Kumar, 1980; Ruthven, 1984; Cerro and Smith, 1969). The chromatographic technique is ideally suited to these lower partial pressure measurements. It is usually experimentally difficult to operate at extremely lower partial pressure, however, due to the nature of the apparatus, it is possible to inject a pulse into the system that has a considerably higher concentration than that permissible for the Henry's law region (Ruthven and Kumar, 1980; Cerro and Smith, 1969). The concentration of the pulse travelling through the column decreases rapidly (Do, 1998), giving an overall concentration profile that is applicable to the Henry law region (Cerro and Smith, 1969; Denayer and Baron, 1997).

As the velocity of the concentration wave through the chromatographic column can be determined from the slope of the equilibrium isotherm, the chromatographic method can be extended to the

determination of the complete single component isotherm (Ruthven and Kumar, 1980; Do, 1998). This method is known as perturbation chromatography (Do, 1998; Denayer and Baron, 1997).

Unlike the methods described above, the chromatographic method involve considerably more theoretical background and calculations in-order to determine the isotherm (Denayer and Baron, 1997; Do, 1998) or the adsorption equilibrium properties (Schneider and Smith, 1968). This fact is the single biggest detraction for this method. Due to the more involved calculations the likelihood of errors being introduced into the results is increased; whether these errors are a result of incorrect assumptions, or simply an accumulation of errors (Do, 1998). However, when the technique is applied correctly, the isotherms measured using this method compare well with those measured using the gravimetric method (Ruthven and Kumar, 1980; Ruthven and Kaul, 1993; Jama et al., 1997) and the volumetric method (Schneider and Smith, 1968).

The real power of the chromatographic method lies not in the measurement of single component adsorption isotherms, but rather that it can be easily extended to the measurement of multicomponent adsorption isotherms (Ruthven and Kumar, 1980; Ruthven, 1984; Do, 1998; Hufton and Danner, 1993). The gravimetric and volumetric methods discussed previously can be modified for multicomponent isotherm measurement, however due to their inability to determine either the composition of the adsorbed phase or the gas phase they would require additional instrumentation (Ruthven and Kumar, 1980).

There are a number of variations on the chromatographic technique, namely:

- Concentration pulse chromatography
- Tracer pulse chromatography
- Perturbation chromatography.

All these variations however have the same basic methodology and equipment in common. The chromatographic apparatus is extremely simple. It ultimately consists of a packed adsorbent bed which is placed in a temperature controlled environment, with a detector attached to the column outlet, a gas supply and sample injector is connected to the column inlet (Do, 1998).

The adsorbent is packed into a tubular reactor. It is necessary to use particles of uniform size, or at least a narrow particle size distribution (Do, 1998; Ruthven, 1984), due to the limitation inherent in the method of data analysis. The natural choice is to place the column into a standard, commercially available, gas chromatograph as they already contain all the gas and sampling systems that will be required. A gas is introduced into the column until the column has stabilised after which a pulse of the adsorbate is introduced into the column. The retention time of the adsorbate is dependent on the strength of the adsorption. Finally the exit concentration is monitored using a suitable detector, for

example a thermal conductivity detector (TCD) or a flame ionisation detector (FID) are amongst the more commonly used (Schneider and Smith, 1968). The shape and width of the peak is a complex function dependent on the strength of the adsorption and the dispersion forces acting in the system (Do, 1998; Ruthven, 1984), however it is normal to obtain a "bell" shaped chromatogram (Do, 1998). The results are less reliable when the chromatographic peak exhibits excessive tailing, normally due to strong adsorption (Hufton and Danner, 1993)

2.1.3.1 Concentration pulse chromatography (CPC)

Concentration pulse chromatography is analogous to the standard gas chromatographic analytical technique used to determine chemical composition (Hufton and Danner, 1993; Muralidharan and Ching, 1997). A pulse of the adsorbate is injected into the carrier gas as either an impulse or as a square input (Do, 1998). This method is extensively for the quick determination of the adsorption equilibrium parameters, particularly the Henry constant and the limiting heat of adsorption (Ruthven and Kumar, 1980; Denayer and Baron, 1997). The equilibrium properties of the adsorption (dq/dC) at the systems conditions are determined from the concentration-retention time curve produced by the detector (Hufton and Danner, 1993; Ruthven and Kumar, 1980) using the method of moments.

2.1.3.2 Tracer pulse chromatography (TPC)

Like the CPC method a pulse of the adsorbate is injected into the carrier gas. The main difference though is that the injected adsorbate is an isotopically labelled compound (Denayer and Baron, 1997; Do, 1998). The detector used must be able to detect the isotopically labelled compound, such as an ionisation cell (Do, 1998). However, the use of an isotopically labelled compound makes this method less attractive as they often expensive and not freely available (Hufton and Danner, 1993).

Hyun and Danner (1985) presented a combined CPC and TPC method (C/TPC) for the measurement of binary component adsorption isotherms. This method makes it possible to perform binary component chromatographic adsorption measurements using a single isotopically labelled adsorbate, as opposed the two that the standard TPC method would require (Hufton and Danner, 1993).

This experimental technique, like the CPC technique, is useful for determining the low pressure equilibrium parameters (Do, 1998; Ruthven and Kumar, 1980). The detector generates a chromatographic peak similar to that produced by the CPC method (Hufton and Danner, 1993). The analysis of this peak determines the ratio of the adsorbed phase to the gas phase (q/C).

2.1.3.3 Method of moments: Evaluation of the experimental data

As already mentioned the analysis of the chromatographic peaks is fairly complex (Ruthven, 1984). Schneider and Smith (1968) and more recently Ruthven (1984) and Do (1998) have all presented treatises on the analysis of chromatographic experimental data. It would therefore be pointless to redevelop the method of analysis here, and this work will simply present the expressions needed to analyse the data.

The basis for the analysis of the experimental data produced by the CPC and TPC method is a series of mass balances performed over the adsorbent particle and the adsorption column (Do, 1998; Ruthven, 1984). The Kubin theory provides a means to solve the mass conservation equations for gas adsorption in a adsorption column (Cerro and Smith, 1969) assuming that the system is isothermal and that the rate of adsorption is directly proportional to the concentration in the gas (Cerro and Smith, 1969). If the linear assumption is valid then the following expression holds (Cerro and Smith, 1969):

$$\frac{\partial C_{ads}}{\partial t} = \mathtt{k}_{ads}\left[\bar{C}_{ads} - \frac{1}{\mathtt{K}}C_{ads}\right] \tag{2.2}$$

By assuming isothermal operation the following expression can be found for the response to a pulse in the adsorbate (Cerro and Smith, 1969; Do, 1998):

$$\mu_1' = \frac{L}{u}(1+\delta_0) + \frac{t_0}{2} \tag{2.3}$$

where

$$\delta_0 = \left(\frac{(1-\varepsilon_b)\,\varepsilon_p}{\varepsilon_b}\right)\left(1 + \frac{\rho_p \mathtt{K}}{\varepsilon_p}\right) \tag{2.4}$$

The first absolute moment (μ_1') can be calculated directly from the chromatogram, using equation 2.5 (Ruthven, 1984; Cerro and Smith, 1969).

$$\mu_1' = \frac{\int_0^\infty t C_{gas}(t)dt}{\int_0^\infty C_{gas}(t)dt} \tag{2.5}$$

2.1.3.4 Perturbation chromatography

The chromatographic methods presented so far are limited to the measurement of isotherms in the Henry law region. However, as has already been mentioned, the chromatographic method can be

extended to measurements over the entire concentration range where the slope of the isotherm can be determined (Ruthven and Kumar, 1980; Do, 1998).

The perturbation method operates in a similar fashion to the methods described above. The major difference is that the column is initially equilibrated with a gas stream containing a known concentration (C^*) of the adsorbate (i.e. the gas stream is an inert carrier gas with a known amount of adsorbate), instead of just an inert gas (Denayer and Baron, 1997; Do, 1998). After the column has reached equilibrium a pulse of the adsorbate, with a concentration of ΔC^*, is injected into carrier gas (where $\Delta C^* \ll C^*$), in the same fashion as for CPC and TPC (Do, 1998). This system therefore has three components (Denayer and Baron, 1997):

- The injected pulse.
- The adsorbing component of the carrier gas.
- The non-adsorbing (inert) component of the carrier gas.

It is clear that the analysis of this system is slightly different than that of the CPC/TPC system. Both Do (1998) and Denayer and Baron (1997) present detailed developments of the expressions used to extract the isotherm parameters from the experimental data and like the moments analysis above this work will only present the final expression required. Denayer and Baron (1997) and Denayer et al. (1998) present the following moments:

$$\mu_1 = \frac{L}{u}\left[(\varepsilon_b + \varepsilon_p) + (1 - \varepsilon_b - \varepsilon_p)\, K_{1,exp}\rho_p RT\right] \tag{2.6a}$$

$$\mu_2 = \frac{L}{u}\left[(\varepsilon_b + \varepsilon_p) + (1 - \varepsilon_b - \varepsilon_p)\, K_{2,exp}\rho_p RT\right] \tag{2.6b}$$

where

$$K_{1,exp} = \frac{k_1'}{1 + b_2 P_2} \tag{2.7a}$$

$$K_{2,exp} = \frac{k_2}{(1 + b_2 P_2)^2} \tag{2.7b}$$

These expressions facilitate the determination of the single component adsorption isotherm (Denayer and Baron, 1997) by simply repeating the experiments at different concentrations (Do, 1998). The Henry adsorption constant can be determined by fitting equation 2.7 versus the partial pressure of the carrier gas adsorbing component (Denayer and Baron, 1997).

2.2 Adsorption isotherm models

Accurate equilibrium data is essential for the proper design of industrial equipment for separations and catalytic systems. However, experimental data is rarely available for the entire range of conditions that are of interest and it would be an onerous task to try and measure all the data. For this reason a number of adsorption equilibrium models have been developed to predict both the single and multi-component isotherms of a system.

Langmuir (1918) developed the first theoretically based model. This has been followed by numerous other models, both theoretical and empirical in nature. These models have been based on kinetics (Ruthven, 1984; Do, 1998; Langmuir, 1918; Wang and Hwang, 2000), thermodynamics (Ruthven, 1984; Ruthven and Loughlin, 1972; Yang, 1987), statistical thermodynamics (Ruthven, 1984, 1976; Nitta et al., 1984b; Derrah et al., 1972; Loos, 1997; Do and Do, 1997), empirical correlations (Ruthven, 1984; Do, 1998; Yang, 1987), and more recently on molecular modelling (Bates et al., 1996; Karavias and Myers, 1991; Smit, 1995; Loos, 1997).

2.2.1 Langmuir adsorption isotherm model

The Langmuir model, described by equation 2.8, developed by Langmuir (1918), was the first published model that applied a coherent theory to the subject of adsorption. This model was developed from a kinetic view point (Ruthven, 1984; Do, 1998). Simply, this model relates the continual process of bombarding molecules onto the surface to the corresponding evaporation of molecules from the surface, giving a zero rate of accumulation at the surface. The Langmuir model is based on a number of assumptions (Ruthven, 1984; Do, 1998):

1. Surface is energetically homogeneous, i.e. the adsorption energy is constant over all sites.
2. Molecules are adsorbed at a fixed number of well defined localised sites.
3. Each site can accommodate only one molecule.
4. There is no interaction between molecules adsorbed.
5. The extent of adsorption is limited to a mono-layer.

$$\theta = \frac{bP_i}{1 + bP_i} \tag{2.8}$$

2.2.2 Gibbs adsorption isotherm model

As an alternative to the kinetic based method used to develop the Langmuir isotherm, it is possible to use a more rigorous thermodynamic theory. Yang (1987) and Ruthven (1984) presented a detailed examination of the Gibbs isotherm, an abbreviated version of which is presented below.

The Gibbs isotherm is derived from the basic thermodynamic properties of the gas phase: the internal energy (U), enthalpy (H), Helmholtz free energy (A) and Gibbs free energy (G). The derivation follows the same logic as the derivation of the well known Gibbs-Duhem equation (Sandler, 1989).

Equation 2.9 is the generic form of the Gibbs adsorption isotherm. In itself this expression (eq. 2.9) is not practical for modelling adsorption isotherms but it does provide a convenient form from which a large number of isotherms can be derived (Ruthven, 1984).

$$n_a \left(\frac{\partial \Phi}{\partial P_i}\right)_T = \frac{RT}{P_i} n_s \quad \text{or} \quad \mathcal{A} \left(\frac{\partial \pi}{\partial P_i}\right)_T = \frac{RT}{P_i} n_s \tag{2.9}$$

Table 2.2 presents a list of the isotherms, derived from the generic Gibbs isotherm and their corresponding equation of state (EOS) (Do, 1998). It is clear that the equations of state used are analogous to the more commonly known gas equations of state, such as the van der Waals equation. As with the gas EOS's, correction terms can be added to correct for deviation from ideal behaviour, this potentially allows for a very flexible isotherm. However, as more corrections are included, the derivations become considerably more complex and tedious (Ruthven, 1984).

Table 2.2: Common isotherm equations derived from the Gibbs isotherm equation, with their corresponding equation of state (eq. 2.9).

Isotherm name	Isotherm	Equation of State
Henry law	$q = K' P_i$	$\pi \mathcal{A} = n_s RT$
Langmuir	$\theta = \frac{bP_i}{1+bP_i}$	$\pi(\mathcal{A} - \beta) = n_s RT$
Virial	$\frac{K' P_i}{n_s} = \exp\left(2A_1 n_s + \frac{3}{2} A_2 n_s^2 + \cdots\right)$	$\frac{\pi}{n_s RT} = 1 + A_1 n_s + A_2 n_s^2 + \cdots$

2.2.3 Virial adsorption isotherm model

As shown above (table 2.2) the virial isotherm model can be derived from the Gibbs adsorption isotherm model (eq. 2.9), using the appropriate equation of state (Ruthven, 1984). The main reason for mentioning the virial isotherm is that it will be used later in this work (section 2.3.2) as a convenient means for extracting the Henry adsorption constant from experimental data.

$$\frac{K'P_i}{q} = \exp\left(2A_1q + \frac{3}{2}A_2q^2 + \cdots\right) \tag{2.10}$$

$$\ln\left(\frac{q}{P_i}\right) = \ln K' + A_1q + A_2q^2 + \cdots \tag{2.11}$$

With strongly adsorbed species it is often difficult to make reliable experimental measurements in the linear region of the isotherm, i.e. there is a practical lower partial pressure limit at which the measurements can be performed. From equation 2.11, a simple plot of $\ln(q/P_i)$ versus q should produce a linear plot at concentrations well above the normal Henry's law limit. Thus the Henry constant can be extracted from an extrapolation of the plot to the zero adsorbed phase concentration (Ruthven, 1984; Ruthven and Kaul, 1996).

2.2.4 Nitta adsorption isotherm model

Recently there has been a large amount of work done on developing a more general adsorption isotherm model, one that hopefully addresses some of the downfalls of the previous generations. It has been reported in literature that the decreases of the adsorption capacity due to decreases in sorbate concentrations are more gradual than that predicted from the Langmuir equation (Nitta et al., 1984b; Do, 1998; Wang and Hwang, 2000). This gradual decrease of the adsorption has been ascribed to the heterogeneous characteristics of an adsorbent's surface (Nitta et al., 1984b; Do and Do, 1997).

Nitta et al. (1984b) proposed the development of a "new" isotherm model that assumes a localised mono-layer adsorption on the surface with an allowance for multi-site adsorption. This is really just an extension of the Langmuir isotherm for localised mono-layer adsorption (Do, 1998). Nitta et al. (1984b) derived his isotherm using statistical thermodynamics. Do (1998) is an excellent source for a concise explanation of the derivation. Equation 2.12 presents the final form of the isotherm model.

$$nbP_i = \frac{\theta}{(1-\theta)^n}\exp\left(-\frac{nu}{k_BT}\theta\right) \tag{2.12}$$

The adsorption affinity, b, is analogous to the Langmuir constant and is defined as (Nitta et al., 1984b; Do, 1998):

$$b = \frac{j_s}{j_g}\cdot\frac{\Lambda^3}{KT}\cdot\exp\left(\frac{\varepsilon}{k_BT}\right) \tag{2.13}$$

An important behaviour of the Nitta isotherm is that the slope of the surface coverage (θ) when plotted against the logarithm of pressure ($\ln P_i$) decreases with increasing values of n, while it increases with

an increase in the interaction parameter u (Nitta et al., 1984b; Do and Do, 1997). This is important because it allows the isotherm to describe some traditionally difficult concepts, such as multiple site occupation (both described by the n parameter), and the effect of adsorbate-adsorbate interaction (u) (Nitta et al., 1984a; Martinez and Basmadjian, 1996).

Martinez and Basmadjian (1996) developed an adsorption isotherm model that is remarkably similar to Nitta et al. (1984b), using a combination of kinetics and statistical thermodynamics. The major difference being that the isotherm incorporates adsorbent heterogeneity, as well as chemical dissociation and clustering effects Martinez and Basmadjian (1996). Another similar model was developed by Do and Do (1997) and again this model accounts for the heterogeneity of the adsorbent. In both cases the "original" Nitta isotherm can be recovered by fixing one or two of the parameters. Admittedly Nitta et al. (1984a) did extend the Nitta et al. (1984b) isotherm to account for the heterogeneity of the adsorbent.

The isotherms developed by Nitta et al. (1984b), Nitta et al. (1984a), Martinez and Basmadjian (1996), and Do and Do (1997) are restricted to mono-layer adsorption. However, Wang and Hwang (2000) extended the Do and Do (1997) isotherm, using a kinetic analysis, to account for multi-layer adsorption. There appears to be no reason why the same approach cannot be incorporated into the other isotherms mentioned here.

The Nitta isotherm, along with the isotherms presented by Martinez and Basmadjian (1996), Do and Do (1997), and Wang and Hwang (2000), easily extended to handle multi-component adsorption.

A feature of the Nitta isotherm is that it can be reduced into some of the better known adsorption isotherm models presented in literature (Nitta et al., 1984b; Do and Do, 1997). Table 2.3 presents some of these isotherms, with the corresponding Nitta isotherm constants. The Nitta isotherm also has the ability to predict the azeotropic behaviour of a multicomponent adsorption (Martinez and Basmadjian, 1996).

Table 2.3: Common isotherms derived from the Nitta isotherm, including the Nitta constants required to derive them.

Isotherm	Equation	n	u
Langmuir	$\theta = \frac{bP_i}{1+bP_i}$	1	0
Fowler-Guggenheim	$bP_i = \frac{\theta}{1-\theta}\exp(-c\theta)$	1	u

2.2.4.1 Physical significance of the Nitta isotherm parameters

It has been shown in literature that the Nitta isotherm model improves the fitting of the experimental data without the loss of physical significance (Nitta et al., 1984b; Do and Do, 1997; Martinez and

Basmadjian, 1996; Wang and Hwang, 2000). This is expected as the Nitta isotherm has more parameters that can be used in fitting than say the Langmuir isotherm (eq. 2.8). However, unlike the virial isotherm, all the parameters are intended to have physical meaning (Do and Do, 1997).

The interaction parameter u represents the adsorbate-adsorbate interaction which is one of the major downfalls of the Langmuir isotherm. The interaction energy (u) can be estimated from the Lennard-Jones 12-6 potential assuming that the adsorbate-adsorbate interaction is pairwise additive (Nitta et al., 1984b; Do, 1998). Equation 2.14 presents the expression that can be used to determine an estimate of u, which is considered to be the maximum adsorbate-adsorbate interaction (Nitta et al., 1984b). By estimating the interaction parameter it is possible to improve the fitting of the Nitta isotherm to experimental data (Nitta et al., 1984a). One of the biggest challenges with the Nitta isotherm is to find unique parameters for the fitting of the experimental data (Martinez and Basmadjian, 1996).

$$u = 3.44\left(\frac{\varepsilon_{LJ}}{n}\right) \tag{2.14}$$

In the development of the Nitta isotherm, when a molecule adsorbs, it is considered to occupy a certain number of neighbouring sites, which is represented by n (Nitta et al., 1984b). The deviation from ideality in mildly non-ideal systems is primarily due to the size effects (Do and Do, 1997), which is described by n. The significance of this parameter is shown in equation 2.15. This shows that the product of the number of sites occupied by a molecule (n_i) and the saturation loading of that molecule ($q_{s,\,i}$) is a unique property of the adsorbent (Martinez and Basmadjian, 1996). This constant provides a convenient means to characterise the adsorbent as it is independent of the adsorbate.

$$n_i q_{s,i} = n_j q_{s,j} = \text{constant} \tag{2.15}$$

The definition of the Nitta isotherm affinity constant (b) is given in equation 2.13. This expression could easily be rewritten as:

$$b = b_0 \exp\left(\frac{\varepsilon}{RT}\right) \tag{2.16}$$

This is very similar to the van't Hoff equation that is normally used to describe the temperature dependency of the adsorption affinity (Ruthven, 1984). It is worth noting that the pre-exponential (b_o) factor is a very weak function of temperature (this is clear from eq. 2.13), therefore it should be safe to assume that b_0 is temperature independent.

2.3 Adsorption equilibrium parameters

In order to characterise the adsorbent and the adsorption a number of physical parameters need to be examined. These parameters are used to further the understanding of the processes involved. They also provide a convenient and practical means by which the adsorption of various compounds and adsorbents can be readily compared.

All the parameters presented in this section have real physical significance and are not intended to be only fitting parameters for the isotherm models. In the analysis and interpretation of equilibrium data for zeolitic adsorption the simple model isotherms (Langmuir, Volmer, etc.) have limited applicability (Ruthven and Loughlin, 1972). Although an isotherm model might adequately describe the experimental data, unless the basic assumptions are correct, it is doubtful whether the parameters yielded from the model will have any real physical significance (Ruthven and Loughlin, 1972).

The parameters required to adequately examine most adsorption systems are (Myers and Siperstein, 2001):

- Adsorption capacity
- Henry adsorption constant
- Heat of adsorption
- Entropy of adsorption

This work uses silicalite-1 as the adsorbent of choice. Silicalite-1 is an all silica adsorbent with a physical structure that is analagous to ZSM-5 (Choudhary and Mayadevi, 1996). It is hydrophobic and stable up to high temperatures. Silicalite-1 provides a non-polar structure for adsorption of relatively small gas molecules (Zhu et al., 1998). It can therefore be considered a model adsorbent for the adsorption of C_6 compounds; n-hexane (n-C_6, linear), 3 methyl pentane (3MP, mono-branched), and 2,3 dimethyl butane (23DMB, double-branched), were the compounds used in this work to examine the adsorption on silicalite-1. It is also considered a model adsorbent for testing adsorption isotherm models based on gas-solid molecular interactions (Zhu et al., 1998).

Table 2.4 presents a concise list of some of the results reported in literature for the adsorption of n-hexane, 3 methyl pentane, and 2,3 methyl butane on MFI type adsorbents (silicalite-1 or ZSM-5). Unfortunately, with adsorption the results obtained on one adsorbent do not necessarily translate to another adsorbent even of the same type (Myers and Siperstein, 2001). The heat of adsorption is shown to be in the region of $60kJ \cdot mol^{-1}$ and is typically 2 to 3 times the normal heat of vapourisation ($\Delta H_{vap,n-C_6} = 28.8kJ \cdot mol^{-1}$) (Ruthven, 1984). It was also shown that the saturation loading decreases with increasing chain length.

Table 2.4: Literature reported values adsorption equilibrium parameters (eq. 2.20) for alkanes on Silicalite-1

k_0 $(mol \cdot kg^{-1} \cdot Pa^{-1})$	$-\Delta H_0$ $(kJ \cdot mol^{-1})$	q_s[a] $(mol \cdot kg^{-1})$	Source
n-Hexane			
	73 ± 2		Anderson et al. (1998)[b]
	66 ± 4		Anderson et al. (1998)
	69.9	1.29	Cavalcante and Ruthven (1995)
$(5.17 \pm 0.31) \times 10^{-12}$	68.8 ± 0.26		Denayer et al. (1998)[c]
1.16×10^{-12}	72	1.22[d] (1.23[e])	Eder and Lercher (1997)
9.18×10^{-14}	70.5	1.45	Sun et al. (1996)
	65		Stach et al. (1983)
3 Methyl pentane			
2.91×10^{-11}	62.8	0.84	Cavalcante and Ruthven (1995)
$(5.00 \pm 0.55) \times 10^{-12}$	66.0 ± 0.18		Denayer et al. (1998)
2,3 Dimethyl butane			
	54.4	0.71	Cavalcante and Ruthven (1995)
$(5.15 \pm 0.29) \times 10^{-12}$	63.4 ± 1.49		Denayer et al. (1998)

[a] $T = 373K$, q_s is considered temperature independent
[b] ZSM-5: unknown Si/Al
[c] ZSM-5: $Si/Al = 137$
[d] $1.3kPa$ & $333K$
[e] $1.2kPa$ & $373K$

2.3.1 Adsorbate capacity

The adsorption in zeolites is complex and the adsorption proceeds as follows (Roque-Malherbe, 2000):

1. Micropore filling. The adsorption in the micropore volume of zeolites is considered as a volume filling process and not as a layer by layer surface coverage. This phenomenon is adequately approximated by the Langmuir equations.

2. Later surface coverage begins, this occurs at high pressures. This process consists of the formation of a mono-layer followed by multi-layer adsorption and capillary condensation on the walls of the mesopores and macropores.

The adsorption capacity is often described as the saturation loading (q_s). The saturation loading term is self explanatory; it is the maximum loading that the adsorbent can accommodate.

The total saturation loading of different molecules may vary significantly. For alkanes q_s is highly dependent on the chain length and the degree of branching (Kapteijn et al., 2000). Linear alkanes can occupy both the straight channels and intersection space on silicalite-1, while the branched molecules preferentially reside in the intersections (Vlugt et al., 1998, 1999). Mono-branched molecules can partially occupy the channel space, while double-branched molecules can only occupy the intersections

(Vlugt et al., 1999). However, at a sufficiently high pressure the molecules are forced to re-arrange resulting in the well documented inflection in the adsorption isotherms of mono-branched and double-branched alkanes on silicalite-1 (Smit and Maesen, 1995; Sun et al., 1998; Yang and Rees, 1997). The presence of the inflection point is also dependent on the adsorption temperature with the inflection becoming less pronounced at higher temperatures. In the case of n-hexane adsorption on silicalite-1 the inflection is ascribed to a rearrangement of the molecules, because at higher pressures the hexane starts to occupy the sinusoidal channels and not just the straight channels (Eder and Lercher, 1997; Olson and Reischman, 1996; Song and Rees, 1997; Vlugt et al., 1998). It is interesting to note that the inflection occurs when the loading reaches approximately 4 molecules/u.c. which corresponds to the number of intersections per unit cell of silicalite-1 (Eder and Lercher, 1997; Gélin et al., 1995). This phenomenon reflects the step-wise filling of the different sites.

It is possible to calculate the theoretical saturation capacity of a zeolite. At it simplest it can be assumed that adsorbed molecules will have a density approximately the same as a liquid molecule (Bellat and Simonot-Grange, 1995a; Webster et al., 1998). Bellat and Simonot-Grange (1995a) have reported that these adsorbate capacity approximations have been found to be in at least the same order of magnitude as the experimentally determined values.

A note worthy of comment about the saturation loading is that due to the small thermal expansion of light alkanes and aromatics the saturation loading is approximately temperature independent (Do and Do, 1997). This factor has been utilised in table 2.4 where the saturation loadings have been presented as being temperature independent, although most of the measurements were performed at $373K$.

2.3.2 Henry Constant (K')

The Henry constant is a commonly used characteristic of the adsorbate-absorbent systems. It is equal to the slope of the adsorption isotherm at low adsorbate pressure, the linear region of the isotherm as the adsorbate partial pressure approaches zero (Ruthven, 1984; Hufton and Danner, 1993). Figure 2.1 presents a graphical explanation of the Henry constant. This parameter is important when designing industrial processes for the removal of low levels of impurities from a gas stream (Ruthven, 1984). It is also an integral part of many of the more complex isotherms (Do, 1998; Nitta et al., 1984a). The Henry's constant represents the strength of the adsorbate-adsorbent interaction, since at these conditions the adsorbate-adsorbate interaction effects are negligible (Hufton and Danner, 1993).

The Henry's law can be expressed in terms of either the pressure or concentration:

$$q = kc_i \text{ or } q = k'P_i \tag{2.17}$$

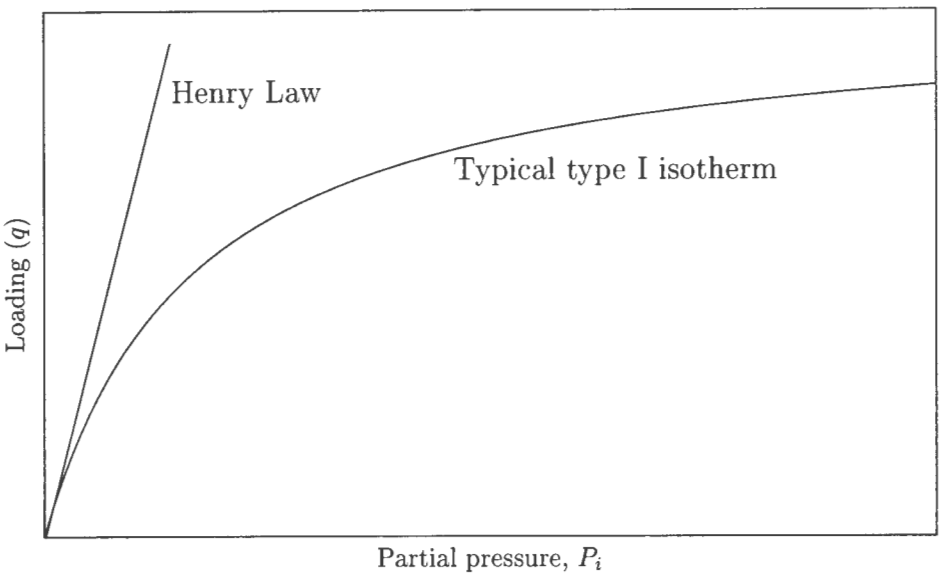

Figure 2.1: Typical type I isotherm, with the Henry law isotherm.

The concentration form is related to the pressure form by equation 2.18, assuming the gas is ideal (Ruthven, 1984).

$$k = k'RT \tag{2.18}$$

The temperature dependency of the Henry constant is normally described by the van't Hoff equation (eq. 2.19).

$$\frac{d\ln K}{dT} = \frac{\Delta U_0}{RT^2} \quad \text{or} \quad \frac{d\ln K'}{dT} = \frac{\Delta H_0}{RT^2} \tag{2.19}$$

or

$$K = K_0 \exp\left(\frac{-\Delta U_0}{RT}\right) \quad \text{or} \quad K' = K'_0 \exp\left(\frac{-\Delta H_0}{RT}\right) \tag{2.20}$$

For comparison purposes the Henry constant is often reported in literature as a dimensionless number. Equation 2.21 presents the dimensionless form of the Henry constant (K) (Loos, 1997).

$$K = k\rho q_s RT \tag{2.21}$$

The Henry adsorption constant is normally determined from experimental data. The virial isotherm model (eq. 2.10) provides a convenient method of extracting the Henry constant from experimental

data that has been measured at partial pressures outside of the Henry law adsorption range (Ruthven, 1984; Ruthven and Kaul, 1996).

It has been shown by Denayer et al. (1998) that the Henry constant (K') obeys a relation (eq. 2.22) with the carbon number (CN) for the adsorption of normal paraffins on ZSM-5. Denayer and Baron (1997) showed a similar finding where the Henry constant of adsorption on faujasite was more dependent on the molecular weight than the degree of branching.

$$K' = A \exp BCN \tag{2.22}$$

2.3.3 Heat of adsorption (ΔH)

The heat of adsorption provides a direct measure of the strength of the bonding between the adsorbate and the adsorbent (Ruthven, 1984; Eder and Lercher, 1996). Another way of putting it is that the heat of adsorption is the minimum energy required to desorb a molecule from the adsorbent.

The heat of adsorption is invariably exothermic (Ruthven, 1984). This is easily proved for gas phase adsorbates. The adsorbed molecule has at most two degrees of translational freedom on the surface, and the rotational freedom of the adsorbed molecule must be less than that of the gas phase molecule (Choudhary and Mayadevi, 1996). Therefore the entropy of adsorption (eq. 2.23) must be negative. The Gibbs free energy for adsorption must be negative for any significant amount of adsorption to occur and as the entropy (ΔS) has already be shown to be negative equation 2.24 implies that the the heat of adsorption (ΔH) must also be negative (Ruthven, 1984).

$$\Delta S = S_{ads} - S_{gas} \tag{2.23}$$

$$\Delta G = \Delta H - T\Delta S \tag{2.24}$$

For an energetically homogeneous adsorbent the heat of adsorption should be constant and independent of the degree of coverage (Martinez and Basmadjian, 1996; Wang and Hwang, 2000). However, in real systems this is rarely the case (Do and Do, 1997). When considering adsorption on a zeolite the Si/Al is an important factor as this governs the cation density which is the main source of the heterogeneity (Ruthven, 1984). Therefore it would be expected that the adsorption on silicalite-1 would provide a near homogeneous surface. Eder and Lercher (1997) and Yang and Rees (1997) have both shown that silicalite has a very small variation in the heat of adsorption with a change in the

coverage for the adsorption of alkanes on silicalite-1. It is also known that smaller alkane adsorption on silicalite-1 exhibits a fairly constant heat of adsorption with an increasing degree of coverage, thus indicating a relatively homogeneous adsorbent (Hufton and Danner, 1993). The heterogeneity of the adsorbent has also been shown to be a factor of the adsorbate. The adsorption of aromatics, alcohols, water, and olefins on silicalite-1 have exhibited a rapid and significant increase in the heat of adsorption with an increase in the degree of coverage. The ratio of the limiting heat of adsorption (lower loading) to the heat of adsorption at intermediate loading can exceed a factor of 2 (Hufton et al., 1995). However, the adsorption of saturated compounds does not exhibit the same sort of rapid increase; indeed the heat of adsorption remains virtually constant from infinite dilution to the saturation limit. It is not uncommon for the isosteric heats of adsorption to increase slowly with loading on silicalite-1. Yang and Rees (1997) attributes this small increase to the increase in adsorbate-adsorbate interaction, rather than any heterogeneity of the adsorbent.

2.3.3.1 Experimental measurement of the heat of adsorption

The heat of adsorption can be measured in variety of ways. Probably the most common is to determine the heat of adsorption from the Henry constant of adsorption. A simple logarithmic plot of the Henry constant versus temperature should yield a straight line, according to equation 2.20. The slope of this line is the heat of adsorption (Atkins, 1994). It should be noted that this heat of adsorption is that at low coverage (Henry law region), and therefore the effects of adsorbate-adsorbate interaction should not be visible (Ruthven, 1984; Do, 1998).

An alternative method of measuring the heats of adsorption is to use a microcalorimeter. This apparatus gives one the ability to measure the heat of adsorption over the entire adsorbate pressure range (Hufton et al., 1995). Atkins (1994) and Eder and Lercher (1996) provide a better description of calorimetry. In practice all that is required is a sensitive thermocouple to be fitted into the sample holder of one of normal adsorbers. This would provide that change in temperature due to adsorption and therefore the enthalpy (Atkins, 1994).

2.3.4 Entropy of adsorption (ΔS)

It is inevitable that the entropy of adsorption is tied to the enthalpy of adsorption. The change in entropy provides insight into the mobility of the adsorbed phase, the larger the change in entropy the greater the loss of mobility (Khelifa et al., 1999). Once the heat of adsorption has been determined, the partial molar entropy of the adsorbed phase can be calculated by equation 2.25 (Ruthven, 1984). The partial molar entropy can be factored into its various contributions, which depend on the degrees of freedom, as shown in equation 2.26.

$$\bar{S}_{ads} - S^{\circ}_{gas} = \frac{\bar{H}_{ads} - H_{gas}}{T} - R\ln\left(\frac{P_i}{P_i^{\circ}}\right) \tag{2.25}$$

$$\bar{S}_{ads} = \bar{S}_{th} + \bar{S}_T + \bar{S}_C \tag{2.26}$$

For localised adsorption the translational entropy ($\bar{S}_T$) is zero and if one considers the surface to be homogeneous then the configuration entropy is given by equation 2.27 (Ruthven, 1984). It is clear that the thermal entropy can then be calculated from equation 2.26.

$$\bar{S}_C = R\ln\left(\frac{1-\theta}{\theta}\right) \tag{2.27}$$

Although this model provides a easy means of evaluating the contributions of the entropies it is unfortunately rarely practical in real systems, particularly for energetically heterogeneous adsorbents, where the contributions of the configurational and the translational entropies are not adequately described by these expressions (Ruthven, 1984).

Choudhary and Mayadevi (1996) present a more practical scheme for determining the entropy from the adsorption data using equation 2.30. These expressions can be resolved into the following equation (eq. 2.31) which provides a simple means to determine the entropy (Zhu et al., 1998).

$$\Delta G = RT\ln\left(\frac{P^{\circ}}{P_i}\right) \tag{2.28}$$

$$\Delta G = q^{st} - T\Delta S \tag{2.29}$$

$$S_{ads} = S_{gas} - \Delta S \tag{2.30}$$

$$\Delta S = (S_{ads} - S_{gas}) = \frac{q^{st}}{T} - R\ln\left(\frac{p_0}{p}\right) \tag{2.31}$$

Choudhary and Mayadevi (1996) presented an alternative scheme to determining the entropy of adsorption. The entropy of adsorption can be estimated by determining the increase in the entropy due to the loss in the numbers of degrees of freedom of the adsorbate. Equation 2.32 presents the method used to estimate this loss of freedom.

$$\begin{aligned} S_{t3D} &= R\ln\left(M^{1.5}T^{2.5}\right) - 9.61 \\ S_{t2D} &= 0.667S_{t3D} + 2.76\ln T - 12.71 \\ \Delta S &= S_{t3D} - S_{t2D} \end{aligned} \tag{2.32}$$

It has been reported in literature (Choudhary and Mayadevi (1996); Bellat and Simonot-Grange (1995b); Chiang et al. (2001)) that the entropy of adsorption decreases with increasing coverage. This is to be expected, because as the loading increases the mobility of the adsorbed molecules will decrease (Choudhary and Mayadevi, 1996).

2.4 Post synthesis modification of zeolites

The use of zeolites as adsorbents is fairly widespread and increasing in popularity (Ruthven, 1988). However, a zeolite may have certain undesirable properties that can be altered by post synthesis treatment:

- The Si/Al ratio
- External acid sites
- Pore opening size

These properties can be modified after the zeolite has been synthesised using a number of well documented methods.

2.4.1 Inertisation

Zeolites are important adsorbents in separation processes (Ruthven, 1984; Coronas et al., 1998). However, due to the nature of zeolites, they have acid sites (when in the hydrogen form), both Brønsted and Lewis sites, which are present in varying degrees dependent on Si/Al ratio (Ruthven, 1984). These acid sites are problematic in the study of the adsorption properties of an adsorbent due to the potential of undesirable reactions occurring. Separation processes are vulnerable to these undesirable reactions, particularly at high temperatures. This is particularly true when olefins are involved (Kantner et al., 1994; Mattox and Rouge, 1967).

Fortunately there are a number of methods available to counter the acid sites present in a zeolite adsorbent. Among these methods are steaming, acid leaching and ion exchange.

2.4.1.1 Steaming

It is possible to reduce the aluminium content of a zeolite by exposing it to a steam environment. This results in the aluminium being removed from the framework of the zeolite (Mattox and Rouge, 1967).

Mattox and Rouge (1967) presented a method used to steam faujasite. The steaming is carried out in fairly harsh condition; temperatures between 420°C and 870°C , in an atmosphere containing at least 80% (by weight) water. This steaming process is applied for five minutes to four hours dependent on the temperature, longer times were used for lower temperatures.

The end result was a zeolite that still maintained its ability to perform the necessary olefin separation, while the isomerisation reaction was suppressed (Mattox and Rouge, 1967). Although the method is effective, care must be taken not to destroy the zeolite's lattice in these extreme conditions.

2.4.1.2 Leaching Method

Kantner et al. (1994) presents a method to reduce the aluminium content of ZSM-5 zeolite. This method was used by Kantner et al. (1994) to reduce the aluminium content of a silicalite sample from about 0.5% to about 0.3%. The basis for this method is the repeated treatment of the zeolite with a strong acid (18% by weight HCL), followed by a treatment with a mild caustic ($NaOH$) solution to neutralise and remove any residual acid impurities.

As with the steaming process, this inertisation method can result in the complete destruction of the zeolite lattice.

2.4.1.3 Ion exchange

A different approach to the inertisation of zeolites is to replace the hydrogen cation, usually with an alkali metal such as Na, K, etc. Rosback and Neuzil (1976) presents a method to ion exchange the cations within the a zeolite lattice (zeolites X and Y) with alkali metals, the end result being an adsorbent for separation processes that has significantly reduced isomerisation activity. This method is based on the earlier work performed by Rosback (1975).

2.4.1.4 Effect of inertisation on adsorption

The adsorption properties of a zeolite are influenced by the following factors (Ruthven, 1984; Choudhary and Srinivasan, 1986):

- Si/Al ratio
- Nature of the cation
- The degree of ion exchange
- Pre-treatment conditions

Choudhary and Srinivasan (1986) have shown that the Si/Al ratio plays an important part in the adsorption of hydrocarbons. In their work they showed that the adsorption of benzene increased as the Si/Al ratio decreased. This is possibly due to the increase in the non-polar nature of the adsorbent.

Wu and Ma (1983) observed that the adsorption capacity of hydrocarbons on alkali metal-exchanged ZSM-5 depends strongly on the radius of the alkali metal cation. It has also been shown by Choudhary and Srinivasan (1986) that the heat of sorption of benzene on HY zeolite increases with Na^+ ion content. The degree of H^+ ion exchange on ZSM-5 (H-Na-ZSM-5) was shown by Choudhary and Srinivasan (1986) to play an important role on the adsorption (again of benzene).

It is interesting to note the method of de-alumination also has an impact on the adsorption. Choudhary and Srinivasan (1986) have shown that steam treated ZSM-5 has a lower adsorption than a ZSM-5 sample that was synthesised with the same Si/Al ratio.

2.4.2 Silanisation

The so called silanisation method is normally associated with the inertisation of the external acidity of a zeolite (Weber, 1998; Röger, 1998). If one considers that on a normal zeolite the bulk of the adsorption occurs on the internal surface (i.e. the macro- and micro-pores), the effect of the external surface tends to be of little importance in the study of adsorption assuming, of course, that the adsorbate being studied has access to the internal surface of the adsorbent. The external acid sites can lead to an increase in non-selective adsorption, which is undesirable from a regeneration point of view in separation processes (Shively and Archer, 1967). In the context of this work silanisation was used as a means of controlling the adsorption properties of the adsorbent, via a process of pore blocking or pore narrowing (Duncan and Möller, 2001; Niwa et al., 1994).

The process of silanising a zeolite was covered in detail by both Weber (1998) and Röger (1998). The continuous flow CVD method detailed by Röger (1998) provides a convenient means to silanise reasonably large quantities of zeolite.

2.4.2.1 Effects of silanisation on adsorption

The effect of silanisation on the adsorption is still not fully understood. It has been suggested that the silanisation technique results in the narrowing of the pore openings, but it is entirely possible that it also results in the blocking of the pore openings (Kim et al., 1996; Weber et al., 2000).

Niwa et al. (1991) presented evidence of the ability to finely control the pore size of NaA using the CVD method (similar to that used by Röger (1998)). The pore mouth "narrowing" was demonstrated using the separation of O_2 and N_2, which is normally performed via kinetic mechanism due to the small difference in the molecules sizes ($0.02nm$). Niwa et al. (1991) has also reported similar success in controlling the pore mouth size of mordenite, for the separation of o- and p-xylene. Niwa et al. (1994) continues the work on pore mouth "narrowing" with a study of light olefins on a continuous-flow CVD'ed zeolite 5A. In this work Niwa et al. (1994) showed that the adsorption of ethylene, propylene, and 1-butene on various silanised 5A zeolites is significantly affected. As the "degree" of silanisation increases the adsorption of the bulkier molecules decreases until the deposited amount of SiO_2 reaches $1.30wt\%$ where the adsorption rate of propylene and 1-butene is extremely slow. This work is consistent with that shown by Niwa et al. (1984b,a, 1991). Niwa et al. (1994) explains this phenomenon using the pore mouth narrowing argument. However, the results do not give a clear indication of the dominant mechanism; pore mouth narrowing or pore mouth blocking. Similar results would be obtained regardless of the silanisation mechanism. In the event of pore mouth blocking the tortorous path length would be increased resulting in a lower adsorption rate. Duncan and Möller (2001) used the ZLC method of diffusion measurement to examine whether the silanisation technique results in pore mouth blocking or narrowing. It was shown by Duncan and Möller (2001) that it was not possible to reliably determine the effect of the silanisation processes on the pore mouth opening.

Chapter 3

Adsorption Microbalance Design and Construction

3.1 Microbalance

The adsorption microbalance system is centred around a *MkII vacuum head* manufactured by *C.I. Electronics Limited.* Originally the microbalance head has a quartz casing, this casing was unsuitable for the work and was replaced with a stainless steel casing manufactured by the Chemical Engineering Department's workshop.

The microbalance used was a null balance, in other words the position of the head did not alter regardless of the change in mass, or counter weight. This was made possible by an electronic bridge circuit which maintains continuous balance using a PID servo system (C.I. Electronics, 1992). This facilitated the installation of a thermowell into the reactor below the microbalance sample pan, without the fear of interfering with the balance. The thermowell allowed the measurement of the reactor temperature near the microbalance sample. The thermocouple was typically less than 1cm from the bottom of the sample holder. The sample temperature was assumed to be the same as the gas temperature, as the reactor could be assumed to be a well mixed system due to the high gas flow rates ($\pm 250 ml/min$).

The microbalance operated on a simple principle. The balance head consisted of a shutter interposed between a lamp and a pair of silicon photo-cells, and a movement coil. As the balance arm moves it causes one of the photo-cells to be exposed to more light. The photo-cells would generate a current proportional to the amount of light they were exposed to. The current was amplified and passed through the movement coil which restored the balance arm to its original position (C.I. Electronics, 1992; Brown, 1988). This servo-action has a number of advantages:

1. It ensures a rapid response.
2. It makes the balance less sensitive to external vibrations.
3. It produces a weight proportional current.

The balance head was controlled using a *MkII Multicard*, supplied by *C. I. Electronics Limited.* This card provided complete access to all the balance functions, it also contained a thermocouple amplifier. The thermocouple amplifier was not used in this system as it could not be used concurrently with the microbalance and would have required continuous mode switching which would have reduced the maximum sampling rate (C.I. Electronics, 1992).

The voltage produced by the movement coil current was taken as the input to the analog to digital converter (ADC). The output from the ADC was a 4 digit binary coded decimal (BCD). The *Multicard* also output the status of the microbalance including an over-range and a polarity bit. The ADC's had a resolution of 1 part in 20 000, which is effectively 14.3 bits (C.I. Electronics, 1992). No indication was provided on the linearity of the ADC and it was assumed that any deviation from linearity in the analog linearising circuitry was accounted for in the resolution provided.

Table 3.1: MkII Microbalance head, and MkII Multicard specifications (C.I. Electronics, 1992).

Specification		
Head Capacity	$1g$	$100mg \pm 10\mu g$
		$10mg \pm 1\mu g$
	$5g$	$200mg \pm 10\mu g$
		$20mg \pm 1\mu g$
Reproduciblity	$10\mu g$	
Temperature Drift	$10\mu g/°C$	
Maximum sampling rate (sample/second)[a]	2	

[a]Thermocouple cannot be read when sampling mass at this rate.

3.1.1 Sample pans, and suspension rods

A piece of fine mesh ($1\mu m$) steel sieve (18mm diameter) was used as the sample pan. The sample pan was carried by a nichrome (20mm diameter) wire sample pan carrier which was made in-house. The sample carrier was then suspended from the balance arm using a boro-silicate suspension rod ($\pm 85mm$ long), which were also produced in-house.

3.2 Gas handling system (rig)

The adsorbate was delivered to the system as a continuous gas stream. The flow-sheet for the rig used is shown in figure 3.1.

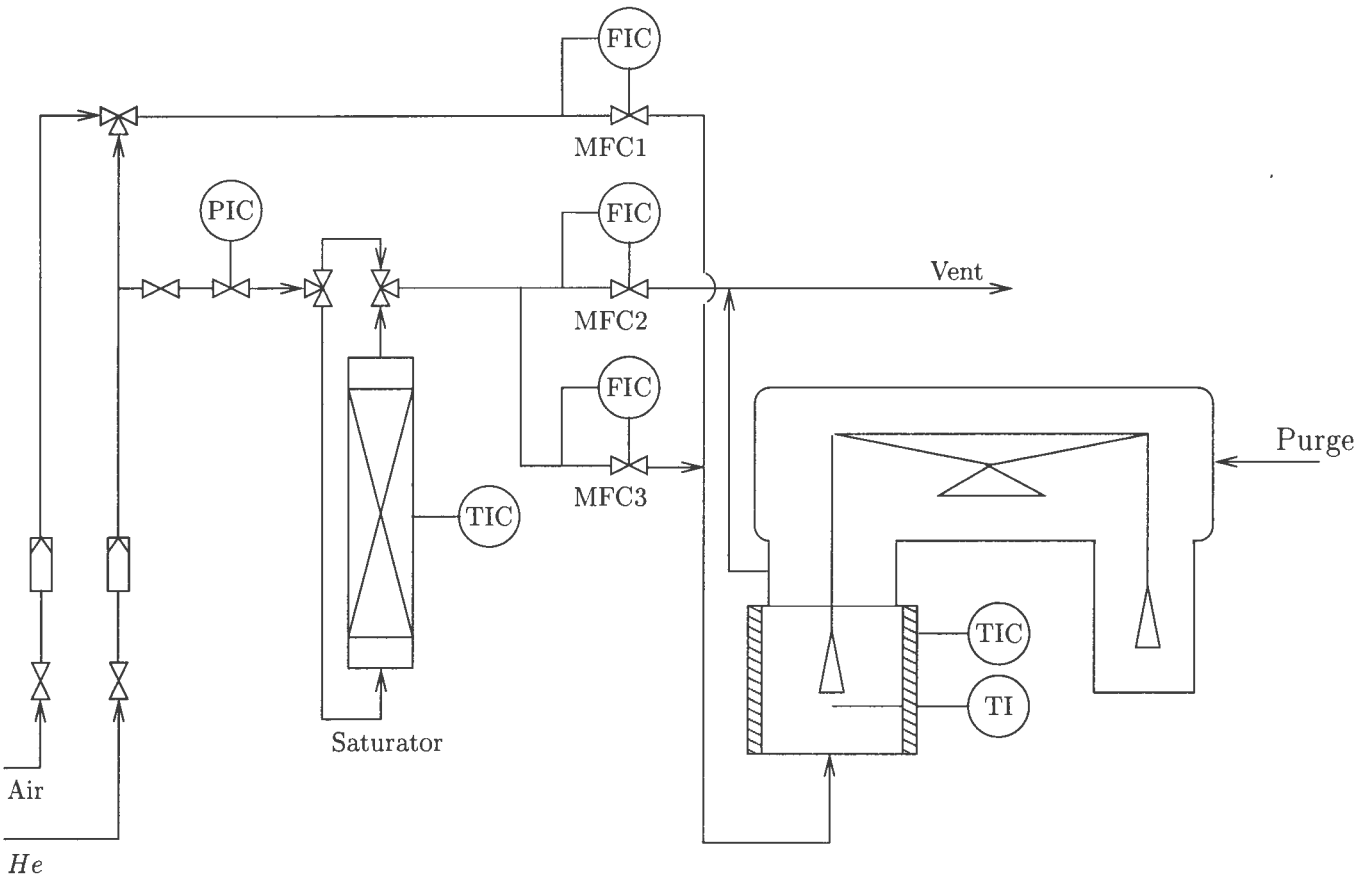

Figure 3.1: Microbalance rig flow-sheet.

The purpose of the rig was to supply a continuous gas flow to the microbalance reactor with a known adsorbate partial pressure. It was also required that the adsorbate's partial pressure could be varied.

The gas flow rate was controlled using three *Unit Instruments* mass flow controllers (MFC). MFC1 was a high flow rate, $\pm 630 ml/min$ (at STP) of helium, *Unit UFC1000*. MFC2 and MFC3 were both *Unit UFC4000s* with a maximum possible helium flow rate of $\pm 30 ml/min$ (at STP).

The adsorbate partial pressure in the balance was controlled using a number of techniques. Firstly, the vapour pressure of the adsorbate varies exponentially with temperature, therefore the saturator temperature was controlled using a refrigerated water bath. Secondly, the flow rate of the saturated carrier gas was controlled by MFC3. Thirdly, the flow rate of the diluent was controlled by MFC1.

Due to the low flow rate of carrier gas required, as low as $0.5 ml/min$, the dead time in the saturator would have been unacceptably large, in excess of $190 min$. This problem was overcome by placing the mass flow controllers after the saturator. By using two mass flow controllers it was possible to have a high enough flow rate ($\pm 16 ml/min$) through the saturator to achieve an acceptable dead time ($< 6 min$), while still being able to achieve the low adsorbate partial pressure in the reactor. The location of the saturator MFCs necessitated installing a pressure regulator before the saturator to

reduce the 2 bar line pressure to 1 bar. This was a safety requirement as glass saturators were used.

MFC1 was normally operated at a high flow rate ($\pm 240 ml/min$) compared to MFC3. This arrangement allowed low partial pressure to be used while the fluctuations, due to the varying saturator vapour pressure, was reduced.

3.2.1 Saturator

Figure 3.2 presents the saturator designed and built for this work. The gas is dispersed into the adsorbate using a gas distribution stick with a porosity 2 frit.

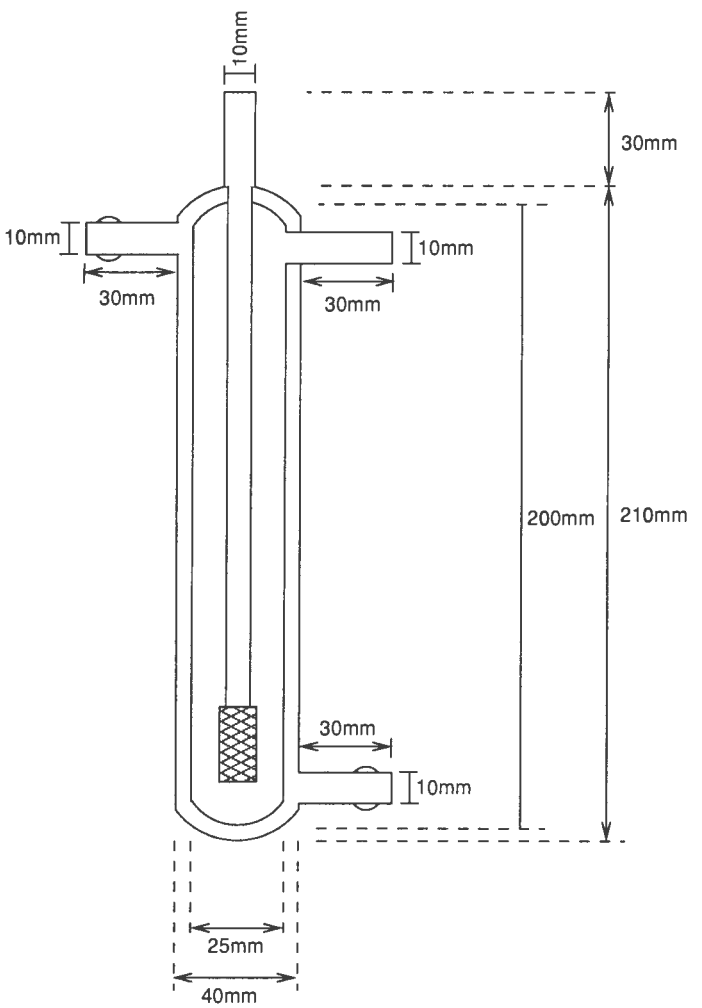

Figure 3.2: Microbalance saturator (bubbler type).

The saturator was tested and found to be stable over the carrier gas flow rates of interest ($0.5 - 30 ml/min$). The saturator was tested by comparing the calculated partial pressures in the reactor with measured partial pressures. The calculated values were found to have a deviate from the measured values by an average of less than 2%.

3.3 Data acquisition and control

Adsorption isotherm measurements took in excess of 24 hours to complete. It would not have been practical to perform these measurement manually because as well as the microbalance data, the operator would have been required to record all the process data manually, such as temperatures and flow rates. The operator would also have been responsible for setting all the experimental set points, such as furnace temperature and carrier gas flow rates. At the start of the project is was therefore decided that the best approach was to completely automate the system. This would not only make the adsorption microbalance more attractive to use, but would also reduce the possibility of human error.

The requirement was that the system be completely automated. Essentially this meant the operator would only have to enter the specific experimental requirements and then start the system. The adsorption microbalance would then complete the experiment without any further human intervention.

The automation required a combination of hardware and software. The remainder of this chapter will discuss the automation, starting with the hardware.

3.3.1 Hardware

The automation hardware was considered to be two made up of two separate sections, the microbalance and the rig. There was little, if any, coupling between them.

The automation hardware for the microbalance had already been addressed using the *C.I. Electronics Ltd. MkII Multicard* and no further hardware was required.

An *Eagle Electronics PC30GA* (*Eagle* card) analog and digital input/output (I/O) boards was used to interface the rig with the computer. This board is a half size, low cost, accurate analog and digital I/O board, intended for an *IBM* compatible computer (Eagle, 1996).

The microbalance reactor temperature was controlled using a *RKC* F9 temperature controller. This type of controller has a 0-5V analog input, used to set the set point, and a 0-5V analog output (the current temperature).

The three mass flow controllers were controlled using power supply units (PSUs) manufactured in-house. These MFC PSUs required a 0-5V analog input (the set point), and output a 0-5V signal, the measured flow rate.

Four thermocouple (TC) amplifiers were constructed in-house based on the *Motorola AD595* thermocouple chips. These thermocouple chips linearised the signal. This simplified the software by requiring

only a simple straight line calibration function thereby removing the need to implement thermocouple look-up tables, or other more complicated calibration methods. The TC chips also handled the cold junction compensation that was required. Once again the output from the TC amplifiers was a 0-5V analog signal.

The rigs valves control was provided by *Burkert* solenoid valves. These valves were available in both 2-way and 3-way variants. All the valves used on the rig had *viton* seats thus making them chemically resistant. The valves were triggered using solid state relays (SSR). The solid state relays were in turn triggered by one of the digital outputs from the *Eagle* card. The saturator's valves were installed in a fail safe configuration, i.e. the saturator's valves would fail to by-pass. Unfortunately the microbalances cooling water valve fails closed which is potentially dangerous, as the the balance head is sensitive to high temperatures.

An *Intel* 133MHz *Pentium (P54C-133)* with 16MB of RAM was used to control the adsorption microbalance apparatus.

3.3.2 Software

The hardware components where tied together by a purpose written *Borland Delphi* (version 4, standard edition) program. *Borland Delphi* is a rapid application development (RAD) system for the *Microsoft Windows (95, 98, NT, & 2000)* platform.

The microbalance program (mbalance) is a large and complicated program with 8000 lines of Object Pascal code. It would not have been beneficial to examine the program in detail but rather to focus on its primary function, namely the control of the adsorption microbalance.

3.3.2.1 Requirements

The Unified Modelling Language (UML) provided a convenient method of capturing the core requirements of an adsorption microbalance system in a easy to read format (OMG, 1999; Bennett et al., 1999). The requirements were presented as textual descriptions from the users perspective. For the purpose of the software design and analysis the balance and the rig were considered to be users of the mbalance program, in addition to the human operator.

Mbalance can be partitioned into four fairly independent sections:

- The balance control.
- The rig control.

- The experimental control.
- The data logger.

Theses sections essentially determined the program modules with the balance control, the rig control, and the data logger being written as in-process servers, while the experimental control section was the client/manager of those servers.

Figure 3.3 shows the functionality that was required by the balance and the interaction between the users and the software is also shown. The ability to configure and read the balance, to zero and calibrate the balance, as well as to save and load calibrations were all implemented in the software.

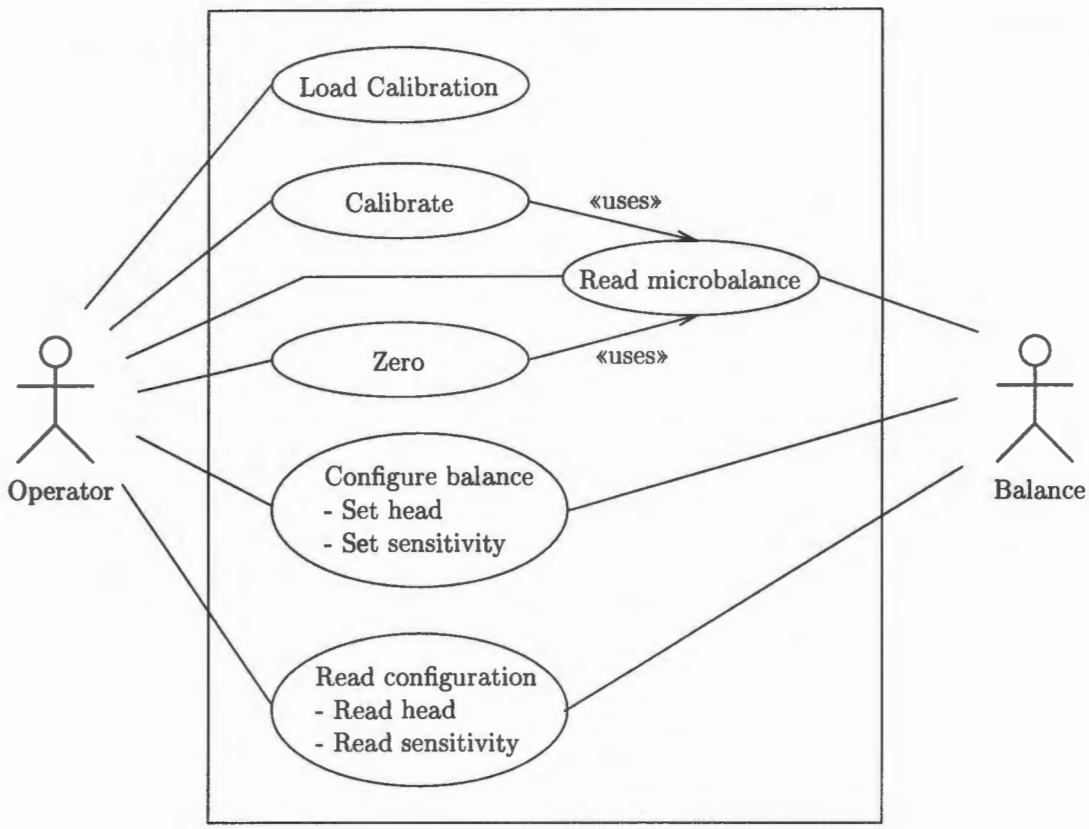

Figure 3.3: Microbalance control use case diagram.

In a similar fashion to the balance the rig's requirements were captured using a use cases diagram, figure 3.4. The calibration factors for the MFCs and the thermocouples were used by the program, although no calibration functionality was provided by the program. The operator could manually add the calibration factors to the rig control's configuration file (rigcntrl.ini)

The experimental section of the program had two basic requirements; the ability to enter the experimental profile and the ability to run the experimental profile. Figure 3.5 shows the experimental requirements in more detail.

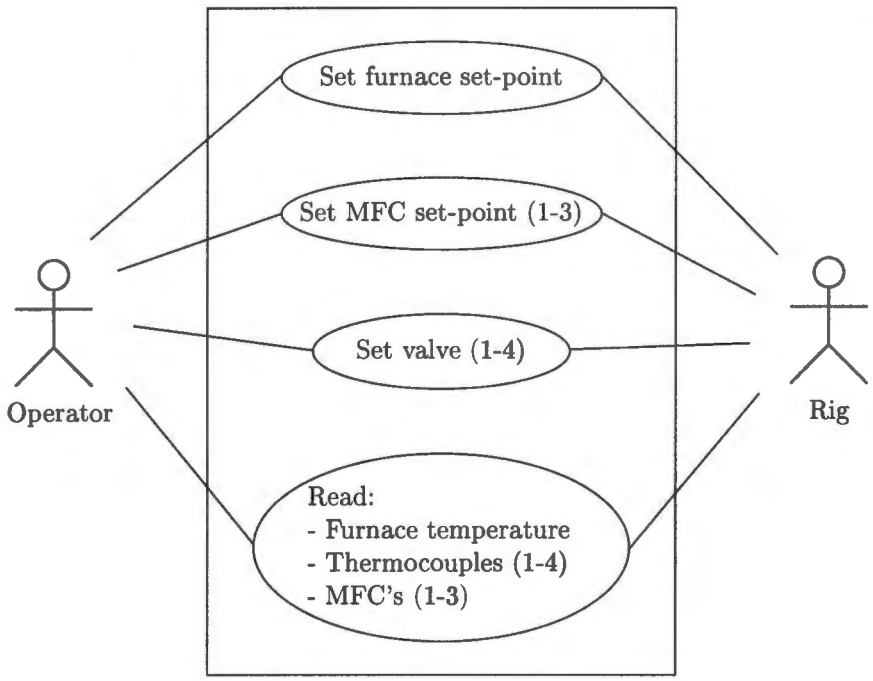

Figure 3.4: Use cases diagram for the rig control.

3.3.2.2 Experimental data

It is clear from the use cases diagrams that the program was required to handle a large amount data, both to setup the experiment and to record the results of the experiment.

Mbalance uses the *Borland database engine (BDE)*, rather than attempting to create a custom data handling system. The *BDE* introduced a powerful and flexible method for manipulating the data.

The experimental database was a *Borland Paradox* table that stored the experimental information, table 3.2 shows the database structure. For each record in the experimental database there was an experimental profile associated with it.

Table 3.2: Experimental information database

Field	Description	Data type
ExpProfile	Link to the experimental profile	FileName
Operator	Operator's name or e-mail address	string
Date	date of the records creation	Date
Adsorbent	The adsorbents name	string
Adsorbent_ref	Reference number for the adsorbent	string
Adsorbent_initmass	Initial mass of the adsorbent	double precision
Adsorbate	Adsorbates used	string
Adsorbate_ref	Adsorbate's reference	string
Adsorbate_purity	The adsorbates purity	string
Comments	General comments	BLOb

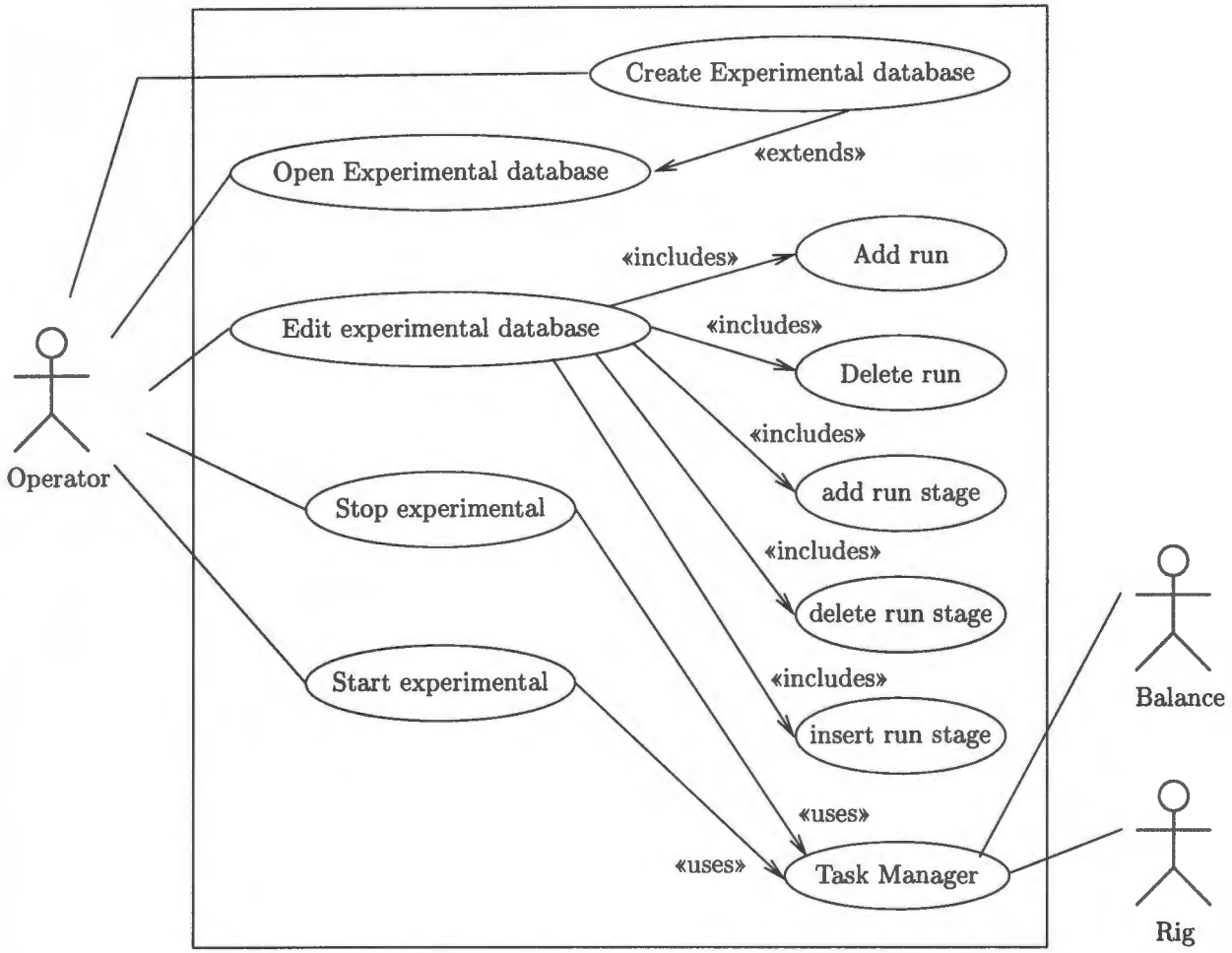

Figure 3.5: The Experimental use cases diagram.

The experimental profile was again a *Paradox* table. This table stored the set point information required for an experiment. Table 3.3 presents the details for the experimental database used. The first row of table 3.3 shows the field provided. The second row presents the field data type. The rows that follow give an example of the data that could be entered.

Table 3.3: An example of an experimental profile database, including the data type definitions.

Step	**Time**	**Furnace temperature**	**MFC1**	**MFC2**	**MFC3**	**Saturator**	**log**
integer	double	double	double	double	double	boolean	boolean
0	0	100	35	50	2	false	false
1	10	150	35	50	100	true	true

The time field used in the experimental profile was a step time, in other words referred to the time that each step would require. When the experiment was started the adsorption microbalance would have been set to the settings specified in step 0. Then over the next 10 minutes the temperature of the furnace would be ramped from 100°C to 150°C, and MFC3's set-point would have ramped from 2% to 100%, the saturator would have been "turned on", and finally the computer would log the data.

The system required that all the ramps be linear.

The experimental database allowed the microbalance system to be remarkable flexible. The only limitation was that only 65536 (16 bit integer index) step were allowed. The practical limitation is the size of the recorded data file which is a both a function of the sample rate and the period over which the samples are recorded. Tests have shown that the software can easily handle 50 000 data points, which equates to 83 hours of data sampled at a period of 5 seconds.

The data generated by the Mbalance was logged, when requested, to a comma delimited ASCII data file which also used the *BDE*. ASCII was chosen as the output format as it facilitates the use of the data with another program that can read flat text files.

3.3.2.3 Design

The use cases diagrams (figures 3.3, 3.4, and 3.5) provided the foundation used to develop the software. These diagrams indicated the main classes needed to achieve the requirements. Figure 3.6 is a UML classes diagram presenting the major classes used and the interaction between the classes.

Figure 3.6 does not show all the classes used by the program, but it does show the basic class hierarchy that was needed to meet the requirements and functions of the system.

The systems partitions discussed above are clearly visible in the classes diagram. The balance control section is handled by the TBalanceControl, which is associated with the TMBalance classes. The rig control is present as TRigControl, which is associated with a number of other classes, such as TFurnace. The experimental control section of the program consisted of TExpProfile, TExpDB and TTaskMan. Finally, the datalogger is made up of TDataLogger and TResultsDB.

TTaskMan, figure 3.6, was responsible for more than just "managing" an experiment (or a task), it was also tasked with tying the program together into a coherent system.

TExpDB provided an interface to the experimental database and the experimental profile database.

TExpProfile used TExpDB to parse the experimental profile data into a data structure that was compatible with TRigControl.

Due to the age of the *MkII Multicard* no *Windows* drivers were available and therefore the hardware interface was written as part of the microbalance program using *Borland's inline assembly language*. The hardware interface was wrapped in the TMBalance, which was used by the TBalanceControl class to provide all the balance functionality.

To improve the reproduciblity of the balance data Brown (1988) recommended the use of a filter on the balance readings. A simple running mean filter (usually using 10 data points) was associated with

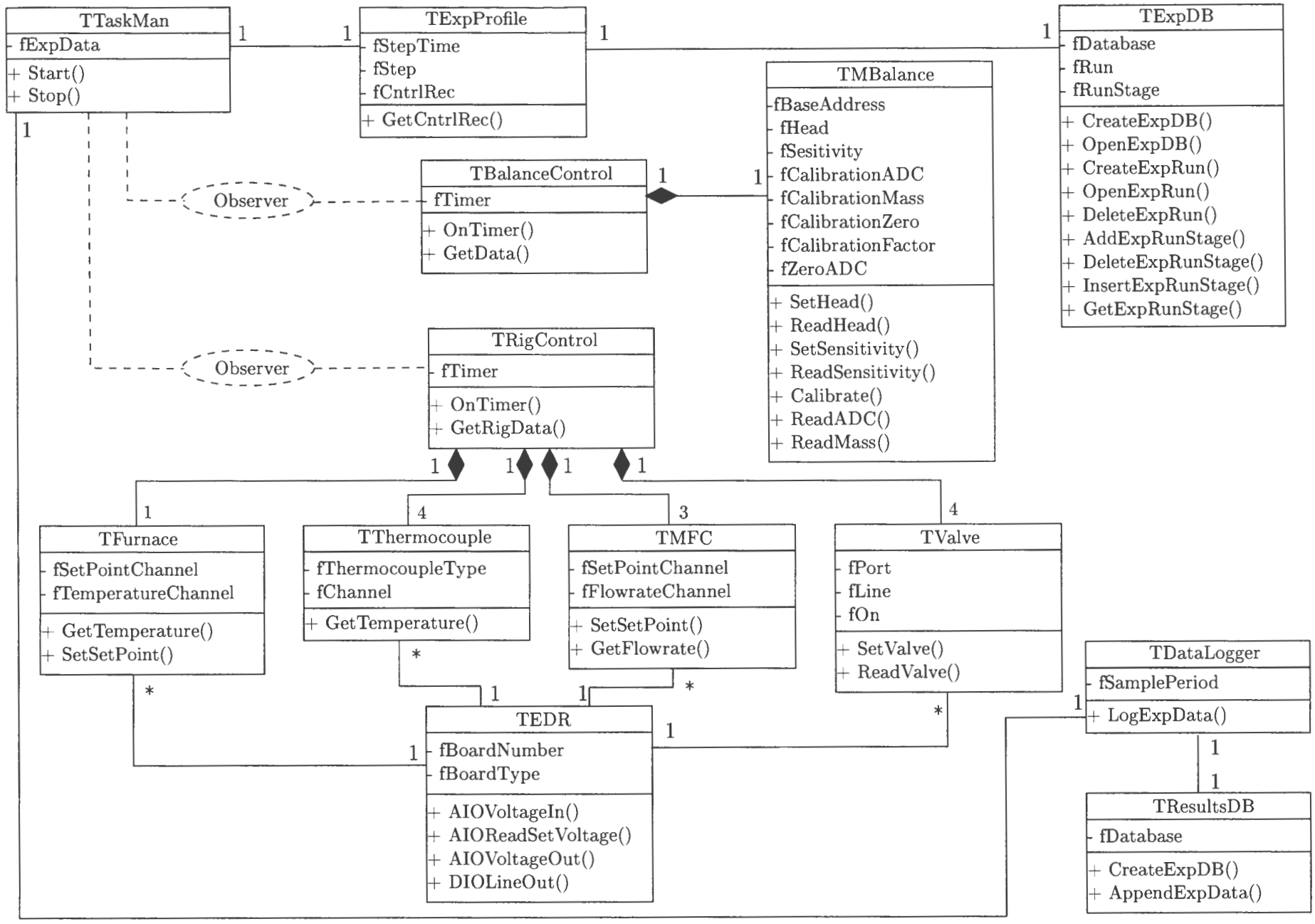

Figure 3.6: UML classes diagram, showing the major classes used in the microbalance program. The classes interaction is also presented in this figure.

the balance data. If necessary this feature can be switched off which is particularly important when making rate measurements.

As figure 3.6 shows, the TBalanceControl class communicates with the rest of the program using an observer design pattern (Gamma et al., 1995; Bennett et al., 1999). This communication pattern increases the degree of decoupling between the various sections of the program.

The rig control section of the mbalance program is very similar to the microbalance control section. In this case the low level hardware interface was provided by the TEDR class which was a wrapper around the drivers provide by Eagle (1999). The rig components were controlled via higher level classes such as the TFurnace class, or the TMFC class. The rig component classes provide a convenient means of hiding the details of the implementation from the remainder of the program.

The final section of the program is the data logger. This section is composed of the TDataLogger, and the TResultsDB classes. The data logger was actually written as two different sections, the data logger and the results database.

The data logger is tasked with handling the sampling of the experimental data. When TTaskMan received new data it would send it to TDataLogger which would determine whether it should be logged. This work used a so-called static data logger. A static data logger records samples at fixed time intervals.

In order to improve the flexibility of the program TDataLogger was implemented as a plug-in. The advantage was that if any other data logger was required they could be added to the system without the need to alter any other part of Mbalance. In fact the addition of a plug-in would not even require recompiling MBalance.

The plug-in framework implemented was based on the *Microsoft COM (component object model)* system (Ly, 1998; Gamma et al., 1995).

The adsorption microbalance system was a complicated system with a number of events occurring concurrently. Figure 3.7 attempts to shows the dynamic nature of the microbalance program. The behaviour shown for TBalanceControl and TRigControl was applicable for the entire life of the program, not just when an experiment was running.

When the program was started the TBalanceControl object was created. As already discussed this object is responsible for controlling the balance. Not only did TBalanceControl provide an interface to the balance, but it also handled the periodic reading of the microbalance. This was accomplished using a timer.

The timer would fire a *Windows* system event at a fixed time interval, which was specified in the configuration file (balcntrl.ini). TBalanceControl would respond to the event by reading the microbalance, followed by notifying the observer objects about the data.

Microsoft Windows is a pre-emptive multitasking system, not a real time operating system. This means that the scheduling of tasks by *Windows* does not take into account the need for accurate timing (Stankovic, 1988). When the timing intervals are small, less than one second, then the use of the *Windows* system timer for accurate time for both data capture and for control is ill advised. Another limitation of *Windows* is that there are only 32 system timers available to the entire system (Inprise, 1998). To compound the timing problem it is not possible to try and account for the inaccuracies in the timing as the possible delays vary depending on a number of factors, such as the present system load, and memory paging (Hilton, 2000).

The MBalance program requires fairly accurate time, particularly for the reading of the balance (normal sample period was 500ms). To overcome the system timer limitation the Mbalance program utilised the the *Microsoft Windows* multimedia timer, using a multi-thread design to improve the response.

The multimedia timer is considerably more accurate than the standard system timer. According to Hilton (2000) the *Windows* multimedia timer allows the use of *Windows* as a "soft" real-time system. This implies that although the system is still not guaranteed to responded to the timer events in a fixed time, the system is considerably more likely to responded. Timing accuracy can be improved to a resolution of approximately one millisecond, which exceeds the MBalance program requirements.

As has already been discussed the TRigControl object worked in the same manner as the TBalance-Control object. Again when a timer event was fired the TRigControl object would read all the rig data and then notify all observer objects.

The activity diagram shows that the TTaskMan object has no timing functionality. The timing is actually provided by the two control objects, TBalanceControl and TRigControl. Essentially the TTaskMan object would wait for one of the control objects to inform it that they had data available. When TTaskMan was told that one of the objects had data available it would check which object had sent the message. If it was TBalanceControl then TTaskMan would read the balance data into a record, it would then pass a record of the all the experimental data, including the latest rig data, to the data logger (TDataLogger). When TRigControl contacted TTaskMan, TTaskMan would read the rig data into a experimental data record and then advance the experimental profile by the required time interval.

Therefore the TRigControl timing was responsible for the experimental profile timing and the TBal-anceControl determined the sample interval timing. The TRigControl timer interval was always set to 1 second, whereas the TBalanceControl timer interval was always set to 500 milliseconds (C.I. Electronics, 1992).

It should be obvious that this algorithm introduces certain limitations. Firstly, the data in the experimental data record is not read at the same time, there could be as much as 500 milliseconds

time difference between the balance data and the rig data. This half second difference was assumed to be sufficiently small that it could be ignored. Secondly, the maximum sample rate is determined by the balance sample period. There would be no practical reason to attempt to sample data faster than the balance can read.

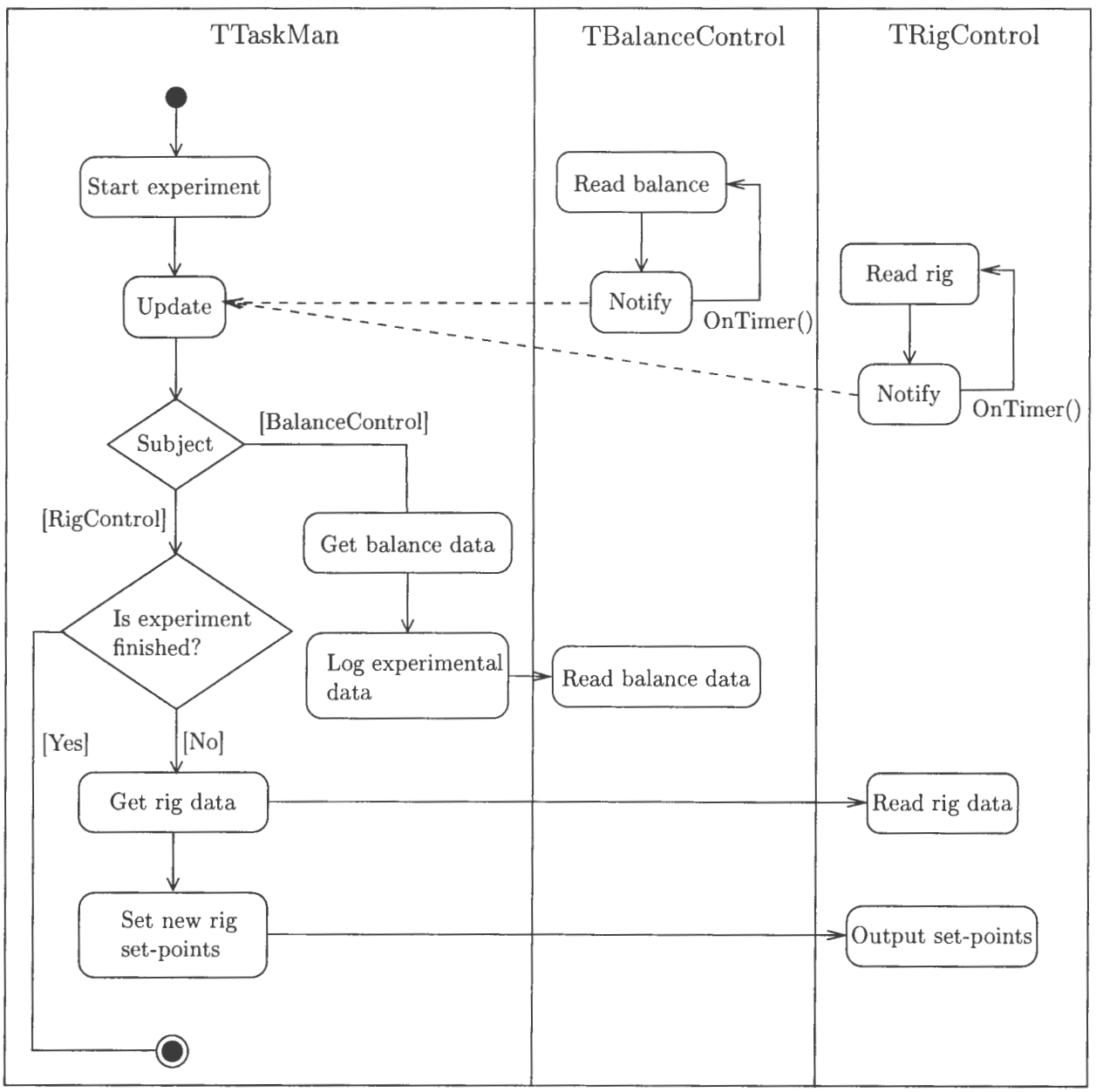

Figure 3.7: Activity diagram for the mbalance program when an experiment has been started.

Chapter 4

Experimental Methods

This chapter presents the experimental methods used to perform the work presented in this thesis. It initially starts with a discussion about the adsorbent and the methods of preparing and modifying the adsorbents. The chapter moves on to look at the isotherm measurement techniques. Finally the methods of calculating physically meaningful parameters from the data is presented.

More detailed information about the materials used can be found in appendix D.

4.1 Adsorbent characterisation

4.1.1 X-ray diffraction (XRD)

A *Philips* X-ray diffractometer using a CuKα radiation source was used to obtain the powder X-ray diffractograms. A wavelength of 1.542Å at 40KV and 25mA with the silicalite 1 in it's hydrogen form was used, with a scanning range of $4 < 2\theta < 47$.

4.1.2 BET surface area

The surface area and the pore volume of the adsorbent was determined by nitrogen adsorption using a *Micromeritics ASAP 2000*. A sample of approximately 0.5g of adsorbent was dried for 24 hours in situ at 350°C under a vacuum (P=0.65Pa). Nitrogen was then adsorbed at its boiling point (77K) using an extended pressure table with 150 pressure points ranging from 0.65Pa to ambient pressure.

4.2 Adsorbent

All the experimental work was performed on a commercial silicalite-1 sample supplied by Süd-Chemie. Table 4.1 present the physical characteristics of the silicalite-1 sample.

Table 4.1: Physical characteristics of Süd-Chemie silicalite-1.

Property	Value
Si/Al	200
Particle size[a] (μm)	0.1-0.2
Surface Area[b] (m^2/g)	317

[a]SEM estimates
[b]BET surface area

4.2.1 Acid/base washing

It is desirable to remove any remaining acidity from the adsorbent prior to using it in any separation processes (Kantner et al., 1994). The aluminium was removed from the silicalite-1 using an acid/base wash technique described by Kantner et al. (1994).

A sample of 20g of silicalite-1 powder was treated with one litre of 18wt% hydrochloric solution, at room temperature, while stirring. After allowing the mixture to settle overnight, the supernatant liquid was decanted. Then a further 1L of fresh 18wt% HCL_aq was added to the mixture while stirring. Again the solid-liquid mixture was allowed to settle overnight. This acid washing procedure was performed a third time.

Finally, after the third acid wash, the supernatant liquid was decanted and the silicalite was washed repeatedly with de-ionised water until the wash water gave a neutral reaction to litmus paper. Due to the small size of the silicalite particles filtration proved impractical and therefore it was necessary to use a centrifuge to improve the recovery of the silicalite. The silicalite sample was centrifuged at 20 000 rpm for 30 minutes after each de-ionised water wash.

A $NaOH$ solution was prepared by dissolving 0.3g of $NaOH$ in 1L of de-ionised water. The $NaOH$ solution was added to the acid treated silicalite, while stirring. The silicalite-1 $NaOH$ solution was allowed to settle overnight, after which supernatant liquid was decanted. The silicalite was then washed once with de-ionised water and again centrifuged.

The wet silicalite-1 was then dried in air overnight at approximately 90°C. Finally the dried silicalite was calcined in air at 400°C for at least 4 hours prior to use.

A total of four samples of silicalite-1 were treated using the acid/base washing technique described above, which were then combined to form a single sample of approximately 50g.

4.2.2 Pelletisation

Due to the small size of the silicalite-1 particles a number of samples were pressed into pellets prior to some of the experimental work in order to avoid high pressure drops, particularly in the silanisation process.

The silicalite pellets were produced by compacting approximately 0.3g of silicalite into a 35mm diameter wafer. This was accomplished by applying 10 tons of pressure to the silicalite, using a mechanical press. The wafer was then lightly ground using a pestle and mortar. The fragments were then sieved to obtain a 212-300μm size fraction. The oversize fraction was returned to the pestle and mortar and the under-size fraction was repressed.

4.2.3 Silanisation

A sample of the silicalite-1 pellets were treated using the silanisation method describe by Röger (1998). The details of the method used are presented below.

4.2.3.1 Reagent preparation

Tetraethoxysilane (TEOS) was used as the silane source for the silanisation process. The TEOS was prepared by "drying" it over zeolite 3A. This was done in order remove the traces of water and ethanol that could influence the silanisation process (Röger, 1998).

4.2.3.2 Experimental apparatus

Figure 4.1 shows the flow sheet for the silanisation apparatus. The apparatus was fitted with a set of automated timer switches which made it was possible to achieve a reasonably high cycle throughput.

Reactor

The silanisation reactor consisted of a 440mm long quartz tube, with an outer diameter of 16mm (14.6mm I.D.), and a porosity 2 quartz frit that was positioned 185mm from the top of the reactor, as shown in figure 4.2. The internal reactor temperature was measured by inserting a stainless steel clad K-type thermocouple into the adsorbent bed during the silanisation process.

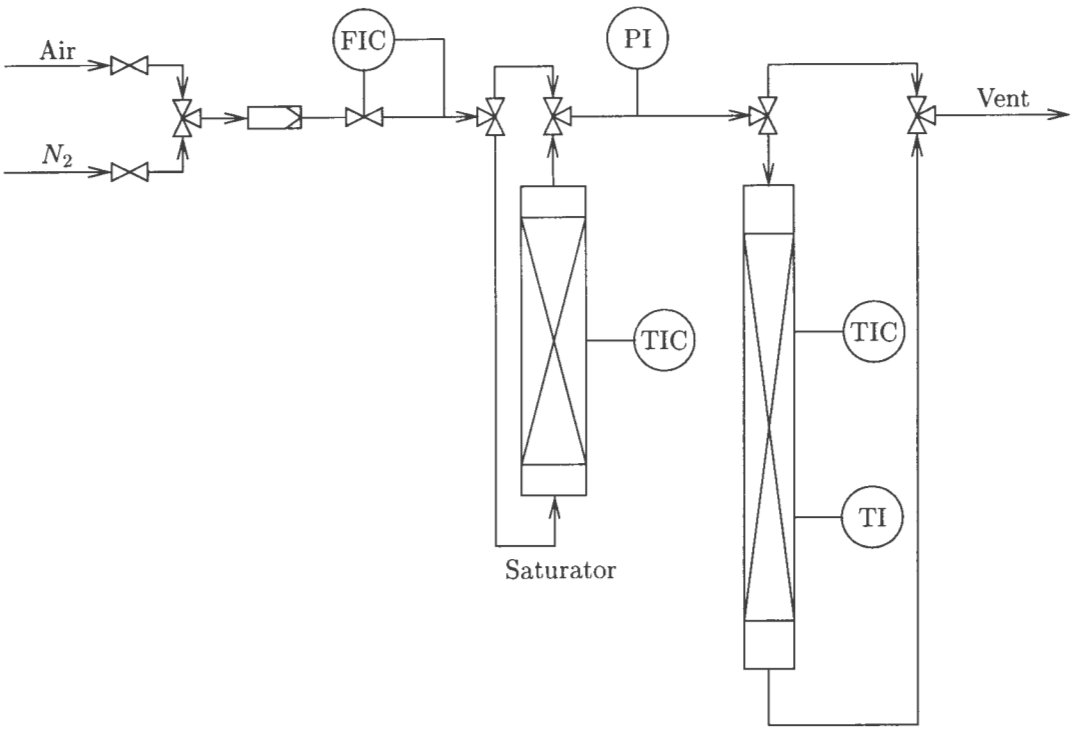

Figure 4.1: Silanisation experimental apparatus flow-sheet

Saturator

The TEOS is fed to the system using a Chromosorb saturator (figure 4.3). This type of saturator consists of two chambers; the lower chamber, which is a reservoir for the TEOS, and the upper chamber, which is packed with Chromosorb P. The TEOS is forced, by capillary action, into the Chromosorb packing and as long as the gas flow rate was reasonably low the Chromosorb packing remained "moist" with TEOS. The carrier gas (N_2) was fed into the bottom of the Chromosorb chamber and exited via the top connection. The saturator temperature was controlled at 15°C by pumping cooling "water" from a refrigerated water bath through the outer jacket of the saturator.

4.2.3.3 Experimental procedure

The silanisation process is cyclical in nature and consists of a number of procedures which are explained in more detail below. Initially approximately 2g of acid/base treated silicalite-1 pellets were loaded into the silanisation reactor. Prior to the start of the silanisation process the adsorbent was calcined in situ for at least 4 hours at 500°C.

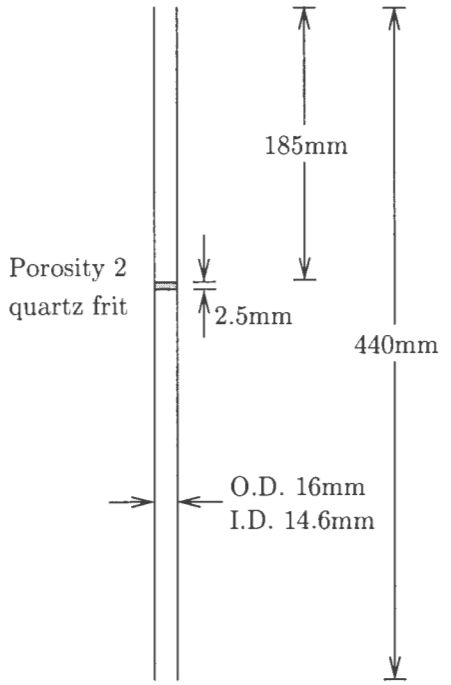

Figure 4.2: Schematic of the silanisation reactor

Silanisation cycle

As already mentioned a silanisation cycle consists of a number of stages. Figure 4.4 represent a single silanisation cycle, based on the temperature profile.

The silanisation cycle starts with a buffer (figure 4.4: stage 1) to allow for small variations in the cycle timing. Following the buffer is the reaction stage (stage 2) where the TEOS is fed to the reactor for 60 minutes at 100°C, after which the weakly adsorbed TEOS is allowed to desorb (stage 3) in a nitrogen atmosphere prior to starting the temperature ramp for the calcination stages (4, 5, and 6). The adsorbent was calcined for two hours (excluding the ramp time) at 500°C in synthetic air. Finally to complete a cycle the reactor is cooled back to the reaction temperature (100°C).

Silanisation series

The silanisation cycles result in small incremental changes to the adsorbent, therefore the silicalite was treated in series of 5 cycles. After each series a small amount (100-150mg) of the adsorbent was removed from the reactor. By doing this the conditions in the reactor varied from series to series, and the details of the reaction conditions are presented in table 4.2. A total of four silanisation series were performed.

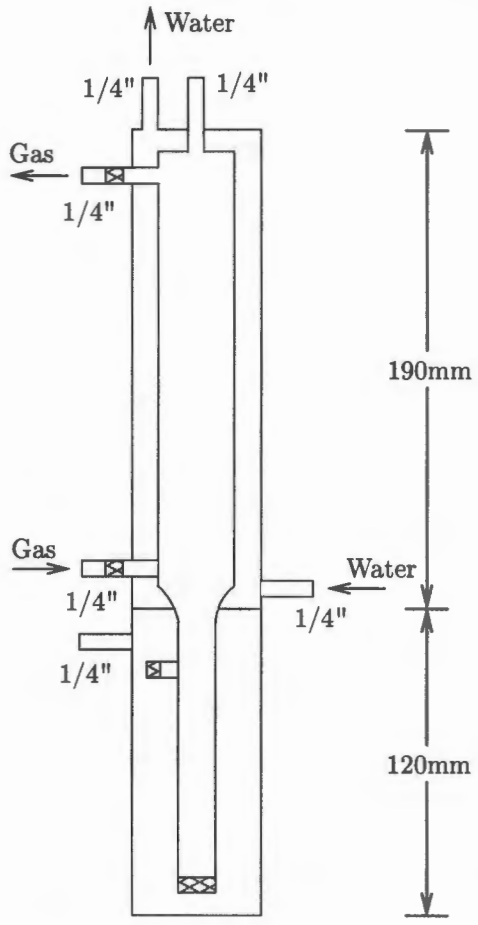

Figure 4.3: Chromosorb saturator used for the silanisation process

4.2.4 Adsorbent Nomenclature

Due to the number of modifications to the adsorbent it was convenient to define a standardised naming scheme. Equation 4.1 below presents the formulation of the adsorbent names that will be used in the rest of this document.

$$\begin{matrix} Adsorbent - Modification \\ IUPAC - A/P/S_i \end{matrix} \tag{4.1}$$

where

- **Adsorbent** refers to the IUPAC name (e.g. MFI for silicalite and ZSM5).
- **Modification** is the post synthesis modification.
  - **A**: Acid/Base washed.

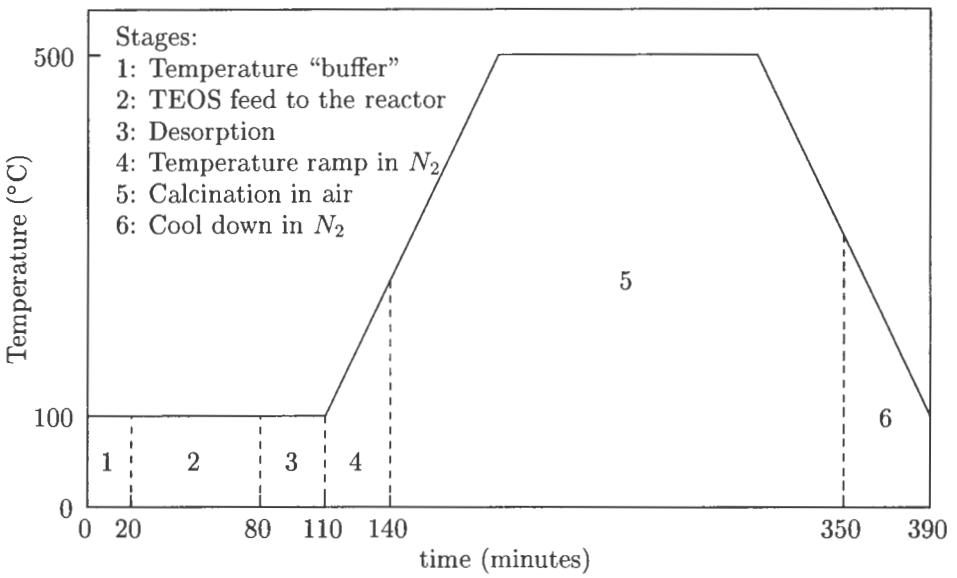

Figure 4.4: A single silanisation cycle, based on the temperature profile.

Table 4.2: Silanisation reaction conditions.

	Number of Cycles	
	10	**15**
T_{rxn} (°C)	100	100
T_{sat} (°C)	16	16
F_{N_2} (ml/min)	97	97
F_{Air} $(\approx ml/min)$	100	100
$P_{rxn,TEOS}$ (Pa)	124	124
Mass (g)[a]	1.8989	1.7479
WHSV[b]	0.026	0.028

[a]Increase in mass due to silanisation not included
[b]Based on the original adsorbent mass

- **P**: Pelleted.
- **S**: Silanised. The subscript i indicates the number of silanisation cycles.

4.3 Microbalance characterisation experiments

4.3.1 Saturator performance

It was necessary to check the performance of the saturator, particularly as the partial pressure is determined via calculations and not direct measurement. The saturator performance was checked using a standard ampule sampling technique. The saturator flow rate and temperature was set, as was the diluent flow rate. Methane was used as an "internal standard", which was introduced into

the gas leaving the adsorber prior to the ampule sampler. The methane gas flow rate was controlled using a porter mass flow controller and thus a known amount of methane was present in the ampules. The partial pressure of the adsorbate was determined using a gas chromatograph with an FID.

4.3.2 Stability

The stability of the microbalance readings are critical to the isotherm measurement. To quantify the stability two areas were investigated; the long term stability and the effect of changing flow rates.

4.3.2.1 Long duration stability

The time taken to measure an isotherm is fairly long (in excess of 24 hours) and it is therefore important to determine the effects of long duration experimental runs. The long run stability was determined by running the microbalance under experimental conditions (excluding the saturator) for a period of 48 hours (well in excess of the normal experimental duration). Table 4.3 shows the experimental conditions chosen.

4.3.2.2 Flow rate stability

Due to the design of the gas delivery system, the total flow rate to the microbalance reactor cannot be kept entirely constant. For obvious reasons (buoyancy and drag) it is essential that the effects of the variable gas flow are quantified. This was accomplished by running the microbalance under near experimental conditions, the major difference being that the gas flow rate was varied over a far greater range than would normally be tolerated (−50% to +100% of the initial value) in the adsorption experiments. The details of the experimental conditions are presented in table 4.3.

Table 4.3: Experimental conditions used to characterisation microbalance's stability.

Parameter	Duration	Flow rate
$T_{bal,int}$ (°C)	100	100
Total reactor flow rate (ml/min)	210	210 (initial)
Flow rate variation (%)		−50 to +100
Mass (mg)	50	50
Run Time(hours)	48	
Sample Rate (samples/min)	10	10

4.3.3 Reactor temperature

Due to the design of the microbalance there is no practical method of measuring the temperature of the absorbent on the sample pan, although there is a thermowell in the centre of the reactor. In

order to determine the thermal characteristics of the microbalance experimentally copper sulphate was thermal decomposed (Brown, 1988).

4.3.4 Response time

It would be advantageous to have some indication of the response of the microbalance to mass changes. This was determined by performing an adsorption experiment with a zeolite Y and n-hexane.

Approximately 50mg of zeolite Y was initially loaded. The adsorbent was calcined in situ for 4 hours at 400°C in air prior to the experiment. The adsorption was performed at 100°C. In order to achieve a fast mass change the n-hexane partial pressure was stepped from 0Pa to approximately 570Pa.

4.4 Adsorption experiments

4.4.1 Reagent preparation

4.4.1.1 Adsorbate preparation

All the reagents used in the adsorption experiments were of HPLC grade (>97%), appendix A provides detailed information on all the reagents used. The reagents were used without any further purification.

4.4.1.2 Adsorbent preparation

Each adsorption experiment used approximately 50mg of adsorbent. Prior to the start of the adsorption measurement the adsorbent was calcined in situ for at least 4 hours at 400°C in air.

4.4.2 Experimental procedure

4.4.2.1 Microbalance calibration

The microbalance was calibrated at regular intervals, normally after every sixth isotherm measurement. Figure 4.5 describes the microbalance calibration method. Special care was taken to ensure that the microbalance readings were stable prior to each of the measurement stages. The quality of the calibration directly impacts on the accuracy of the isotherm measurements.

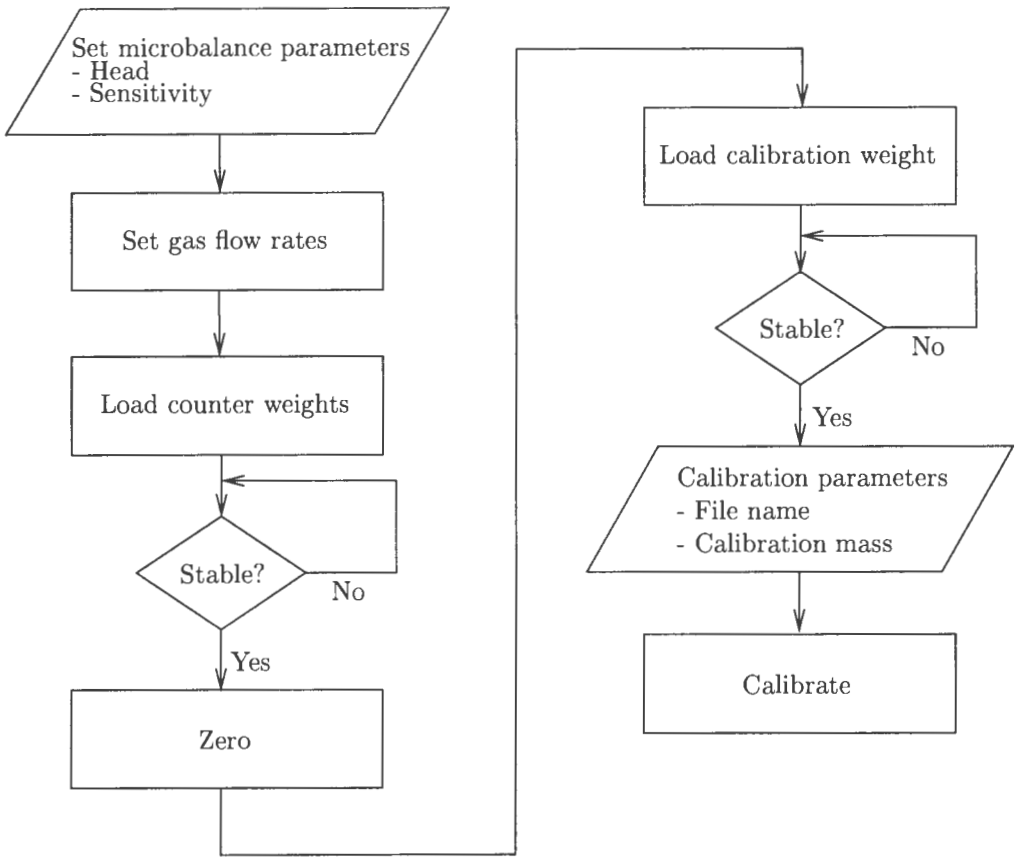

Figure 4.5: Microbalance calibration method flow-sheet

4.4.2.2 Isotherm measurements

The aim of the isotherm measurements was to collect the gravimetric data at known partial pressures. This aim was accomplished by performing a number of step changes to MFC3's set point, and therefore the partial pressure of the adsorbent to the reactor, as shown in figure 4.6. After each step change the system was given sufficient time to stabilise before sampling the microbalance. The stabilisation time varied, and therefore the microbalance was considered to be stable when the standard deviation of the sample mass was less than $10\mu g$.

In an attempt to minimise the time taken to perform an isotherm measurement the step changes were not kept constant but were rather increased over the period of the experiment. The initial portions of the isotherm had small step changes (2%), this is logical as the most rapid change in the isotherm is in the low partial pressure region. The step changes in the later stages of the experiment were increased to 10% to speed up the the experimental process. Table 4.4 presents the normal MFC3 set point profile used.

It is obvious that the experimental method will lead to a changing total gas flow rate to the microbalance reactor, which is undesirable due to buoyancy and drag considerations. Therefore an effort was

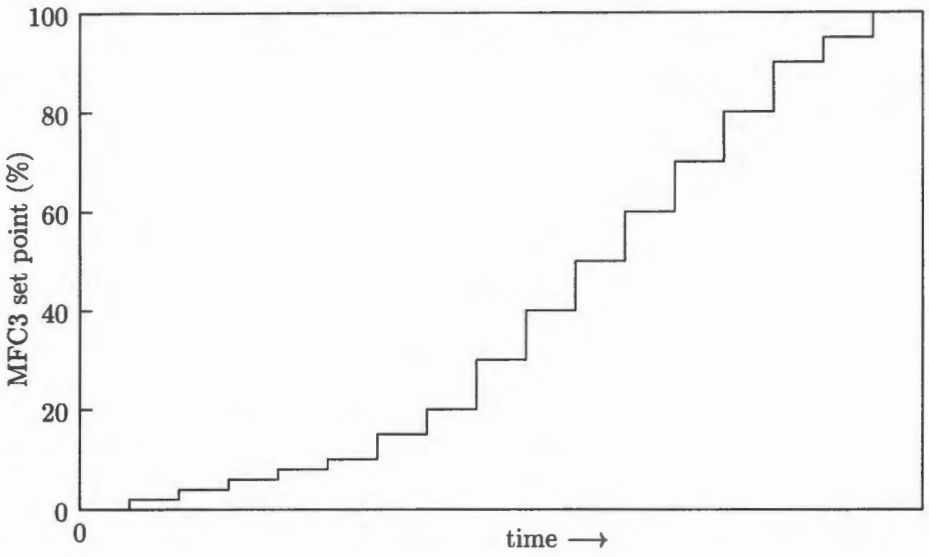

Figure 4.6: Mass flow controller 3's (MFC3's) experimental profile.

Table 4.4: Mass flow controller 3's (MFC3's) experimental set point profile.

set point (%)	Step change (%)
0 - 20	2
20 - 40	4
40 - 90	10
90 - 100	5

made to maintain a constant total flow rate to the microbalance reactor. This was achieved by varying the set-point of MFC1 over the experimental period. The result of this was that the increase in the flow to the microbalance reactor was never more than 10%, and usually less than 5%.

A number of identical experimental runs were performed using different initial sample masses in order to determine the effect of the sample mass on the adsorption results. The effect of whether the sample was in pelletised or powdered format was also checked by using repeated experiments.

4.5 Data evaluation

4.5.1 Partial pressure

The partial pressure of the adsorbate and the TEOS in the respective reactors was determined using equation 4.2 below.

$$P_{bal,i} = P_{sat,i} \frac{F_{sat}}{F_{sat} + F_{dil}} \tag{4.2}$$

The partial pressure of the adsorbates was determined using the data and correlations provided by the Dauber and Danner (1992). The TEOS partial pressure was determined from the Antoine's equation. The correlation constants are available in appendix A.

4.5.2 Weight hourly space velocity

The weight hourly space velocity is defined as the ratio between the mass flow of the reactant per hour to the mass of the adsorbent in the reactor, equation 4.3.

$$WHSV = \frac{\dot{m}}{m_{adsorbent}} \tag{4.3}$$

4.5.3 Henry's constant

The Virial equation (equation 4.4) provides a useful means of determining the Henry's constant from experimental data (Ruthven, 1984; Barrer and Davies, 1970). This method is especially useful when there is no reliable experimental data in the initial linear region as happens with strongly adsorbed compounds.

$$K'P = q \exp\left(A_1 q + A_2 q^2 + \cdots\right) \tag{4.4}$$

A plot of $\log(q/P)$ versus q should approach linearity in the lower partial pressure region and this linear region provides a easy means of extracting the Henry's constant.

4.5.4 Heat of adsorption

The temperature dependence of K' is given by:

$$K' = K_0 e^{-\Delta H/RT} \tag{4.5}$$

Thus, from equation 4.5, the heat of adsorption ($\Delta H/R$) can be determined from a plot of $\ln K'$ versus $1/T$, which should produce a straight line (Ruthven, 1984; Ruthven and Kaul, 1996).

4.5.5 Isosteric heat of adsorption

The isosteric heat of adsorption was determined by first plotting a series of isosteres. This was simply done by plotting the logarithmic pressure versus the inversion temperature at constant loadings. The Clasius-Clapeyron equation (eq. 4.6)was fitted to each of the isosteres, which provided the isosteric heat of adsorption for that loading (Ruthven, 1984; Yang and Rees, 1997).

$$\left.\frac{\partial \ln P}{\partial T}\right|_q = \frac{q^{st}}{RT^2} \tag{4.6}$$

4.5.6 Entropy of adsorption

The differential molar entropy of adsorption at standard pressure (P°) was determined from the isosteric heat of adsorption using equation 4.7.

$$\begin{aligned} \Delta S = S_{ads} - S_{gas} &= R \ln\left(\frac{P^\circ}{P}\right) + \frac{\Delta H}{T} \\ &= R \ln\left(\frac{P^\circ}{P}\right) - \frac{q^{st}}{T} \end{aligned} \tag{4.7}$$

Chapter 5

Characterisation of the adsorption microbalance

In order to use the adsorption microbalance system constructed for this project with any confidence it was necessary to examine the performance and the limitations of the system. The analysis has the added function of highlighting the areas of the microbalance that would show the largest benefits from improvements.

5.1 Reproduciblity

For the microbalance system to be of any practical use it needed to produce repeatable results. The reproduciblity was examined using the adsorption of n-hexane on the parent catalyst (MFI) at 100°C.

The repeatability of the n-hexane adsorption on MFI is excellent, as shown in figure 5.1. The sum of squared errors, based on the loading, is $7.48 \times 10^{-3} mol \cdot kg^{-1}$.

5.2 Mass readability

The readability refers to the limits within which the mass can be read with any degree of confidence. The upper limit is straight forward as it is determined by the physical limitation of the hardware, the *MkII* microbalance head. The manufacturer's stated limits is $100mg$, from table 3.1. This roughly translates to 20 000 A/D counts which is the limit of the A/D converter.

The lower limit is not clear. Essentially this limit is determined by the errors present in the microbalance readings and it is not practical to attempt to assign any significance to readings that are

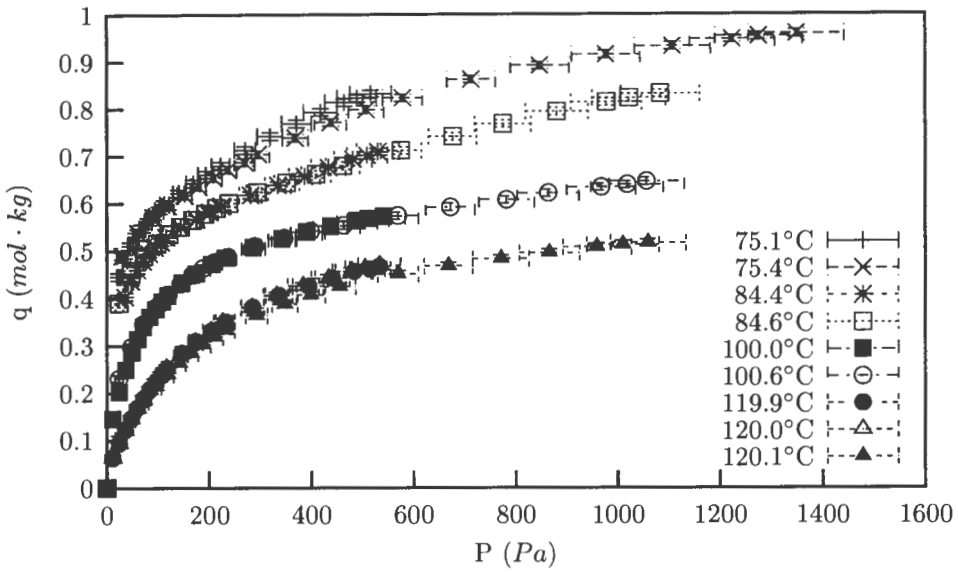

Figure 5.1: Repeatability of n-hexane adsorption on MFI at various temperatures.

smaller than the error. There are two chief sources of error present in the microbalance system, the calibration error and noise.

From the experimental data, see appendix D, the standard deviation of the mass readings vary by an appreciable amount, from close to $0\mu g$, i.e. no deviation, to as much as $60\mu g$. From the experimental data it would be reasonable to accept a noise standard deviation of about $4\mu g$, which would give an error of approximately $8\mu g$ ($t = 1.96$ for large samples).

The calibration of the microbalance introduces a further source of error. The error in the calibration is handled as an offset from the true value. The standard deviation of the calibration error is approximately constant at $\pm 10\mu g$, for all the experimental runs performed. Within a 95% confidence interval this means that the error in the mass readings is approximately $30\mu g$ ($t = 3$ for small sample populations).

These two error sources are cumulative in nature. It is clear that the error in the mass readings is dominated by the calibration error. If it is accepted that the error sources are fairly constant, the combined error in the mass readings is reasonably constant at approximately $30\mu g$ (again within a 95% confidence interval). The smallest mass change that is statistically readable is therefore $30\mu g$.

5.3 Stability

Stability is a measure of the variance in the microbalance readings. The readings are susceptible to a number of variables; the drift over time and variations in the flow rate being the most significant.

5.3.1 Long duration stability

To facilitate the long run times the microbalance must be able to produce stable readings over an extended period of time. This requirement was investigated by running the apparatus under experimental conditions for 24 hours. Figure 5.2 shows the stability of the microbalance over the 24 hour period. It can be seen that there is a definite correlation between the balance head temperature, which was assumed to be the same as the ambient temperature, and the drift in the mass readings.

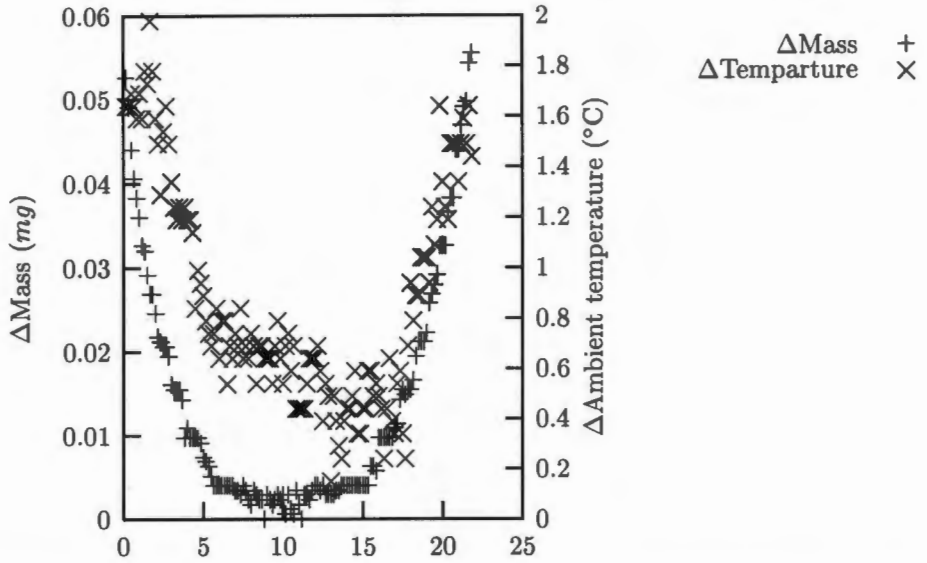

Figure 5.2: Variation in microbalance mass readings over extended run times.

It is clear from figure 5.2 that the balance readings are not stable over an extended run time. When plotted in conjunction with the ambient temperature it can be seen that the balance readings appear to be influenced by the ambient temperature in an approximately linear manner. This phenomenon is easily explained by considering the effect of thermal expansion on the balance's beam.

Due to the limitation of the apparatus where there are no facilities to control the head temperature, the effects of the temperature variations could not be examined in detail.

Due to the small temperature range (>2°C), in comparison to the error in the temperature (±1.4°C), there is a large amount of noise in the temperature readings. Bearing this in mind it is only possible to give a rough estimate of the drift in the mass reading due to temperature. From figure 5.2 it can be seen that the drift in the mass readings due to temperature variations is approximately linear, particularly if the tail of the stability curve is considered. By simple linear regression the mass readings drift by $31\mu g/°C$. This is considerably larger than the value published by C.I. Electronics (1992) of $10\mu g/°C$, although the error in the regression alone as a result of noise is $\pm 20\mu g$.

The results presented in this work have not been corrected for this drift.

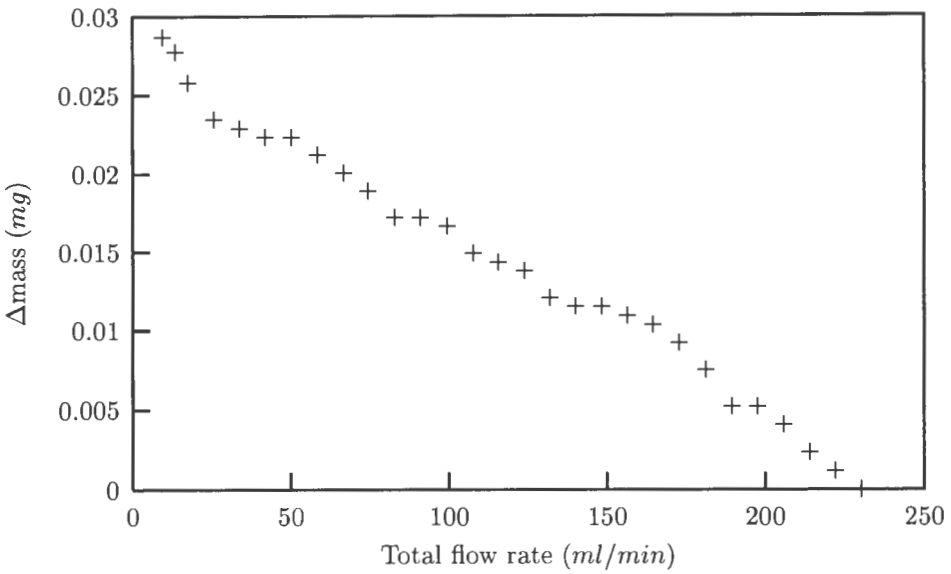

Figure 5.3: Mass readings stability with variations in the total reactor flow rate.

5.3.2 Flow rate stability

By the nature of the microbalance system it is expected to be susceptible to variation in the mass readings due to variation in the reactor flow rate.

The mass readings show an approximately linear relation with the variation in the total reactor flow, figure 5.3. The linear relation is a little surprising, as the variation in the mass is due to the increased drag exerted on the sample pan. The relation between velocity and volumetric flow rate in this instance is not linear (equation 5.1).

$$D = \frac{1}{2} C_D \rho \mathcal{A} v^2 \tag{5.1}$$

The change in microbalance mass readings is relatively small. Therefore, if the changes in flow rate are minimised then the mass reading can be used without the need to apply any corrections. In the context of this work an effort was made to keep the change in the total flow rate less than $15ml/min$, which translates to a mass change of less than $2\mu g$ (assuming a linear relation). This mass change is negligible compared to the error in the mass readings.

5.4 Response

The microbalance system exhibits a response time, much like any other flow apparatus. This response time can be broken down into a couple of variables; the "dead time" in the system and the time it takes to deliver the adsorbate to the balance. In the context of this work the "dead time" refers to

the mixing characteristic, i.e. whether the balance adsorber is PFR or CSTR in nature, as well as the mass flow in the system.

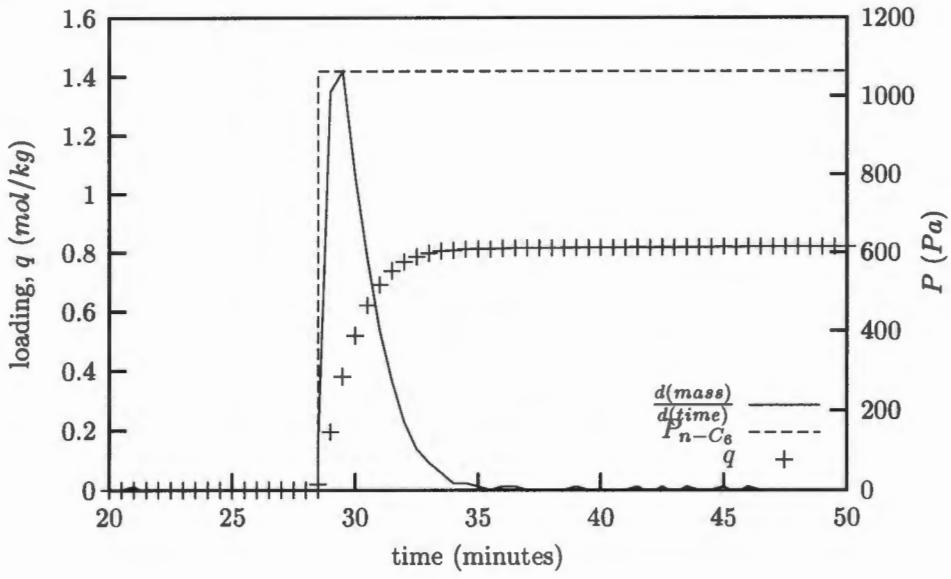

Figure 5.4: Response time of the microbalance to the adsorption of n-hexane on zeolite Y.

Unlike a vacuum system where the adsorbate is propagated through the system rapidly, the feeding of the adsorbate to the adsorber is comparatively slow. A simple calculation showed that it would take about 27 seconds to feed the required amount of adsorbate into the reactor, assuming that all the adsorbate is adsorbed, which obviously was not the case, therefore the response time was significantly longer. The first order derivative, figure 5.4, clearly shows the response of the microbalance system to a step change in the partial pressure. A response time of approximately 7.5 minutes was found.

If the dead volume associated with the saturator is negated, as was done is this case, then the adsorber's volume will dominate. If it is assumed that the mixing characteristics in the adsorber are approximately equivalent to those of a CSTR and if it is assumed that the system will reach equilibrium within three times the residence time, then the the dead time of system is in the order of 79 seconds under "normal" experimental conditions (flow rate $\approx 210ml/min$).

It is clear that the "dead times" discussed above do not account for the measured response time. The assumption in the measurement was that there should be no visible sorption effect of the n-hexane on the zeolite Y. This is quite reasonable as zeolite Y is a large pore zeolite. Regardless of the lack of agreement, the response time does indicate that the system should be given a minimum of 7.5 minutes before any adsorption effect could be measured.

5.5 Error analysis

There were two independent errors present in the experimental data; the error in the loading and the error in the partial pressure. A full description of the error analysis performed on the microbalance data is presented in appendix B. Below is an abridged version, including an indication of the error. The errors in the experimental data were represented by means of error bars.

5.5.1 Loading error

The error in determining the molar loading was caused by a variety of sources, where the calibration error of the microbalance, the resolution of the microbalance and the noise present in the readings were considered to be the most significant. Equation 5.2 describes the variance in the molar loading on the adsorbent. It was assumed that the error in the molar mass was insignificant and it has therefore not been included.

$$\sigma_q^2 = M\left(\frac{\sigma_{\hat{m}}^2}{\hat{m}_{baseline}^2} + \frac{\hat{m}^2}{\hat{m}_{baseline}^4}\sigma_{\hat{m}_{baseline}}^2\right) \tag{5.2}$$

It was observed from the experimental data that the mass loading was between 7-8$mol \cdot kg^{-1}$. This error was approximately constant within an experimental run, due to the loading error being dominated by the microbalance calibration error. This represents an average error in the loading of approximately 2%. However, due to the constant nature of the error, this means the error is considerably larger, approximately 5%, in the low loading region.

5.5.2 Partial pressure error

Due to the lack of direct measurement of the partial pressure, it was considered the most significant source of error. Firstly it was necessary to check the performance of the saturator.

5.5.2.1 Saturator

The partial pressure in the microbalance reactor was determined by calculation rather than a direct measurement, as would be done in a vacuum system. A basic assumption of the microbalance system was that the carrier gas leaving the saturator is completely saturated.

The performance of the saturator was checked for degree of saturation of n-hexane at lower temperatures (≈ -1.5°C) and low flow rates (0 – 18 ml/min), using the method presented in chapter 4.

Figure 5.5 shows the correlation between the measured and the calculated partial pressures. Except for the single point at about $410Pa$, the calculated partial pressures were close to the measured values. Based on the limited data, the saturator could be expected to deliver a gas stream that was within 2% of total saturation.

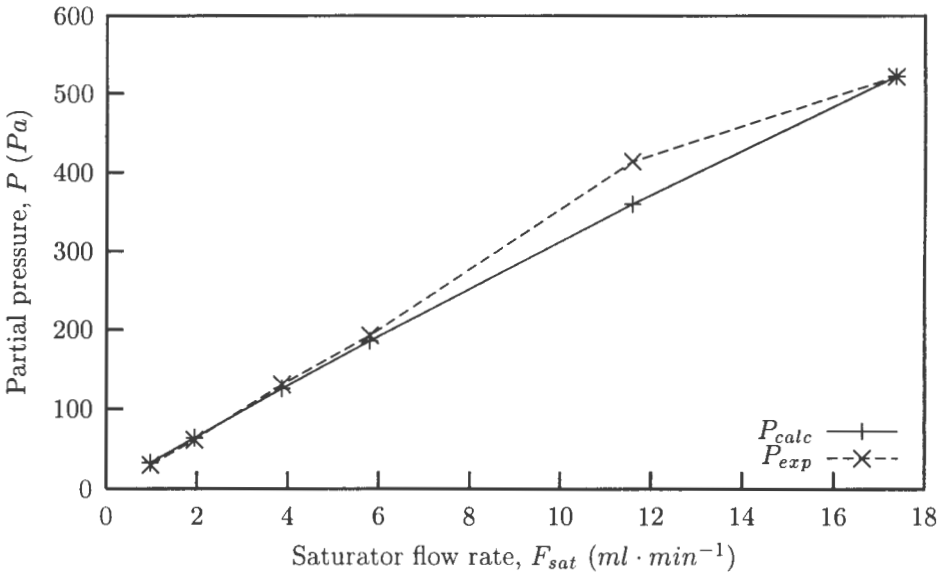

Figure 5.5: Correlation between the measured partial pressure and the calculated partial pressure of n-hexane at low temperature (−1.5°C) and low rate.

5.5.2.2 Partial pressure error

The error in the partial pressure was a function of the mass flow controllers used to control the partial pressure and the saturator partial pressure. The saturator partial pressure was assumed to be equal to the vapour pressure of the gas in the saturator. The vapour pressure was determined using the temperature dependent regression data published by Dauber and Danner (1992), via equation 5.3. Dauber and Danner (1992) estimated the error to be less than 3%. However this excluded the variance in the temperature and it is clear that, due to the exponential nature of equation 5.3, that even a small variation in temperature can have a significant effect on the partial pressure.

$$P^* = \exp\left[A + \frac{B}{T} + C\ln T + DT^E\right] \tag{5.3}$$

The error in the saturator partial pressure was calculated from equation 5.4. The error in the measured temperature was observed to be about 1.2°C, indicating that the temperature measurement was the greatest source of error.

$$\sigma^2_{P^*} = \left(\exp\left[A + \frac{B}{T} + C\ln T + DT^E\right]\left(-\frac{B}{T^2} + C\frac{1}{T} + DET^{E-1}\right)\right)^2 \sigma^2_T \tag{5.4}$$

The partial pressure error is described by equation 5.5. This error varied by an appreciable amount, from about 6.5% to 35%. The most significant level of error was observed in the low partial pressure region. These errors are extremely large in comparison with the error shown when the saturator performance was checked. However, it should be remembered that the error presented here is a theoretical error and is essentially the worst case scenario.

$$\begin{aligned}\sigma_P^2 = &\left(\frac{F_{MFC3}}{F_{MFC1}+F_{MFC3}}\right)^2 \sigma_{P_{sat}}^2 \\ &+ \left(P_{sat}\frac{F_{MFC3}}{(F_{MFC1}+F_{MFC3})^2}\right)^2 \sigma_{F_{MFC1}}^2 \\ &+ \left(P_{sat}\frac{F_{MFC1}}{(F_{MFC1}+F_{MFC3})^2}\right)^2 \sigma_{F_{MFC3}}^2\end{aligned} \tag{5.5}$$

Chapter 6

Results and discussion

The experimental work performed is presented in this chapter along with the analysis and discussion of these experimental results. More detailed information regarding the experimental results can be found in the appendices.

The experimental work was performed using the techniques and methods described in chapter 4. This work entailed the measurement of adsorption isotherms for three "ideal" C_6 paraffins; n-hexane, 3 methyl pentane, and 2,3 dimethyl butane. The adsorption of these compounds has been well documented for the adsorption on silicalite-1. The adsorbates were chosen as they provide a gradual increase in the degree of branching, while retaining the same carbon number. All the adsorptions were performed on a silicalite-1 and four post synthesis modified samples of the silicalite-1. The post synthesis modifications included pelletisation, de-alumination, and two silanised samples.

6.1 Silcalite-1 adsorption (MFI)

6.1.1 Henry constant

Figure 6.1 presents six isotherms showing the adsorption of n-hexane on the parent silicalite powder (MFI). The virial isotherm model (eq. 2.11) was fitted to the data in order to determine the Henry constant, as described in chapter 4.

The repeatability for the hexane adsorption was shown to be excellent (fig. 6.1) and the virial isotherm model fit appears to be excellent for all the isotherms presented in figure 6.1. It is clear that the Henry constant extrapolated from the "high" temperature isotherms ($373K$ and $393K$) were accurate as the isotherm measurements were made at a low enough loading to observe the linear behaviour at low partial pressures. Unfortunately, this was not the case for the lower temperature isotherms

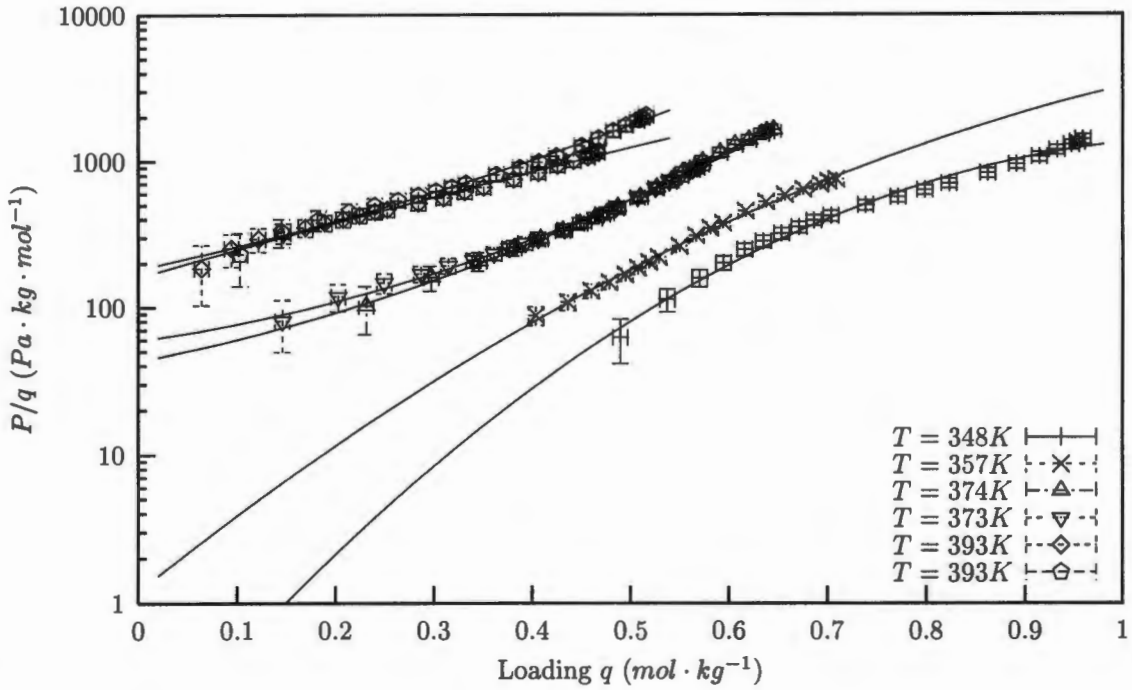

Figure 6.1: n-Hexane adsorption isotherm on MFI showing the Virial adsorption isotherm model fit. The lines represent the virial isotherm model.

($348K$ and $357K$). Here the isotherms were measured at significantly higher loadings which, as shown in figure 6.1, are well outside the linear Henry region. Although the virial isotherm can be used to predict the Henry constant for data outside the linear region, as the data gets further from the linear region, the accuracy of the Henry constant prediction deteriorates (Ruthven and Kaul, 1996). For these isotherms it appears that the extrapolated Henry constant is significantly larger than would be expected. It would appear reasonable to expect these low temperature isotherms to "level off" in a similar fashion to the observation for the higher temperature isotherms. The primary reason for the lack of sufficient low temperature adsorption data is that the adsorption is considerably stronger at low temperatures and therefore, in order to measure the isotherm at a loading comparable to the higher temperature isotherm, it would be necessary for the measurements to be performed at a significantly reduced partial pressure (as low as $2Pa$). This is difficult experimentally.

The Henry constants that were determined for the higher temperature isotherms compare well with the values published in literature, as shown in table 6.1. As expected the "low" temperature isotherms do not compare well with published data.

The pelletisation process was shown to have no discernible effect on the adsorption isotherms (fig. 6.2). The n-hexane isotherm at $374K$ on MFI and MFI-P compared well, particularly if the experimental error was considered. This observation is re-enforced by the similarity of the Henry constants determined for the two isotherms, an important factor, as this work aims to compare the adsorption properties of the parent (MFI) adsorbent with the pelleted post synthesis modified adsorbents.

Table 6.1: Adsorption Henry constants for the adsorption of n-hexane on MFI.

Temperature K	Henry constant (k') $mol \cdot kg^{-1} \cdot Pa^{-1}$			
	This work	Denayer et al. (1998)	Eder and Lercher (1997)	Sun et al. (1996)
348	11.8	1.10×10^{-1}	7.45×10^{-2}	3.51×10^{-3}
357	8.38×10^{-1}	6.03×10^{-2}	3.98×10^{-2}	1.90×10^{-3}
374	1.69×10^{-2}	2.10×10^{-2}	1.32×10^{-2}	6.45×10^{-4}
393	5.50×10^{-3}	7.21×10^{-3}	4.31×10^{-3}	2.16×10^{-4}

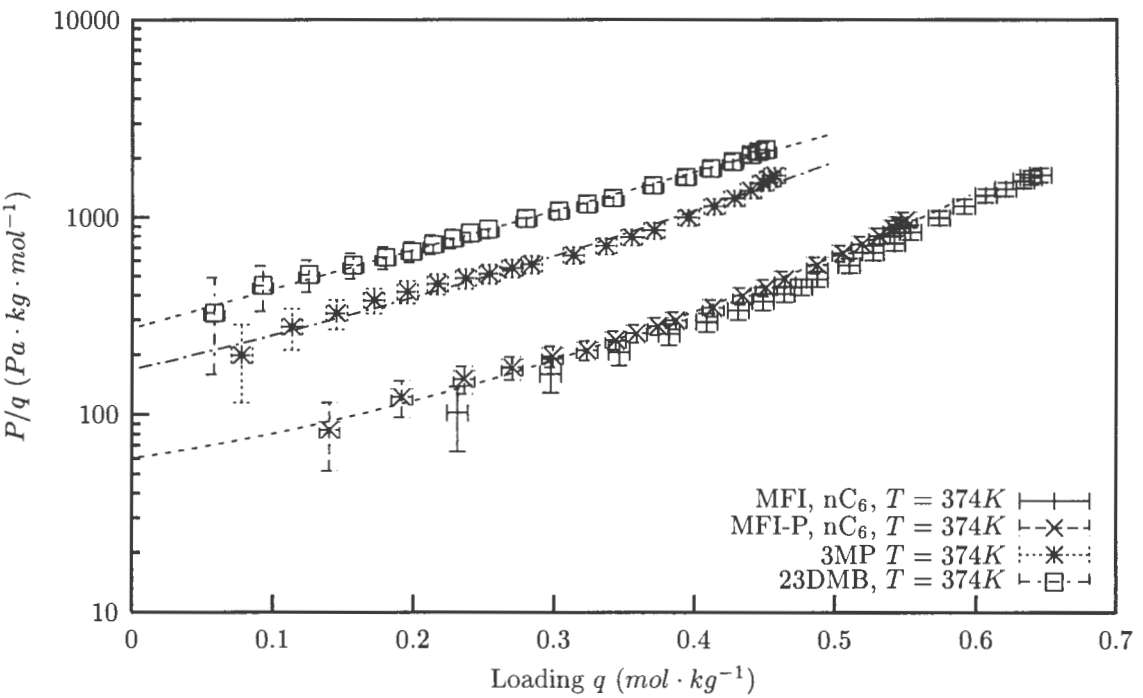

Figure 6.2: The effect of the degree of branching on the Henry constant for the adsorption on the pelleted adsorbate (MFI-P).

As shown with the n-hexane adsorption on MFI the Henry constants found for the adsorption of the branched C_6's (3MP and 23DMB) compared well with values published by Cavalcante and Ruthven (1995) for the 3 methyl pentane, and Denayer et al. (1998) for the 2,3 dimethyl butane (shown in table 6.2). It has also been shown in table 6.2 that the published literature values for the Henry constants vary appreciably, as do all adsorption properties (Myers and Siperstein, 2001). As anticipated the degree of branching was shown to play an important role in the strength of the initial adsorption and the Henry constants exhibit the following trend: $nC_6 > 3MP > 23DMB$.

6.1.2 Heat of adsorption

The limiting heat of adsorption was determined using the Henry constants determined previously. The method used was described in detail in chapter 4. Figure 6.3 shows the van't Hoff plot generated

Table 6.2: Henry constant at $374K$, extrapolated from the virial isotherms for the branched adsorbates on the pelleted adsorbate (MFI-P).

Adsorbate	**Henry constant (k')** $mol \cdot kg^{-1} \cdot Pa^{-1}$		
	This work	Cavalcante and Ruthven (1995)	Denayer et al. (1998)
n-hexane	1.66×10^{-2}		
3 methyl pentane	5.94×10^{-3}	1.72×10^{-2}	8.26×10^{-3}
2,3 dimethyl butane	3.68×10^{-3}		3.69×10^{-3}

for the Henry constants calculated for the adsorption of n-hexane.

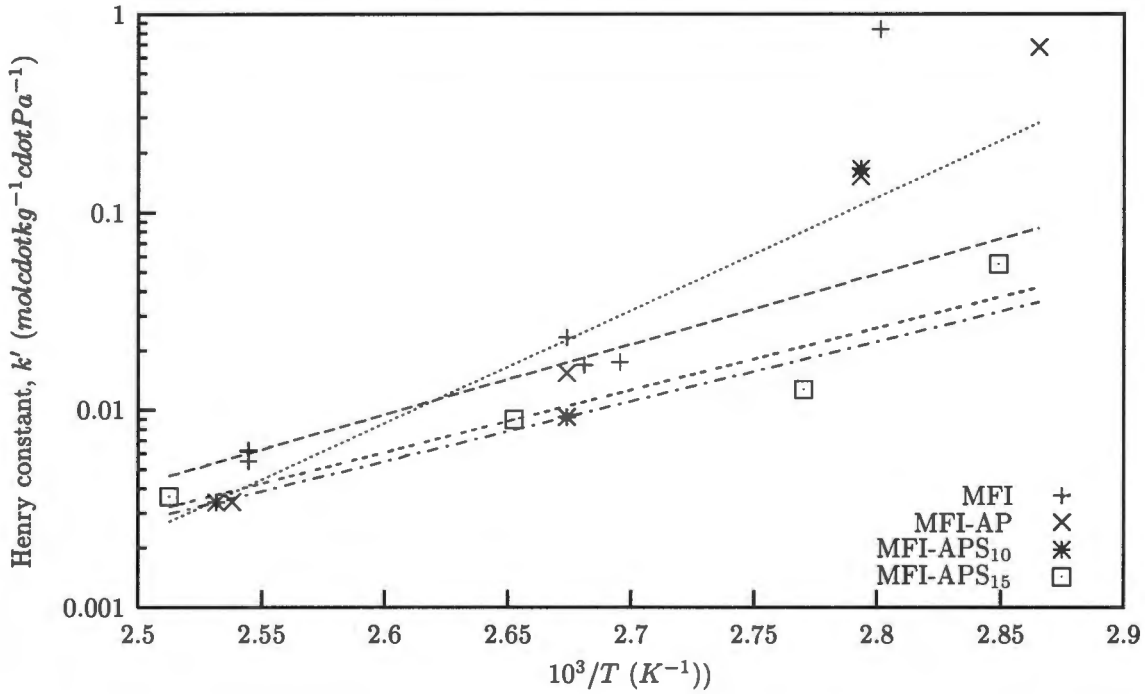

Figure 6.3: Van't Hoff plots for the adsorption of hexane showing the temperature dependency of the Henry constants

Due to the concern over the accuracy of the Henry constants for the low temperature isotherms the van't Hoff equation (eq. 2.20) was only fitted to the $373K$ and $393K$ isotherms, although this was not desirable. The heat of adsorption determined ($\Delta H = -68.2kJ \cdot mol^{-1}$) agrees well with those published previously, see table 2.4.

6.1.3 Isosteric heat of adsorption

The isosteric heat of adsorption was determined from the experimental data by first producing a number of isosteres, figure 6.4. These were used to determine the variation in the heat of adsorption with loading (fig. 6.5) which is an important indication of the energy heterogeneity of the adsorbent.

Table 6.3: Van't Hoff equation (eq. 2.20) parameters for the adsorption of n-Hexane on various adsorbents.

Adsorbent	$-\Delta H$	k_0'
	$kJ \cdot mol^{-1}$	$mol \cdot kg^{-1} \cdot Pa^{-1}$
MFI	68.18	5.22×10^{-12}
MFI-AP	109.40	1.19×10^{-17}
MFI-APS_{10}	58.19	6.86×10^{-11}
MFI-APS_{15}	60.43	3.78×10^{-11}

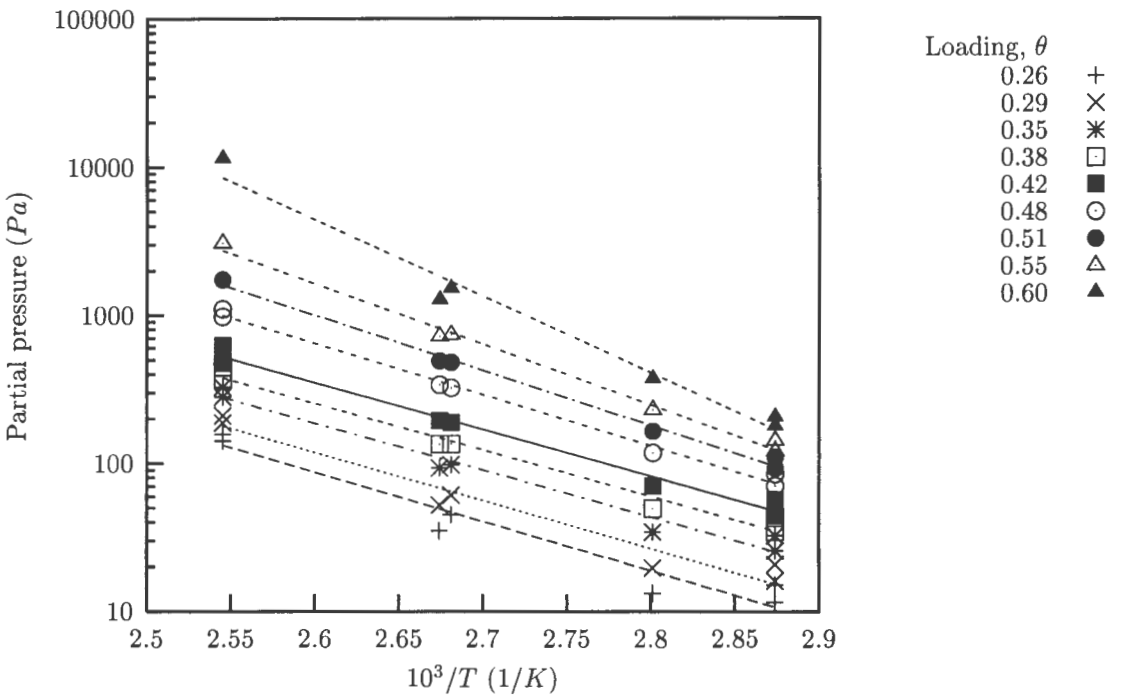

Figure 6.4: Adsorption isosteres for the adsorption of hexane on MFI.

Yang and Rees (1997) showed that the isosteric heat of adsorption tends to increase with coverage. In contrast to their results, this work shows that the isosteric heat of adsorption initially decreased slowly (by $\approx 8.1 kJ \cdot mol^{-1}$), followed by a rapid increase. The minimum appeared to be at a loading of approximately 0.37. The implication of this large variation in the isosteric heat of adsorption was that the silicalite-1 adsorbent (MFI) was not energetically homogeneous.

6.1.4 Entropy of adsorption ($-\Delta S$)

The entropy of adsorption (eq. 2.31) naturally followed the trend shown in the isosteric heat of adsorption (fig. 6.5). It was shown in figure 6.6 that the entropy of adsorption was initially constant until a coverage of approximately 0.37, after which the entropy of adsorption showed a rapid increase indicating that the adsorbed phase was becoming considerably less mobile. It has been shown in literature (Eder and Lercher, 1997; Vlugt et al., 1998) that the adsorption of n-hexane undergoes a

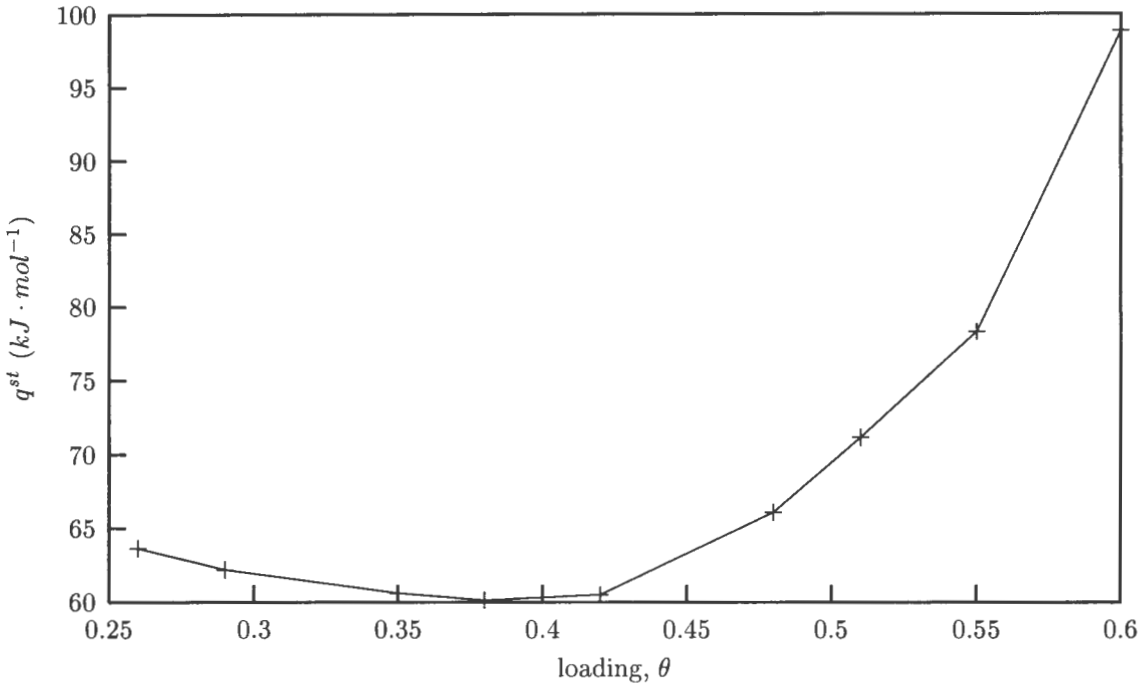

Figure 6.5: Change in the isosteric heat of adsorption with coverage for the adsorption of hexane on MFI.

re-arrangement when the loading reaches approximately 4 molecules/u.c. (when $q \approx 0.699$). This has been shown to coincide with an increase in the entropy of adsorption. The n-hexane isotherms presented in this work do not exhibit the inflection point at the 4 molecules/u.c. loading which precludes the use of this argument to explain the increase in the entropy. It also possibly indicates that the adsorption did not proceed in the fashion described by Roque-Malherbe (2000), where the micropores are initially filled followed by the surface coverage.

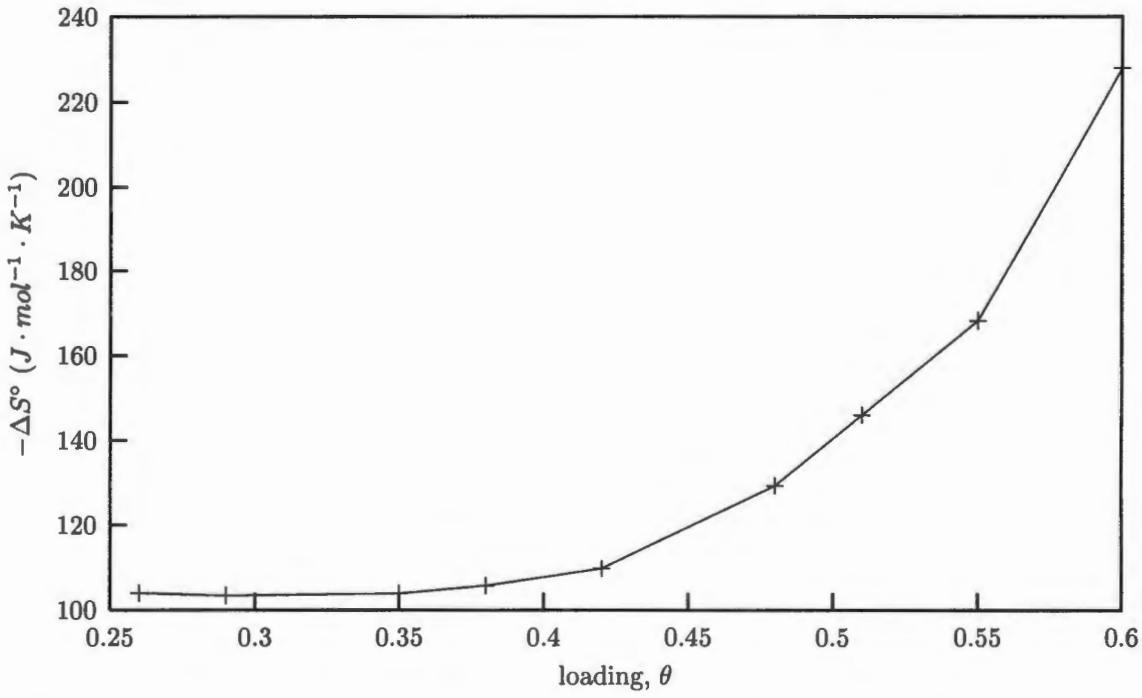

Figure 6.6: Change in the differential molar entropy of adsorption at standard pressure with coverage for hexane adsorption on MFI.

6.2 Effect of de-alumination on the adsorption

The silicalite-1 adsorbent was de-aluminated using the acid leaching process described in chapter 4 in an attempt to remove the remaining unwanted acid sites from the silicalite-1 adsorbent. The effects on the adsorption of this de-alumination process was examined here using the same techniques presented above for the investigation of the silicalite-1 (MFI).

A concern of the acid leaching de-alumination process was that the zeolite crystallinity would be altered. Figure 6.7 presents the x-ray powder diffraction of the parent silicalite and the acid leached silicalite. These XRD's showed that there was no appreciable lose of crystallinity.

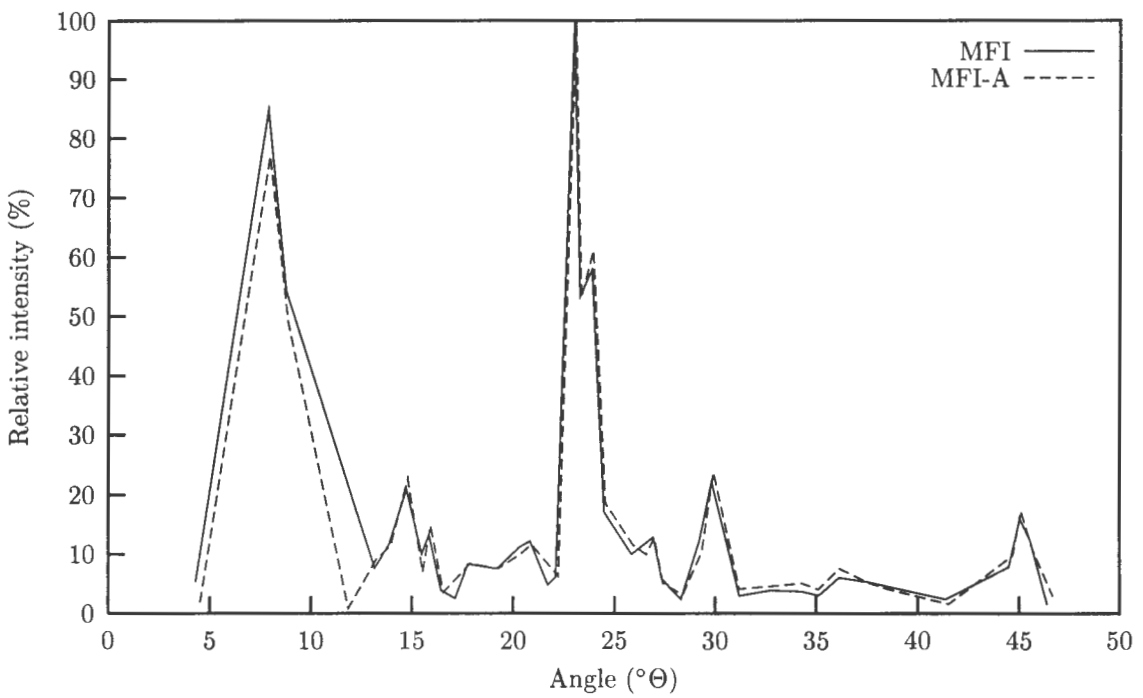

Figure 6.7: Comparison of the x-ray powder diffraction of the parent adsorbent (MFI), and the acid leached adsorbent (MFI-A).

6.2.1 Henry constant

As the crystallinity remained largely unchanged, the adsorption was expected to be unaffected by the acid leaching process. Similarly to the parent adsorbent the Henry constants (fig. 6.8) for the "low" temperature isotherms ($349K$ and $358K$) are larger than would be the case if the isotherm had been measured at a lower partial pressure. Once again the two "high" temperature isotherms appear to have been measured at a sufficiently low loading to accurately predict their Henry constants. The Henry constants determined, table 6.4, for the acid leach adsorbent were sufficiently close to the parent adsorbent to be considered the same, particularly for the $374K$ isotherm.

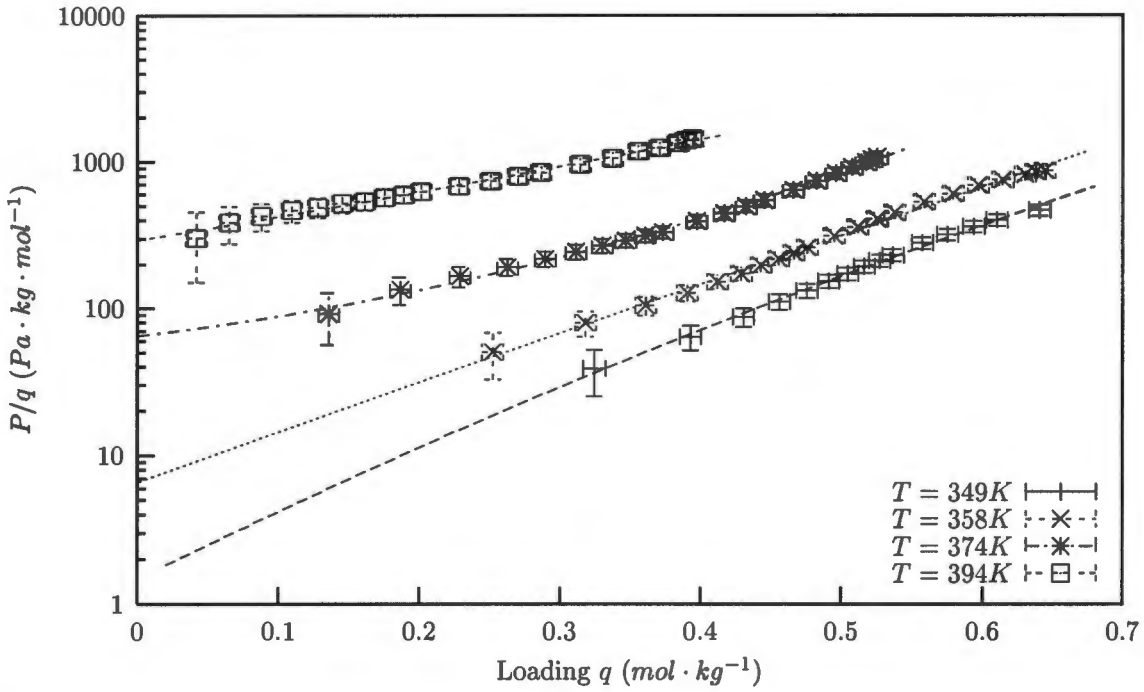

Figure 6.8: Virial isotherm model fit for the adsorption of hexane on acid leached adsorbent (MFI-AP).

Table 6.4: Henry constants for the adsorption of n-hexane on MFI-AP.

Temperature K	Henry constant (k′) $mol \cdot kg^{-1} \cdot Pa^{-1}$		
	n-C_6	3MP	23DMB
349	6.78×10^{-1}		
358	1.52×10^{-1}		
374	1.54×10^{-2}	4.46×10^{-3}	2.10×10^{-3}
394	3.419×10^{-3}		

The Henry constants for the branched C_6 compounds (fig. 6.9) adsorbing on the MFI-AP was shown to follow the same trend as seen with these adsorbates on the MFI adsorbent; $nC_6 > 3MP > 23DMB$. The Henry constant determined for these compounds, table 6.4, were similar to those found on the MFI adsorbent (table 6.2). Therefore, based on the Henry constants data, it was seen that the silicalite-1 was not significantly altered by the de-alumination.

6.2.2 Heat of adsorption

Due to the nature of the van't Hoff equation (eq. 2.20), even small variations in the Henry constants can yield large differences in the heat of adsorption. The heat of adsorption determined for the MFI-AP adsorbent, figure 6.3, was found to be considerable higher ($109.40 kJ \cdot mol^{-1}$) than that determined for the MFI adsorbent ($68.18 kJ \cdot mol^{-1}$). An examination of the virial isotherm model

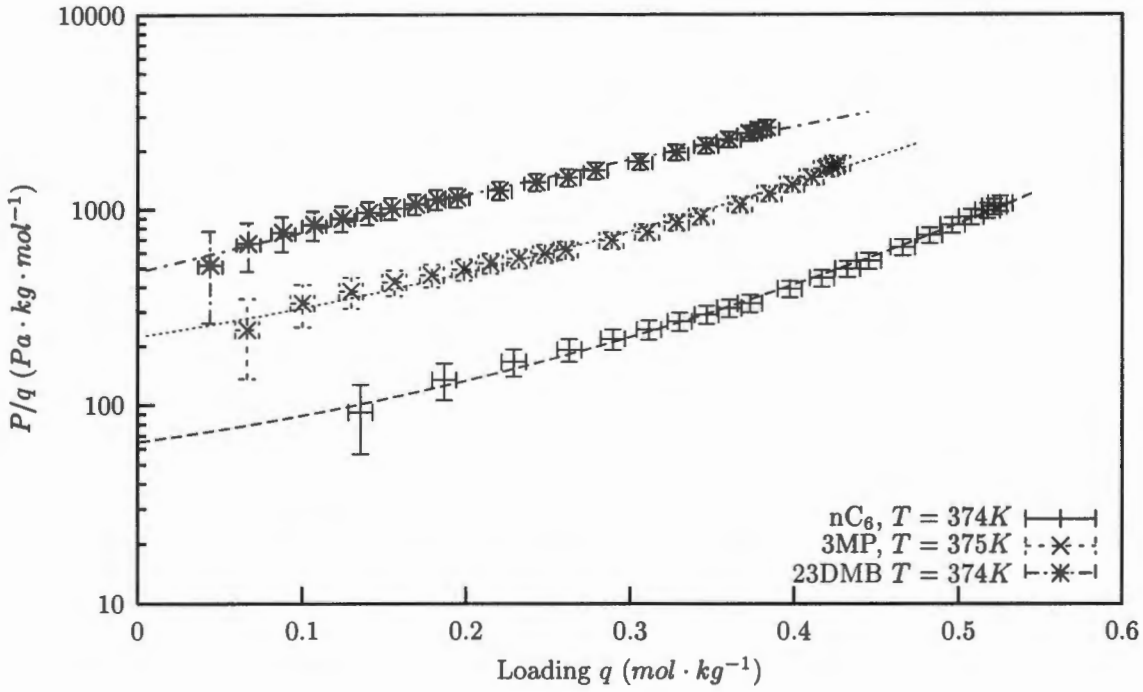

Figure 6.9: The effect of the degree of branching on the Henry constant for adsorption on MFI-AP.

fits (fig. 6.8) indicate that, as with the MFI adsorbent, the "low" temperature ($349K$ and $358K$) isotherms over-predicts the Henry constant. However, even if the fit for the van't Hoff equation is reduced to the two "high" temperature isotherms, the heat of adsorption was still in the region of $92kJ \cdot mol^{-1}$. This was considerably higher than the expected value for the adsorption of hexane on silicalite-1, although it was still within the normally accepted limits. The heat of adsorption is normally 2-3 times the normal heat of vapourisation ($\Delta H_{vap} = 28.8kJ \cdot mol^{-1}$).

6.2.3 Isosteric heat of adsorption

A plot showing the change in the isosteric heat of adsorption, for the adsorption of n-hexane on the MFI-AP with increasing coverage, (fig. 6.11) was generated from the adsorption isosteres (fig. 6.10). It was reasonable to expect that the isosteric heat of adsorption would show that the de-aluminated adsorbent was more energetically homogeneous (Ruthven, 1984). However, as shown in figure 6.11, the isosteric heat of adsorption initially decreased with coverage and was then followed by a rapid increase, with a minimum at approximately 0.37 coverage. The general trend was the same as that shown for the adsorption of n-hexane on the MFI adsorbent, however, the initial decrease was shown to be considerably more severe for the MFI-AP adsorbent. This would indicate that the heterogeneous nature of the parent adsorbent (fig. 6.5) was in fact exacerbated by the acid leaching process. This is contrary to the results shown by Ruthven (1984) where the de-alumination of zeolites resulted in a reduction of the change in the isosteric heat of adsorption with a corresponding change in the coverage.

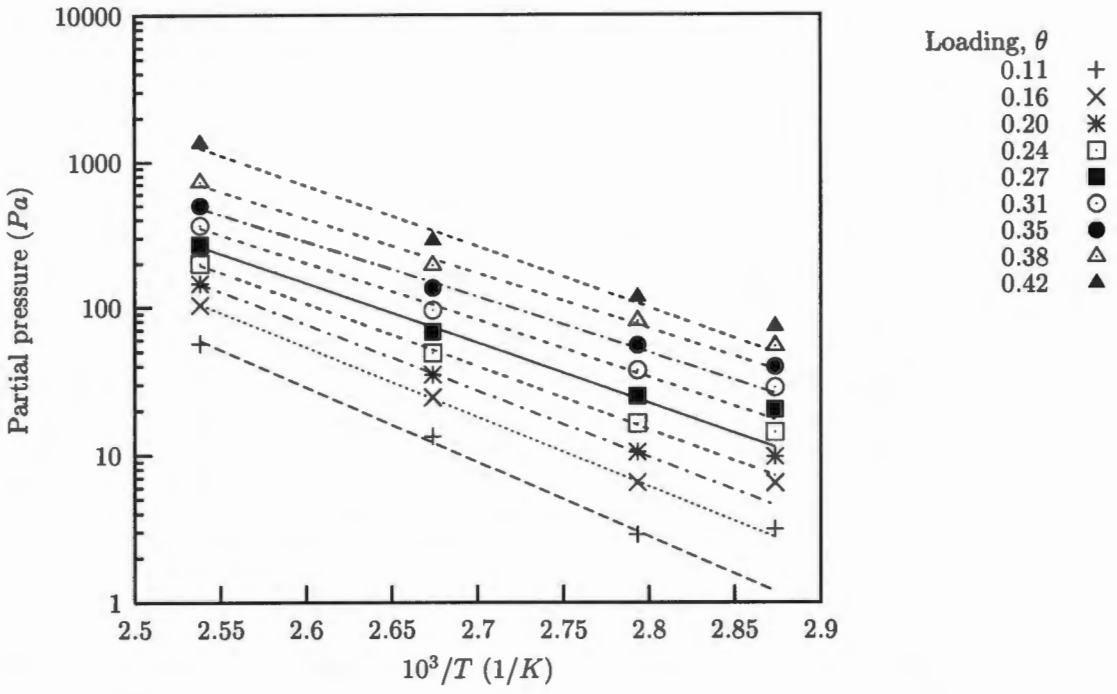

Figure 6.10: Adsorption isosteres for the adsorption of hexane on MFI-AP.

The position of the minimum for the isosteric heat of adsorption for the MFI adsorbent and the MFI-AP adsorbent was shown to be at approximately the same coverage.

6.2.4 Entropy of adsorption ($-\Delta S$)

As with the MFI adsorbent, the same trend was observed in the isosteric heat of adsorption that was observed in the adsorption entropy (fig. 6.12), with an initial decrease in the entropy until the coverage reached $\theta \approx 0.35$, at which point there was a rapid increase. This indicates that the adsorbed phase becomes more mobile in the initial phase of the adsorption, followed by a sudden decrease in the mobility of the adsorbed phase. As the minimum points for the MFI adsorbent and the MFI-AP adsorbent were at approximately the same coverage, it could indicate that the means by which the adsorption proceeds has not been significantly altered and that only the heterogeneity of the initially accessible surface has changed with the de-alumination.

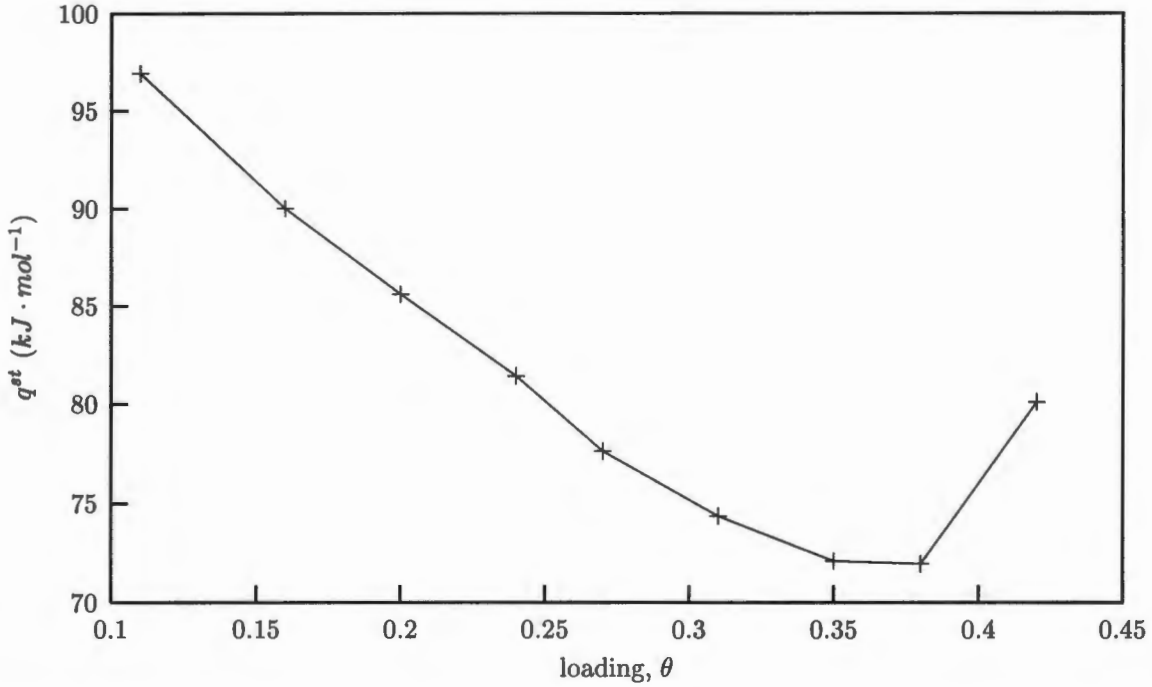

Figure 6.11: Change in the isosteric heat of adsorption with coverage for the adsorption of hexane on MFI-AP.

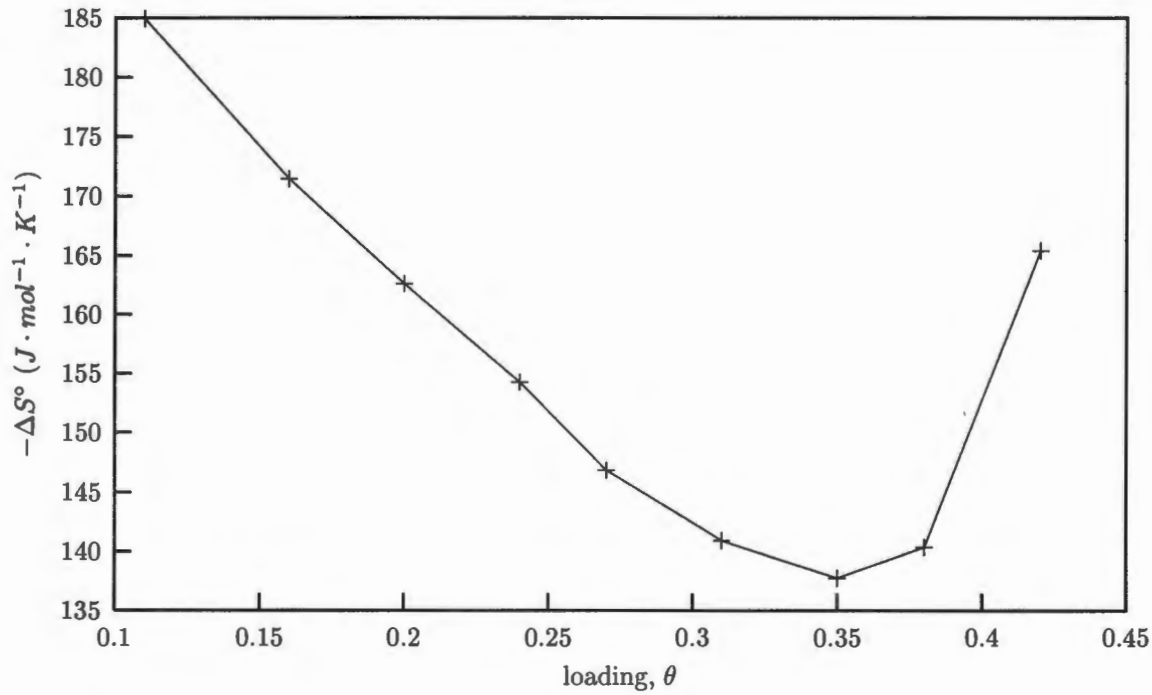

Figure 6.12: Change in the differential molar entropy of adsorption at standard pressure with coverage for hexane adsorption on MFI-AP.

6.3 Effect of silanisation on the adsorption

Two silanised adsorbents were produced from the de-aluminated adsorbent using the technique described in chapter 4. The first sample was subject to 10 silanisation cycles (MFI-APS_{10}), whereas the second sample underwent 15 silanisation cycles (MFI-APS_{15}). The purpose of the silanisation was twofold; firstly to inertise the external surface of the adsorbent to remove any residual acid sites present on the external surface (Röger, 1998) and secondly, and more importantly, the silanisation process has been shown by Niwa et al. (1984b) as an appropriate method to control the pore openings of the zeolite, either via a pore blocking mechanism or a pore narrowing mechanism. The adsorption of the paraffins on these silanised samples were examined and compared to the adsorption of both the parent silicalite-1 and the acid leached silicalite-1.

6.3.1 Henry constant

Figure 6.13 presents the virial isotherm model fits for the adsorption of n-hexane on the 10 and 15 cycle silanised adsorbents. The Henry constants (table 6.5) for the silanised adsorbents show a slight but consistent decrease when compared with each other and they also show a decrease in comparison to the MFI adsorbent. It should be noted that the decreases are small and within the limits of the experimental error. The trend exhibited was MFI > MFI-APS_{10} > MFI-APS_{15}. The exception was the Henry constant found for the n-hexane isotherm at $351K$ which was significantly lower than the corresponding Henry constants on the MFI and MFI-AP adsorbents, however this value was suspect due to the lack of sufficient low coverage adsorption data.

An interesting observation was that the shape of the adsorption isotherms for the silanised adsorbent are different from that of the parent adsorbent (MFI).

The silanisation process only affects the external surface of the adsorbent (Weber, 1998). Adsorption in microporous materials theoretically proceeds via the micropore being initially filled (Roque-Malherbe, 2000) and so the Henry constant should not be significantly altered by the silanisation process, particularly as the technique used to measure the Henry constant was an equilibrium method. In other words, so long as the adsorbate has access to the internal surface of the adsorbent, then the effects of silanisation should not be significant.

As with the adsorption of hexane on the silanised adsorbents, the adsorption of the 3 methyl pentane and the 2,3 dimethyl butane exhibited a small decrease in the Henry constants in comparison to the parent adsorbent. The change shown in the Henry constants were sufficiently small to be within the limits of experimental error.

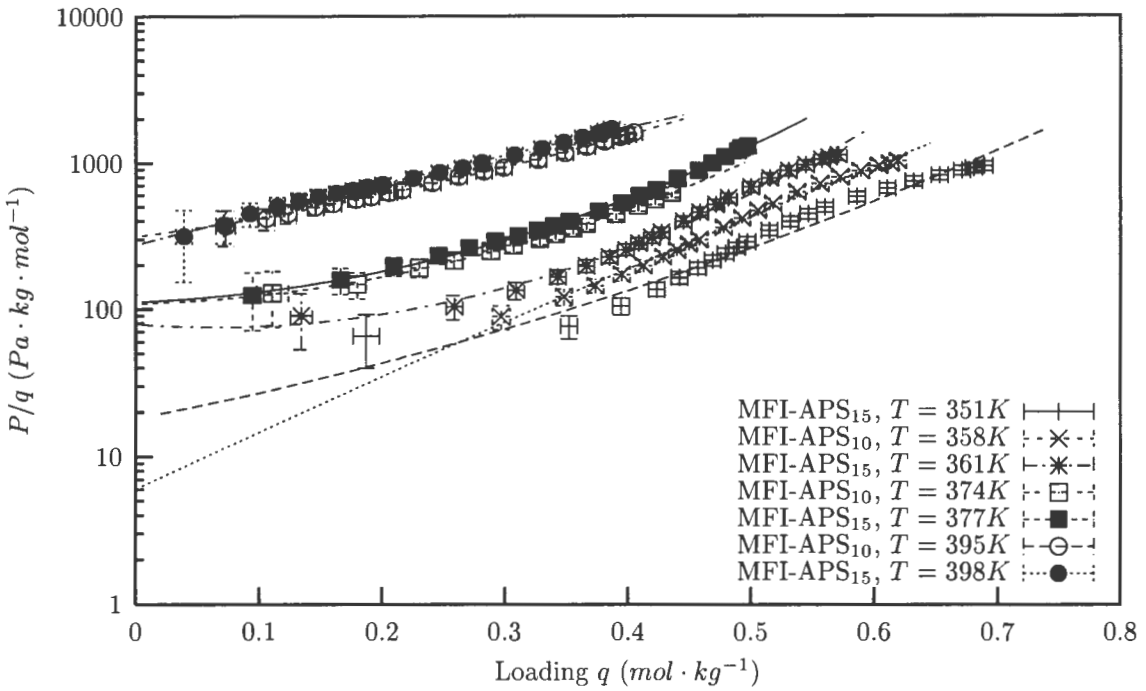

Figure 6.13: The effect of silanisation on the Henry constant

6.3.2 Heat of adsorption

Figure 6.3 shows an interesting phenomenon where the van't Hoff fits for the MFI, MFI-APS$_{10}$, and MFI-APS$_{15}$ were approximately parallel indicating that the silanisation process has consistently reduced the adsorption strength at zero loading of the n-hexane on the various adsorbents. If the van't Hoff plots were truly parallel then the heats of adsorption would be identical which was not the case. The heat of adsorption for the MFI-APS$_{10}$ ($\Delta H = 58.2kJ \cdot mol^{-1}$) was lower than the heat of adsorption for the adsorption of n-hexane on the parent silicalite (see table 6.3). This would indicate that the initial adsorption strength has been slightly decreased.

The heat of adsorption for the 15 cycle silanised sample showed a small increase ($\Delta H = 60.4kJ \cdot mol^{-1}$) when compared to the heat of adsorption for the 10 cycle sample. However, the difference between the ΔH's is sufficiently small that it is reasonable to assume that the heats of adsorption for the two silanised samples is the same and therefore the degree of silanisation does not have any significant effect on the adsorption.

6.3.3 Isosteric heat of adsorption

The isosteric heats of adsorption for the silanised adsorbents (fig. 6.17) show the same trend as the MFI-AP adsorbent with the isosteric heat of adsorption initially decreasing, until it reached a minimum at about $\theta \approx 0.57$, after which the q^{st} underwent a rapid increase with the increase in

Table 6.5: Henry constants for the adsorption of n-hexane on the silanised de-aluminated silicalite-1, the MFI Henry constants are provided for comparison purposes

Temperature K	**Henry constant (k')** $mol \cdot kg^{-1} \cdot Pa^{-1}$		
	MFI[a]	MFI-APS$_{10}$	MFI-APS$_{15}$
351	7.32×10^{-2}		5.50×10^{-2}
358	4.63×10^{-2}	1.66×10^{-1}	
361	3.83×10^{-2}		1.27×10^{-2}
374	1.74×10^{-2}	9.20×10^{-3}	
377	1.46×10^{-2}		8.95×10^{-3}
395	5.42×10^{-3}	3.40×10^{-3}	
398	4.64×10^{-3}		3.64×10^{-3}

[a]Calculated from van't Hoff equation

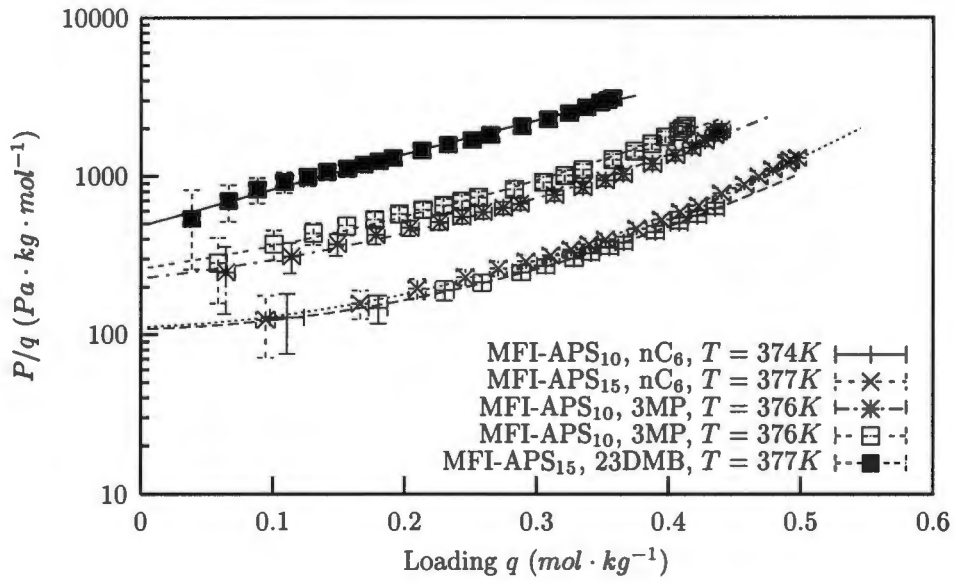

Figure 6.14: The effect of the degree of branching on the adsorption on silanised adsorbents.

loading. If it is assumed that the external surface of the adsorbent has been coated with a silica layer (Weber, 1998; Niwa et al., 1984b), then the source of the heterogeneity must be in the internal surface.

It was observed that the isosteric heat of adsorption for the MFI-APS$_{15}$ is consistently higher than that of the MFI-APS$_{10}$ adsorbent although the extent of the heterogeneity does not appear to have been significantly altered. The rate of change of the q^{st} with coverage is approximately the same for both the 10 cycle and the 15 cycle silanised samples. This re-enforces the argument that the heterogeneity must be on the internal surface of the adsorbent.

Table 6.6: The effect of branching on the Henry constants for the adsorption on the silanised adsorbents.

Temperature K	Henry constant (k′) $mol \cdot kg^{-1} \cdot Pa^{-1}$		
	n-C_6	3MP	23DMB
MFI-APS_{10}			
376	8.33×10^{-3} [a]	4.41×10^{-3}	
MFI-APS_{15}			
376	9.40×10^{-3}	3.83×10^{-3}	2.07×10^{-3}

[a]Calculated form the van't Hoff equation

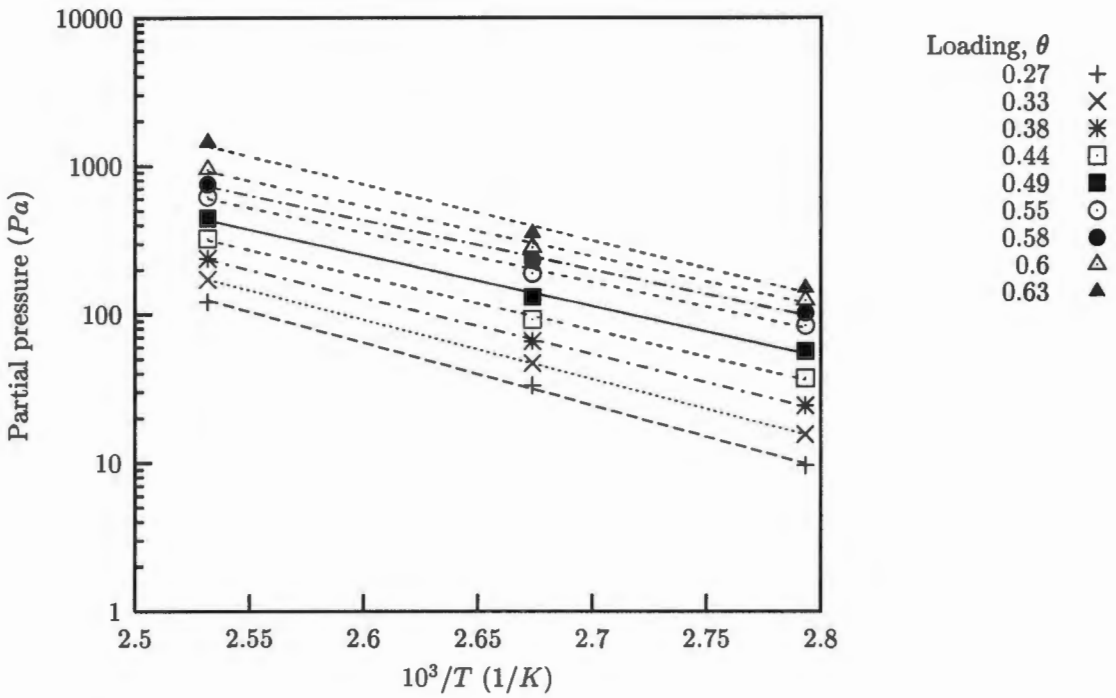

Figure 6.15: Adsorption isosteres for the adsorption of hexane on MFI-APS_{10}.

6.3.4 Entropy of adsorption

The adsorption entropy for the adsorption of n-hexane shows a similar trend to the isosteric heat of adsorption. As with both the parent adsorbent and the de-aluminated adsorbent, the adsorbed phase initially undergoes an increase in mobility, followed by a sudden decrease after the coverage has reach approximately 0.55, indicating that there is a definite change in the adsorption process. As this minimum was observed on all the adsorbents this change in the adsorption must be an artifact of the internal structure of the adsorbent, particularly if it is assumed that the external surface area of the adsorbate was inertised by the silanisation process.

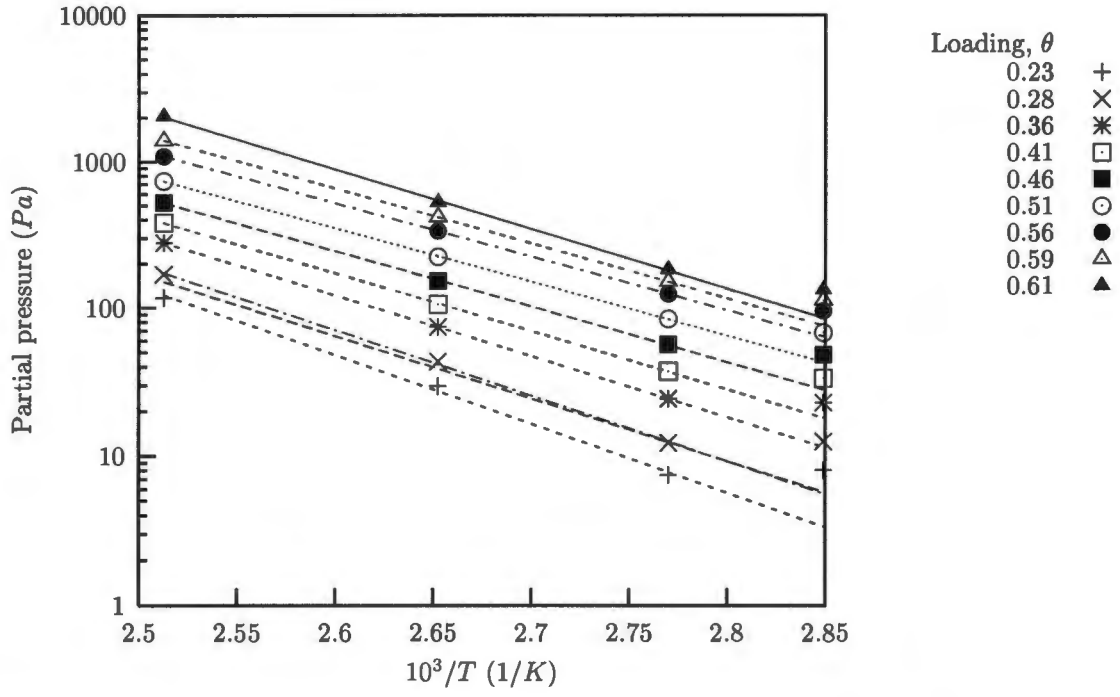

Figure 6.16: Adsorption isosteres for the adsorption of hexane on MFI-APS$_{15}$.

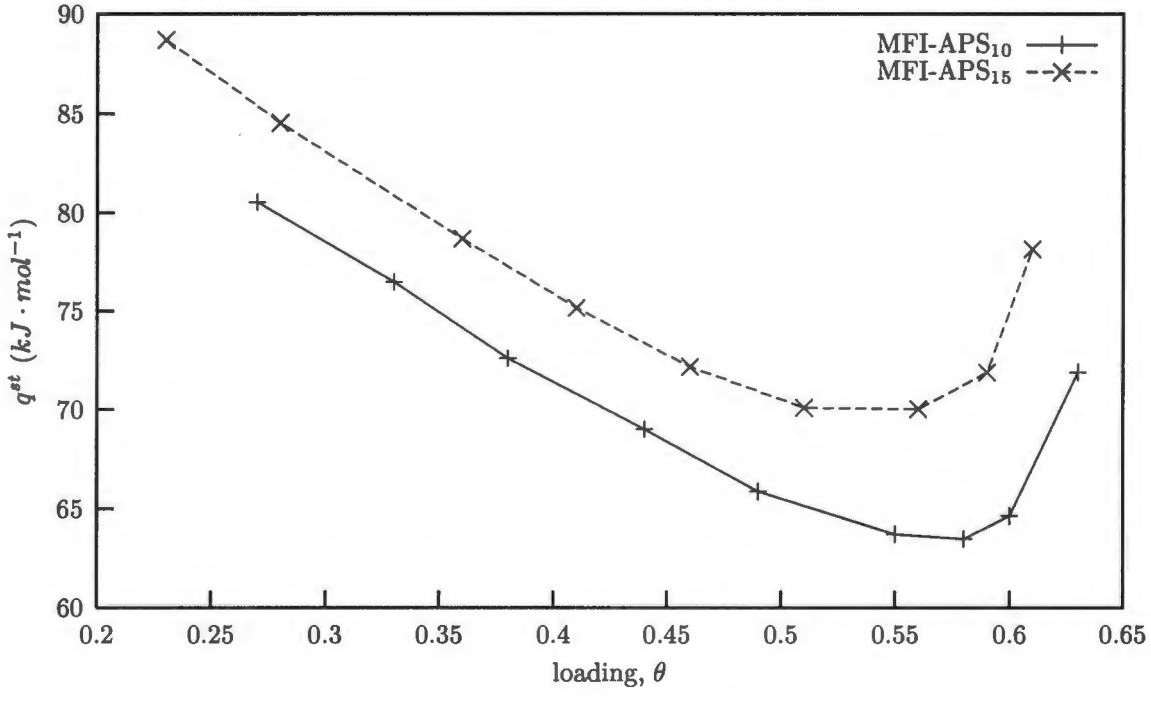

Figure 6.17: Change in the isosteric heat of adsorption with coverage for the adsorption of hexane on silanised adsorbents.

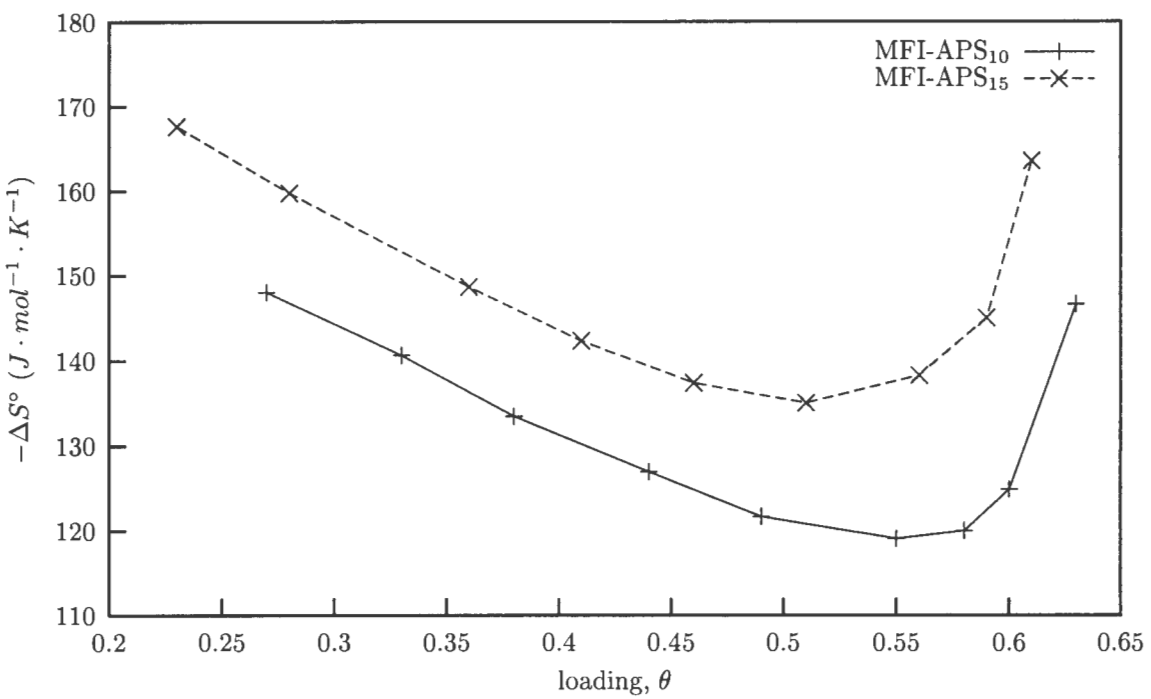

Figure 6.18: Change in the differential molar entropy of adsorption at standard pressure with coverage for hexane adsorption on the silanised adsorbents.

Chapter 7

Conclusions

Based on the findings presented in the previous chapters (chapter 5 and chapter 6) the following conclusions were drawn.

The repeatability of the adsorption isotherms measured using the adsorption microbalance was shown to be extremely good. Successive isotherm measurements were shown to be repeatable, well within the limits of the experimental error. The experimental work was performed within a small mass range ($30mg$-$60mg$). In this range it was found that the microbalance could accurately and repeatably measure the mass to within $30\mu g$. The stability of the microbalance readings were affected by the temperature of the microbalance head and the flow rate. Variation in the microbalance head temperature resulted in significant changes in the balance readings. Although the flow rate to the balance was a potential source of error, it was controlled by ensuring that the total change in the flow rate to the balance was less than 10%, resulting in an insignificant variation in the mass readings. The response of the microbalance to changes in the adsorbate partial pressure was found to be rapid, significantly less than the time allowed for the system to reach equilibrium. An analysis of the error in the experimental adsorption isotherm data revealed that the primary source of error was in the partial pressure calculations, which was shown to be as high as 35% at low partial pressure with an average of 10%, the error associated with the loading measurement was found to be significantly less with an average of only 2%. It should be noted that although the partial pressure error was significant, this was the worst case scenario for the partial pressure. It is therefore indicated that the microbalance could be significantly improved by improving the means of determining the partial pressure. However the microbalance system still produced results that matched well with literature. It should be safe to concluded that the microbalance system was a reliable tool for the measurement of adsorption isotherms.

The adsorption at $373K$ and $393K$ of n-hexane, 3 methyl pentane, and 2,3 dimethyl butane on the parent silicalite adsorbent produced adsorption parameters that were reconcilable with literature

results for the adsorption of these compounds on silicalite-1. The adsorption of these compounds at $348K$ and $357K$ did not produce adsorption parameters that compared as well as the high temperature isotherms. The difficulty experienced with the low temperature isotherms was wholly the result of insufficient low loading experimental data, due to the practical difficulty of performing measurements at the low partial pressures required. However, the high temperature isotherms provided sufficient information for the adsorption energy profiles to be determined. The excellent comparison between the high temperature isotherms and corresponding literature results complements the conclusion that the adsorption microbalance system was a reliable and versatile tool for the measurement of adsorption isotherms.

The pelletisation of the silicalite was shown to have no visible impact on the adsorption of either the linear or branched compounds. This facilitated the comparisons between the powdered parent adsorbent and the pelleted post synthesis modified adsorbents.

It was shown that the isosteric heat of adsorption for the adsorption of n-hexane on the parent adsorbent was not constant with loading. Thus the adsorbent was not energetically homogeneous, contrary to the expectations for silicalite-1. The examination of the entropy of adsorption highlighted the change in the adsorption. Increases in the adsorption entropy have been observed in literature in connection with the re-arrangement of the n-hexane into the sinusoidal channels. The entropy increase presented here occurred at a significantly lower loading than the 4 molecules/u.c. that is often quoted. It appears that the adsorption occurs in two stages, with the initial stage corresponding to a decrease in the isosteric heat and approximately constant entropy. This is followed by an increase in both the isosteric heat of adsorption and the entropy of adsorption indicating that the adsorption process was significantly different at the higher pressures.

The de-alumination of the parent silicalite resulted in an adsorbent that showed similar adsorption traits to those of the parent adsorbent. No satisfactory explanations were found for the significant differences in the heat of adsorption. It was found that the acid leaching process resulted in a adsorbent that was considerable more heterogeneous than the parent, with the initial adsorption stage being the most severely affected. However, the apparent two stage adsorption process that was observed on the parent was retained in the de-aluminated adsorbent.

The silanised de-alumination adsorbents yielded adsorption parameters that compared better with the parent adsorbent than the de-aluminated adsorbent, indicating that the acid leaching process had indeed affected the external surface of the adsorbent. It was shown that the degree of silanisation had an impact on the the Henry adsorption constants, with the Henry constant being reduced with an increase in the degree of silanisation. The heat of adsorption for n-hexane on the silanised adsorbents was lower in comparison with the parent silicalite, although there was no discernible difference between the heats of adsorption for the 10 cycle and 15 cycle silanised adsorbents.

The heterogeneous nature of the adsorbent was still observed on the silanised adsorbents, where the isosteric heat and entropy of adsorption followed the same trend as the de-aluminated adsorbent. This leads to the conclusion that the heterogeneous nature of the adsorbent, that was exacerbated by the acid leaching, was located on the internal surface of the adsorbent. It was also observed that the an increase in the degree of silanisation shifted both the isosteric heat of adsorption and the entropy of adsorption to a higher energy. This indicates that more energy is required for the adsorbate to access the internal surface of the adsorbent and thus the access to the internal structure of the zeolite has been restricted. It is not known whether this restricted access to the internal surface of the zeolite was the result of a pore narrowing or a pore blocking mechanism.

In conclusion the adsorption microbalance was a valuable tool for the measurement of adsorption isotherms. It was also shown that adsorption provides a simple method to provide information about a microporous material that would otherwise be difficult to obtain.

References

Abrams, L. and Corbin, D. R. (1995). Probing intrazeolite space. *Journal of Inclusion Phenomena and Molecular Recognition in Chemistry*, 21:1–46.

Anderson, B. G., de Gauw, F. J. M. M., Noordhoek, N. J., van IJzendoorn, L. J., van Santen, R. A., and de Voigt, M. J. A. (1998). Mass transfer of alkanes in zeolite packed-bed reactors studied with positron emission profiling (pep). 1. experiments. *Ind. Eng. Chem. Res.*, 37:815–824.

Atkins, P. W. (1994). *Physical Chemistry.* Oxford University Press, 5th edition.

Barrer, R. M. and Davies, J. A. (1970). Sorption in decationated zeolites. *Proc. R. Soc. London*, A(320):289.

Bates, S. P., van Well, W. J. M., van Santen, R. A., and Smit, B. (1996). Energetis of n-alkanes in zeolites: A configurational-bias monte carlo investigation into pore size dependence. *J. Am. Chem. Soc.*, 118:6753–6759.

Bellat, J. and Simonot-Grange, M. (1995a). Adsorption of gaseous p-xylene and m-xylene on NaY, KY, and BaY zeolites. part1: Adsorption equilibria of pure xylenes. *Zeolites*, 15:124–130.

Bellat, J. and Simonot-Grange, M. (1995b). Adsorption of gaseous p-xylene and m-xylene on NaY, KY, and BaY zeolites. part2: Modelling. enthalpies and entropies of adsorption. *Zeolites*, 15:219–227.

Bennett, S., McRobb, S., and Farmer, R. (1999). *Object-Oriented System Analysis and Design.* McGraw-Hill Publishing Company.

Berlier, K., Olivier, M., and Jadot, R. (1995). Adsorption of methane, ethane, and ethylene on zeolite. *J. Chem. Eng. Data.*, 40:1206–1208.

Brown, M. E. (1988). *Introduction to thermal analysis.* Chapman and Hall Ltd.

Cavalcante, C. L. and Ruthven, D. M. (1995). Adsorption of branched and cyclic paraffins in Silicalite-1. 1. equilibrium. *Ind. Eng. Chem. Res.*, 34:177–184.

Cerro, R. L. and Smith, J. M. (1969). Effects of heat release and nonlinear equilibrium on transient adsorption. *I & EC Fundamentals*, 8(4):796–802.

Chiang, Y., Chiang, P., and Huang, C. (2001). Effects of pore structure and temperature on voc adsorption on activated carbon. *Carbon*, 39:523–534.

Chihara, Z., Suzuki, M., and Kawazoe, K. (1976). Effect of heat of generation on measurement of adsorption rate by gravimetric method. *Chemical Engineering Science*, 31:505–507.

Choudhary, V. R. and Mayadevi, S. (1996). Adsorption of methane, ethane, ethylene, and carbon dioxide on silicalite 1. *Zeolites*, 17:501–507.

Choudhary, V. R. and Srinivasan, K. R. (1986). Sorption and diffusion of benzene in H-ZSM-5: Effect of Si/Al ratio, degree of cation exchange and pretreatment conditions. *Journal of Catalysis*, 102:328–337.

C.I. Electronics (1992). *MultiCard Manual.* C. I. Electronics Limited, 2 Brunel road, Churchfields, Salisbury, Wilts. SP2 7PX, 2nd edition.

Coronas, J., Noble, R. D., and Falconer, J. L. (1998). Separations of C_4 and C_6 isomers in ZSM-5 tubular membranes. *Ind. Eng. Chem. Res.*, 37:166–176.

Dauber, T. E. and Danner, R. P. (1992). *Physical and thermodynamic properties of pure chemicals. Data compilation project.* AIChE.

Davies, O. L. and Goldsmith, P. L., editors (1980). *Statistical methods in research and production.* Longman Group Limited.

Denayer, J. F., Souverijns, W., Jacobs, P. A., Martens, J. A., and Baron, G. V. (1998). High-temperature low-pressure adsorption of branched C_5-C_8 alkanes on zeolite Beta, ZSM-5, ZSM-22, zeolite Y, and Mordenite. *Journal of Physical Chemistry B*, 102:4588–4597.

Denayer, J. F. M. and Baron, G. V. (1997). Adsorption of normal and branched paraffins in faujasite zeolites NaY, HY, Pt/NaY and USY. *Adsorption*, 3:251–265.

Derrah, R. I., Loughlin, K. F., and Ruthven, D. M. (1972). Sorption of ethylene, propylene and cyclopropane in 5A zeolite. *J. Chem. Soc., Faraday Trans.*, 68:1947–1955.

Do, D. D. (1998). *Adsorption analysis: Equilibria and kinetics.* Imperial College Press.

Do, D. D. and Do, H. D. (1997). A new adsorption isotherm for heterogeneous adsorbent based on the isosteric heat as a function of loading. *Chemical Engineering Science*, 52(2):297–310.

Duncan, W. L. and Möller, K. P. (2001). The effect of silanistion on the intracrystalline diffusivity of ZSM-5. In *The proceedings of the 14th international zeolite conference.* to be published.

Eagle (1996). *User manual for the PC30F and PC30G series boards.* Eagle Technology, 31 Hout street, Cape Town, South Africa, 5th edition.

Eagle (1999). *EDR: Software develops kit for Eagle Technology boards.* Eagle Technology, 31 Hout street, Cape Town, South Africa, 2.28 edition.

Eder, F. and Lercher, J. A. (1996). Alkane sorption on siliceous and aluminophosphate moleculer sieves. a comparative study. *J. Phys. Chem.*, 100:16460–16462.

Eder, F. and Lercher, J. A. (1997). Alkane sorption in molecular sieves: The contribution of ordering, intermolecular interactions, and sorption on brønsted acid sites. *Zeolites*, 18:75–81.

Eigenmann, F., Maciejewski, M., and Baiker, A. (2000). Gas adsorption studied by pulse thermal analysis. *Thermochimica Acta*, 359:131–141.

Gamma, E., Helm, R., Johnson, R., Vlissides, J., and Booch, G. (1995). *Design Patterns: Elements of reusable object-oriented software.* Addison-Wesley Publishing Company.

Gay, D. M. (1990). Usage summary for selected optimization routines. Computing science technical report 153, AT&T Bell Laboratories, Murray Hill, NJ 07974.

Gélin, P., Dutel, J. F., and Mentzen, B. F. (1995). p-xylene adsorption on silicalite measured by a quasi-equilibrium gravimetric technique. *Microporous Materials*, 4:283–290.

Halliday, D. and Resnick, R. (1988). *Fundamentals of physics.* John Wiley & Sons, 3rd edition.

Hershkowitz, F. and Madiara, P. D. (1993). Simultaneous measurement of adsorption, reaction, and coke using a pulse microbalance reactor. *Ind. Eng. Chem. Res.*, 32:2969–2974.

Hilton, E. F. (2000). *Manual for the Real Time Controls Laboratory, RTiC-Lab.* efhilton@alum.mit.edu, 0.6.3 edition.

Hufton, J. R. and Danner, R. P. (1993). Chromatographic study of alkanes in silicalite: Equilibrium properties. *AIChE Journal*, 39(6):954–961.

Hufton, J. R., Ruthven, D. M., and Danner, R. P. (1995). Adsorption and diffusion of hydrocarbons in silicalite at very low concentration: effect of defect sites. *Microporous Materials*, 5:39–52.

Hunger, M. and Horvath, T. (1997). Sorption of methanol on zeolite HBeta investigated by in situ MAS NMR spectroscopy. *Catalysis Letters*, 49:95–100.

Hyun, S. H. and Danner, R. P. (1985). Gas adsorption isotherms by use of perturbation chromatography. *Ind. Eng. Chem. Fundam.*, 24:95.

Inprise (1998). *Delphi 4 Developer's Guide.* Inprise Corporation, 100 Enterprise Way, Scotts Valley, CA 95066-3249, USA.

Jama, M. A., Delmas, M. P. F., and Ruthven, D. M. (1997). Diffusion of linear and branched c_6 hydrocarbons in silicalite studied by the wall-coated capillary column chromatographic method. *Zeolites*, 18:200–204.

Jasra, R. V. and Bhat, S. G. T. (1988). Adsorptive bulk separations by zeolite molecular sieves. *Separation science and technology*, 23(10 & 11):945–989.

Kantner, E., Savage, D. W., and Bellows, R. J. (1994). Zeolite composition for use in olefinic separations. U.S. Patent 5,292,990, U.S. Patent & Trademark Office.

Kapteijn, F., Moulijn, J. A., and Krishna, R. (2000). The generalized maxwell-stefan model for diffusion in zeolites: Sorbate molecules with different saturation loadings. *Chemical Engineering Science*, 55:2923–2930.

Karavias, F. and Myers, A. L. (1991). Monte carlo simulation of binary gas adsorption in zeolite cavities. pages 411–432.

Khelifa, A., Derriche, Z., and Bengueddach, A. (1999). Adsorption of propene NaX zeolite exchanged with Zn^{2+} and Cu^{2+}. *Applied Catalysis A: General*, 178:61–68.

Kim, J.-H., Ishida, A., Okajima, M., and Niwa, M. (1996). *J. Catal.*, 161:387–392.

Langmuir, I. (1918). The adsorption of gases on plane surfaces of glass, mica and platinum. *J. Am. Chem. Soc.*, 40:163–172.

Lestak, F. and Collins, C. (1997). Advanced distillation saves energy and capital. *Chemical Engineering*, pages 72–76.

Loos, J. B. W. P. (1997). *Modelling of Adsorption and Diffusion of Vapours in Zeolites.* PhD thesis, Delft University.

Ly, B. (1998). Implementating a plug-in framework. *http://www.techvanguards.com.*

Martinez, G. M. and Basmadjian, D. (1996). Towards a general gas adsorption isotherm. *Chemical Engineering Science*, 51(7):1043–1054.

Mattox, W. J. and Rouge, B. (1967). Separating alpha monoolefins using a steamed faujasite molecular seive. U.S. Patent 3,331,882, U.S. Patent & Trademark Office.

Meier, W. M. and Olson, D. H. (1978). *Atlas of Zeolite structure types.* Juris Druck und Verlag AG, Zurich.

Miller, I., Freund, J. E., and Johnson, R. A. (1990). *Probability and statistics for engineers.* Prentice-Hall Inc.

Muralidharan, P. K. and Ching, C. B. (1997). Determination of multicomponent adsorption equilibria by liquid chromotography. *Ind. Eng. Chem. Res.*, 36:407–413.

Myers, A. L. and Siperstein, F. (2001). Characterization of adsorbents by energy profile of adsorbed molecules. *Colloids and Surfaces A: Physicochem. Eng. Aspects*, 187-188:73–81.

Napier-Munn, T. J. (1998). *An introduction to comparative statistics and experimental design for minerals engineers.* Julius Kruttschnitt Mineral Research Centre, University of Queensland, 2nd edition.

Nitta, T., Shigetomi, T., Kuro-Oka, M., and Katayama, T. (1984a). An adsorption isotherm of multi-site occupancy model for heterogeneous surface. *Journal of Chemical Engineering of Japan*, 17:45–51.

Nitta, T., Shigetomi, T., Kuro-Oka, M., and Katayama, T. (1984b). An adsorption isotherm of multi-site occupancy model for homogeneous surface. *Journal of Chemical engineering of Japan*, 17(1):39–44.

Niwa, M., Kato, S., Hattori, T., and Murakami, Y. (1984a). Fine control of the pore-opening size of the zeolite mordenite by chemical vapour deposition of silicon alkoxide. *J. Chem. Soc., Faraday Trans. 1*, 80:3435–3145.

Niwa, M., Morimoto, S., Kato, M., Hattori, T., and Murakami, Y. (1984b). Fine control of pore size of H-mordenite by vapor-phase deposition of $Si\,(OCH_3)_4$. *Proc. 8th Int. Cong. Catal.*, IV:701–711.

Niwa, M., Yamazaki, K., and Murakami, Y. (1991). Separation of oxygen and nitrogen due to the controlled pore-opening size of chemical vapor deposited zeolite A. *Ind. Eng. Chem. Res.*, 29:38–42.

Niwa, M., Yamazaki, K., and Murakami, Y. (1994). Separation of lower olefins by chemical vapor deposited zeolite A. *Ind. Eng. Chem. Res.*, 33:371–374.

Olson, D. H. and Reischman, P. T. (1996). Structure-related paraffin sorption in ZSM-5. *Zeolites*, 17:434–436.

OMG (1999). *OMG unified modelling language specification.* Object Management Group (OMG), 1.3 edition.

Patashnick, H., Rupprecht, G., and Wang, J. C. F. (1980). A new real time monitoring instrument for suspended particulate mass concentration: The TEOM. *Prepr.-Am. Chem. Soc., Div. Pet. Chem.*, 25:188–193.

Post, M. F. M., van Bekkum, H., Flanigen, E. M., and Jansen, J. C. (1991). *Introduction to zeolites and practice*, chapter Diffusion in zeolite molecular sieves. Elsevier, Amsterdam, The Netherlands.

Robens, E. (1995). Early gravimetric adsorption measurements. *Colliods and Surfaces A: Physicochemical and Engineering Aspects*, 104:375–376.

Röger, H. P. (1998). *Application of the transformation of 1,2,4-trimethylbenzene to monitor the chemical vapour depsotion of tetraethoxysilane over ZSM-5.* PhD thesis, University of Cape Town.

Roque-Malherbe, R. (2000). Complementary approach to the volume filling theory of adsorption zeolites. *Microporous and Mesoporous Materials*, 41:227–240.

Rosback, D. H. (1975). Process for separating olefins by adsorption. U.S. Patent 3,888,939, U.S. Patent & Trademark Office.

Rosback, D. H. and Neuzil, R. W. (1976). Method for manufacturing an adsorbent useful for olefin separation. U.S. Patent 4,048,111, U.S. Patent & Trademark Office.

Ruthven, D. M. (1976). Sorption of oxygen, nitrogen, carbon monoxide, methane, and binary mixtures of these gases in 5A molecular sieve. *AIChE Journal*, 22(4):753–759.

Ruthven, D. M. (1984). *Principles of adsorption and adsorption processes.* John Wiley & Sons Inc.

Ruthven, D. M. (1988). Zeolites as selective adsorbents. *Chemical Engineering Progress*, pages 42–50.

Ruthven, D. M. and Kaul, B. K. (1993). Adsorption of aromatic hydrocarbons in NaX zeolite. 1. equilibrium. *Ind. Eng. Chem. Res.*, 32:2047–2052.

Ruthven, D. M. and Kaul, B. K. (1996). Adsorption of n-hexane and intermediate molecular weight aromatic hydrocarbons on LaY zeolite. *Ind. Eng. Chem. Res.*, 35:2060–2064.

Ruthven, D. M. and Kumar, R. (1980). An experimental study of single-component and binary adsorption equilibria by a chromatographic method. *Ind. Eng. Chem. Fundam.*, 19:27–32.

Ruthven, D. M. and Loughlin, K. F. (1971). The sorption and diffusion of n-butane in Linda 5A molecular sieve. *Chemical Engineering Science*, 26:1145–1154.

Ruthven, D. M. and Loughlin, K. F. (1972). Sorption of light paraffins in Type-A zeolites. *Faraday Trans. I*, 68:696–708.

Sakuth, M., Meyer, J., and Gmehling, J. (1995). Vapor phase adsorption equilibria of toluene + 1-propanol mixtures on y-zeolites with different silicon to aluminum ratios. *J. Chem. Eng. Data*, 40:895–899.

Sandler, S. I. (1989). *Chemical and engineering thermodynamics.* John Wiley & Sons, Inc., 2nd edition.

Schneider, P. and Smith, J. M. (1968). Adsorption rate constants from chromatography. *AIChE Journal*, 14(5):762–771.

Shively, J. H. and Archer, E. D. (1967). Silanized crystalline alumino-silicates. South African Patent D.69,690-F, South African Patent Office.

Silva, J. A. C. and Rodrigues, A. E. (1997). Sorption and diffusion of n-pentane in pellets of 5A zeolite. *Ind. Eng. Chem. Res.*, 36:493–500.

Smit, B. (1995). Simulating the adsorption isotherms of methane, ethane, and propane in the zeolite silicalite. *J. Phys. Chem.*, 99:5597–5603.

Smit, B. and Maesen, T. L. M. (1995). *Nature*, 374:42.

Song, L. and Rees, L. V. C. (1997). Adsorption and transport of n-hexane in silicalite-1 by the frequency response technique. *J. Chem. Soc., Faraday Trans.*, 93(4):649–657.

Stach, H., Thamm, H., Jänchen, J., Fiedler, K., and Schirmer, W. (1983). Experimental and theoretical investigations of the adsorption of n-paraffins, n-olefins and aromtaics on silcalite. In Olson, D. and Bisio, A., editors, *The proceedings of the 6th international zeolite conference*, pages 225–231. Butterworths.

Stankovic, J. (1988). Misconceptions about real-time computing. *IEEE computer*, 21(10).

Sun, M. S., Shah, D. B., Xu, H. H., and Talu, O. (1998). Adsorption equilibria of C_1 to C_4 alkanes, CO_2 and SF_6 on silicalite. *J. Phys. Chem. B.*, 102:1466–1473.

Sun, M. S., Talu, O., and Shah, D. B. (1996). Adsorption equilibria of C_5-C_{10} normal alkanes in silicalite crystals. *J. Phys. Chem.*, 100:17276–17280.

Vlugt, T. J. H., Krishna, R., and Smit, B. (1999). Molecular simulations of adsorption isotherms of linear and branched alkanes and their mixtures in silicalite. *J. Phys. Chem. B.*, 103:1102–1118.

Vlugt, T. J. H., Zhu, W., Kapteijn, F., Moulijn, J. A., Smit, B., and Krishna, R. (1998). Adsorption of linear and branched alkanes in zeolite silicate-1. *J. Am. Chem. Soc.*, 120:5599–5600.

Wang, C. and Hwang, B. (2000). A general adsorption isotherm considering multi-layer adsorption and heterogeneity of adsorbent. *Chemical Engineering Science*, 55:4311–4321.

Weber, R. W. (1998). *The inertisation of the zeolites ZSM-5, mordenite and beta by chemical vapour deposition using tetraethoxysilane.* PhD thesis, University of Cape Town.

Weber, R. W., Möller, K. P., and O'Connor, C. T. (2000). *Microporous and Mesoporous Materials*, 35-36:533–543.

Webster, C. R., Drago, R. S., and Zerner, M. C. (1998). Molecular dimensions for adsorptives. *J. Am. Chem. Soc.*, 120:5509–5516.

Wu, P. and Ma, Y. H. (1983). The effect of cation on adsorption and diffusion in ZSM-5. In Olson, D. and Bisio, A., editors, *The proceedings of the 6th international zeolite conference*, pages 251–260. Butterworths.

Yang, R. T. (1987). *Gas separation by adsorption processes.* Butterworth Publishers.

Yang, R. T., Chen, Y. D., Peck, J. D., and Chen, N. (1996). Zeolites containing mixed cations for air separation by weak chemisorption-assisted adsorption. *Ind. Chem. Eng. Res.*, 35:3093–3099.

Yang, Y. and Rees, L. V. C. (1997). Adsorption of normal hexane in silicalite-1: An isosteric approach. *Microporous Materials*, 12:117–122.

Zhu, W., de Graaf, J. M. V., Broeke, L. J. P. V. D., Kapteijn, F., and Moulijn, J. A. (1998). TEOM: A unique technique for measuring adsorption properties. light alkanes in silicalite-1. *Ind. Chem. Eng. Res.*, 37:1934–1942.

Appendix A

Materials

Table A.1: List of chemical, reagents and gases.

Reagent	Supplier	Purity
Chemicals		
n-Hexane (nC_6)	Sigma-Aldrich	$> 97\%$
n-Hexane (nC_6)	BDH	$> 97\%$
2,3 Dimethyl butane (23DMB)	Riedel de Haën	98%
3 methyl pentane	Sigma-Aldrich	99%
Tetraethoxylsilane (TEOS)	Fluka	$> 98\%$
HCl	Riedel de Haën	32%
NaOH	Saarchem	97%
Gases		
Synthetic air	Fedgas	99.99%
Helium 4.5	Fedgas	99.996%
Helium 5	Fedgas	99.999%
Miscellaneous		
3A molecular sieve	Merck	$> 2.5mm$ 5%
		$< 1.6mm$ 2%
Quartz wool	Supelco	
Chromosorb P	Supelco	60/80 mesh

Table A.2: List of equipment.

Description	Manufactor	Model
Balances		
Microbalance	C.I. Electronics	MkII Standard Head
Microbalance I/O card	C.I. Electronics	Multicard II
Microbalance housing	Chemical Engineering Department	
Flowmeters		
Mass flow controllers	Unit Instruments	UFC-4000 (0-20$ml \cdot min^{-1}$)
Mass flow controllers	Unit Instruments	UFC-1500 (0-630$ml \cdot min^{-1}$)
Furnaces and Temperature controllers		
Furnace Heating coil	Unitemp	
Heating tape	Flexiheat	
Temperature controller	RKC Instruments	REX-F9
Thermocouples	Unitemp	type K
Glassware		
Quartz tubing and frits	Heraeus	
Saturators	Scientific Glassblowers	
Electronics		
I/O cards	Eagle electronics	PC30GA
MFC PSU	Chemical Engineering Department	
Thermocouple amplifiers	Chemical Engineering Department	
Thermocouple chips	Motorola	AD595
Gas chromatograph		
Gas chromatograph	Hewlett Packard	5890 series II
Miscellaneous		
Valves, fittings, filters	The Swagelok Company	
Soleniod valves	Bürkert	
Regulator	Air Products	
Stainless steel tubing	Pace	

Table A.3: Adsorbate vapour pressure regression constants (Dauber and Danner, 1992).

Adsorbate	Temperature range (K)	A	B	C	D	E
n-Hexane	177.83-507.60	1.0465×10^{2}	-6.9955×10^{3}	-1.2702×10^{1}	1.2381×10^{-5}	2.0000
3 Methyl pentane	110.25-504.43	8.6139×10^{1}	-6.1648×10^{3}	-9.8546	9.2741×10^{-6}	2.0000
2,3 Dimethyl butane	145.19-499.98	8.2333×10^{1}	-5.8771×10^{3}	-9.3142	9.0123×10^{-6}	2.0000

Appendix B

Error analysis

The error analysis of the experimental data generated by the microbalance is complex and tedious. This appendix describes the error analysis detail. The experimental errors were determined using the method presented. All the calculations were programmed into a series of *Python* scripts to remove the tedium of determining the errors.

B.0.5 Adsorbate loading error calculations

The adsorbate loading was determined via a number of calculations; ranging from the microbalance calibration to the molar loading calculations. The calculations used are presented below in the sequential order in which they were applied.

B.0.5.1 Microbalance calibration

In order to understand the analysis of the calibration variance it is necessary to look at the calibration procedure. The physical procedure was presented in chapter 4. However, the internals of the calibration method were not presented. The calibration factor is determined using the simple linear relation shown in equation B.1 (C.I. Electronics, 1992).

$$C = \frac{m_{cal}}{ADC_{cal} - ADC_{zero}} \tag{B.1}$$

When the microbalance is zeroed a number of ADC readings are averaged, normally about 10 ADC readings. To complicate matters, these ADC readings are themselves averages from the running mean filter (chapter 3). The calibration ADC readings are produced in the same manner.

Unfortunately, the variance associated with the averaged ADC_{cal} and ADC_{zero} could not be determined as the individual data points were not recorded by the software. In hindsight this is not significant and it can be safely assumed that the variance introduced by the averaged ADC readings can be ignored. This assumption is well supported by examining the standard deviations present in the experimental data and it was observed during the calibration process.

Table B.1 presents the error introduced in the calibration of the microbalance. The tolerance is often defined as being $\pm 3\sigma$ (Napier-Munn, 1998). Using this relation the standard deviation can be determined for the given tolerances.

Table B.1: Published errors and tolerances for the *MK2* Microbalance (C.I. Electronics, 1992).

Parameter	Tolerance	σ
m_{cal}	0.006mg	0.002mg
ADC_{cal}	$\frac{1}{20000}$	
ADC_{zero}	$\frac{1}{20000}$	

For the purpose of instrument calibration it is common to assume that one variable has a negligible error (Davies and Goldsmith, 1980). In the calibration of the microbalance this assumption is especially true for the ADC measurements, as shown in table B.1. The variance of a simple arithmetic equation is given by B.2 (Davies and Goldsmith, 1980; Napier-Munn, 1998).

$$\begin{aligned} \text{if } z &= a_1x_1 + a_2x_2 + \cdots + a_nx_n \\ \text{then } \sigma_z^2 &= a_1^2\sigma_1^2 + a_2^2\sigma_2^2 + \cdots + a_n^2\sigma_n^2 \end{aligned} \tag{B.2}$$

Thus the calibration variance is given by equation B.3.

$$\sigma_c^2 = \frac{\sigma_{m_{cal}}^2}{ADC_{cal} - ADC_{zero}} \tag{B.3}$$

B.0.5.2 Mass reading

The mass was determined using the calibration factor, as shown in equation B.4 (C.I. Electronics, 1992). Therefore, there was propagation of the error from the calibration to the mass readings.

$$m = C\,(ADC - ADC_{zero}) \tag{B.4}$$

The variance in the mass reading is handled in exactly the same manner as the calibration factor. As with the calibration factor, the ADC readings used are not single readings but a running average

and, again like the calibration method, the variance associated with the averaged ADC readings is considered to be negligible and thus ignored. Using the expression B.2 the mass variance can be estimated using equation B.5.

$$\sigma_m^2 = (ADC - ADC_{zero})^2 \sigma_C^2 \tag{B.5}$$

For an adsorption experiment each adsorption step had a number of mass readings, from 10 to in excess of 400 depending on the sampling rate. The mass readings were then summarised into a single mean value. The effect of this procedure was that there were then two independent sources of errors introduced into the mean value. Figure B.1 is a block diagram of the data model used to analyse the variance of the mass readings.

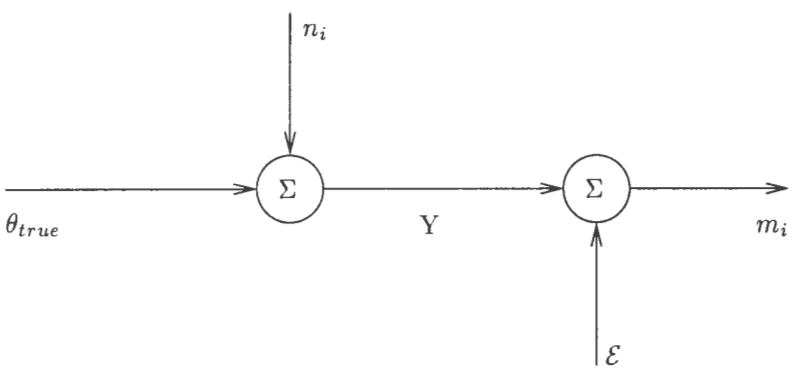

Figure B.1: Statistical model of the experimental mass readings.

θ_{true} represents the "true" value of the mass being measured by the microbalance. The system was susceptible to a certain amount of noise, such as electrical noise and physical vibrations. This noise is represented by n_i, in figure B.1. As the system does not directly measure the mass but rather uses a calibration factor, there was an error ($\mathcal{E}$) introduced by the calibration factor. This calibration error was considered to be an offset from the true value.

Both m_i, and $\mathcal{E}$ were considered to be independent random variables. However, in order to simplify the development of the error, $\mathcal{E}$ was also considered to be a constant and therefore $\mathrm{E}\{\mathcal{E}\} = 0$ (Miller et al., 1990; Davies and Goldsmith, 1980).

$$m_i = \{m_1, m_2, \cdots, m_N\} \tag{B.6}$$

From figure B.1 the mass readings are simply a summation of the terms, as shown in equation B.7.

$$m_i = \theta_{true} + n_i + \mathcal{E} \tag{B.7}$$

By treating n_i and $\mathcal{E}$ as random variables the following expressions can be derived:

$$\begin{aligned} \text{let } \hat{\bar{m}} &= \frac{\sum m_i}{N} \\ &= \frac{\sum \theta_{true} + n_i + \mathcal{E}}{N} \\ &= \theta_{true} + \frac{\sum n_i}{N} + \mathcal{E} \end{aligned} \tag{B.8}$$

The expectation is given by equation B.9, assuming that both n_i and $\mathcal{E}$ have a normal distribution.

$$\mathrm{E}\left\{\hat{\bar{m}}\right\} = \mathrm{E}\left\{\theta_{true} + \frac{\sum n_i}{N} + \mathcal{E}\right\} = \theta_{true} \tag{B.9}$$

Therefore the variance is given by the following:

$$\begin{aligned} \mathrm{Var}\left\{\hat{\bar{m}}\right\} &= \mathrm{Var}\left\{\frac{\sum n_i}{N} + \mathcal{E}\right\} \qquad \text{(B.10)} \\ &= \mathrm{Var}\left\{\frac{\sum n_i}{N}\right\} + \mathrm{Var}\left\{\mathcal{E}\right\} \\ &= \frac{\mathrm{Var}\left\{n\right\}}{N} + \mathrm{Var}\left\{\mathcal{E}\right\} \\ &= \frac{\sigma_n^2}{N} + \sigma_{\mathcal{E}}^2 \\ \therefore \sigma_{\hat{\bar{m}}} &= \sqrt{\frac{\sigma_n^2}{N} + \sigma_{\mathcal{E}}^2} \qquad \text{(B.11)} \end{aligned}$$

The estimator for the mass ($\hat{\bar{m}}$) is unbiased, as $\mathrm{E}\left\{\hat{\bar{m}}\right\} = 0$.

Lastly, an estimate of σ_n could be determined because $\mathcal{E}$ was assumed to be constant for all measurements.

$$\begin{aligned} \sigma_n^2 &= \sigma_m^2\Big|_{\mathcal{E}=constant} \\ \therefore \sigma_n^2 &= \frac{\sum \left(m_i - \hat{\bar{m}}\right)^2}{N-1} \end{aligned} \tag{B.12}$$

B.0.5.3 Mass loading

The mass loading (q_m) was nothing more than the normalised change in mass for each adsorption "step". Equation B.13 presents this in a more readable manner.

$$q_m = \frac{\hat{\bar{m}} - \hat{\bar{m}}_{baseline}}{\hat{\bar{m}}_{baseline}} \tag{B.13}$$

The variance for a general function can be determined in the following manner (Davies and Goldsmith, 1980; Napier-Munn, 1998).

$$\begin{aligned} &\text{if } X = f(x_1, X_2, \cdots, x_n) \\ &\text{then } \mathrm{Var}\{X\} = \left(\frac{\partial X}{\partial x_1}\right)^2 \mathrm{Var}\{x_1\} + \left(\frac{\partial X}{\partial x_2}\right)^2 \mathrm{Var}\{x_2\} + \cdots + \left(\frac{\partial X}{\partial x_n}\right)^2 \mathrm{Var}\{x_n\} \end{aligned} \tag{B.14}$$

Thus the mass loading variance ($\sigma^2_{q_m}$) is:

$$\sigma^2_{q_m} = \frac{\sigma^2_{\hat{\dot{m}}}}{\hat{\dot{m}}^2_{baseline}} + \frac{\hat{\dot{m}}^2}{\hat{\dot{m}}^4_{baseline}} \sigma^2_{\hat{\dot{m}}_{baseline}} \tag{B.15}$$

B.0.5.4 Molar loading

The loading is more commonly stated as a molar loading, the variance for which can easily be extended from equation B.15 as it was assumed that the error in the molar mass was insignificant. Equation B.16 presents the variance in the molar loading (q).

$$\sigma^2_q = M\sigma^2_{q_m} \tag{B.16}$$

B.0.6 Partial pressure

B.0.6.1 Flow rates

The flow rate of the carrier gas through the saturator was the cumulative flow rates of MFC2 and MFC3 as shown in figure 3.1. However, the total flow rate of the carrier gas to the reactor is sum of the flow rate through MFC1 and MFC3, given by equation B.17. The variance in the total reactor flow rate was only due to the variance in the flow rate through MFC1 and MFC3, and the variance in MFC2 can safely be ignored.

$$F_{adsorber} = F_{MFC1} + F_{MFC3} \tag{B.17}$$

The mass flow controllers were calibrated using a soap bubble flow meter and a stop watch. The implication is that the error in the flow rate measurement can be attributed to the experimental error and the errors in the apparatus can discarded as being insignificant. The calibration data was fitted to a simple linear relation, equation B.18.

$$F = \beta V + \alpha \tag{B.18}$$

The error introduced by the measurement of the voltage is negligible in comparison with the measurement of the flow rate. Therefore, it is reasonable to assume that the error in the calibration curve is solely due to the experimental error in the flow rate measurements which is a common assumption in data regression (Davies and Goldsmith, 1980; Miller et al., 1990). The variance around the calibration line is given by equation B.19.

$$s^2 = \frac{\sum \left(F_i - \hat{F}\right)}{N-2} \tag{B.19}$$

The variance in the predicted flow rates was determined using equation B.20 (Davies and Goldsmith, 1980; Miller et al., 1990). This variance is the variance of the mean, sometimes referred to as the standard error.

$$\begin{aligned} s_i^2 &= s^2 \left(\frac{1}{N} + \frac{(V_0 - \bar{V})^2}{S_{xx}} \right) \\ \text{where: } S_{xx} &= \sum_{i=1}^{N} (V_i - \bar{V})^2 \end{aligned} \tag{B.20}$$

Equation B.20 provides a means to estimate the error associated with a single prediction of the flow rate. But, like the mass readings, the final flow rate was the result of the averaging of a number readings. The variance in the averaged flow rates can be determined in the same manner as the averaged mass readings variance, via equation B.11 (where $\hat{\bar{m}} = \hat{\bar{F}}$ and $\sigma_\varepsilon = s_i$).

As mentioned previously, equation B.17, the total flow rate to the microbalance was the sum of the flows through two mass flow controllers (MFC1 and MFC3). This implies, from equation B.2, that the variance in the flow rate is the sum of the relevant variances. Equation B.21 presents the flow rate variance.

$$\sigma^2_{adsorber} = \sigma^2_{MFC1} + \sigma^2_{MFC3} \tag{B.21}$$

B.0.6.2 Saturator Temperature

The saturator temperature is one of the most significant variables in the reactor's partial pressure. Even small changes in the temperature have disproportionately large effects on the total pressure, due to the exponential relationship between temperature and vapour pressure, equation B.22.

The saturation temperature was measured on a continuous basis and like the measurement of the other process variables it was subject to a calibration to convert the voltage into something more meaningful. The variance in the temperature calibration was handled in exactly the same fashion as the flow rate variance.

Firstly, the variance in the calibration was determined using equation B.19. This was followed by the determination of the single measurement variance, via equation B.20. Finally, the variance in the averaged temperature (for each adsorption "step") was determined using equation B.11.

B.0.6.3 Vapour Pressure

Using the temperature, the vapour pressure could be determined using the temperature dependent data published by Dauber and Danner (1992). The vapour pressure data was presented in the form of constants for the regression equation (equation B.22).

$$P^* = \exp\left[A + \frac{B}{T} + C\ln T + DT^E\right] \tag{B.22}$$

Dauber and Danner (1992) estimated that the error in the vapour pressure to be less than 3%, for all compounds of interest. However, this error did not account for any variance in the temperature.

The propagation of the error in the temperature through the vapour pressure calculation (equation B.22) was estimated using the method outlined by equation B.14.

$$\begin{aligned} \mathrm{Var}\{P^*\} &= \frac{\partial P^{*\,2}}{\partial T}\sigma_T^2 \\ \therefore \sigma_{P^*}^2 &= \left(\exp\left[A + \frac{B}{T} + C\ln T + DT^E\right]\left(-\frac{B}{T^2} + C\frac{1}{T} + DET^{E-1}\right)\right)^2 \sigma_T^2 \end{aligned} \tag{B.23}$$

From equation B.23 it was obvious that even a small error in the temperature will have an exponential effect on the vapour pressure. The error in the vapour pressure was assumed therefore to be solely due to the error in the temperature.

The variance in the temperature was handled in the same manner as the flow rate variance. Firstly the variance in the calibration was determined and this was then combined with the variance due to noise in the averaged experimental data.

B.0.6.4 Reactor Partial pressure

The partial pressure in the reactor was determined using the ideal gas law on an open system. Equation B.24 presents the final form of the relationship used.

$$P_i = P_{i,sat}\frac{F_{MFC3}}{F_{MFC1} + F_{MFC3}} \tag{B.24}$$

Equation B.25 presents the function for the error propagation through the partial pressure function.

$$\begin{aligned}
\mathrm{Var}\{P_i\} &= \left(\frac{\partial P_i}{\partial P_{i,sat}}\right)^2 \sigma^2_{P_{i,sat}} + \left(\frac{\partial P_i}{\partial F_{MFC1}}\right)^2 \sigma^2_{F_{MFC1}} + \left(\frac{\partial P_i}{\partial F_{MFC3}}\right)^2 \sigma^2_{F_{MFC3}} \\
\sigma^2_{P_i} &= \left(\frac{F_{MFC3}}{F_{MFC1} + F_{MFC3}}\right)^2 \sigma^2_{P_{i,sat}} \\
&+ \left(P_{i,sat}\frac{F_{MFC3}}{(F_{MFC1} + F_{MFC3})^2}\right)^2 \sigma^2_{F_{MFC1}} \\
&+ \left(P_{i,sat}\frac{F_{MFC1}}{(F_{MFC1} + F_{MFC3})^2}\right)^2 \sigma^2_{F_{MFC3}}
\end{aligned} \tag{B.25}$$

B.0.7 Confidence interval

All experimental errors were published within the 95% 2-sided confidence interval. Equation B.26 was used to estimate the confidence interval. Values for the t parameter are available in most statistics publications, such as Davies and Goldsmith (1980) or Miller et al. (1990).

$$\begin{gathered}
\bar{x} - t_{\alpha/2}s < \mu < \bar{x} + t_{\alpha/2}s \\
\text{where } \alpha = 1 - Confidence/100
\end{gathered} \tag{B.26}$$

Appendix C

Model fitting

All the isotherm model fits present in this work were performed using the techniques presented in this appendix. The parameters determined for the model fits are also present.

C.1 Model fitting

The model fitting was performed by minimising the error between the calculated model result and the experimental results. Equation C.1 shows the objective function used in all the model fitting procedures. A reduced squared error was found to provide better model parameters, as it prevents the high pressure/loading data from dominating the sum of squared errors.

$$OF = \sum \left(\frac{P_{calc,i} - P_{exp,i}}{P_{exp,i}} \right)^2 \tag{C.1}$$

Due to the nature of the isotherm models and experimental data the isotherm models were fitted either on the loading (q_i) or the pressure (P_i). The choice of the variable used in the objective function was dependent on the form of the isotherm model, the objective function variable was required to be the explicit variable of the isotherm model. For example in the both the virial and the Nitta isotherm the partial pressure was the most practical choice for the objective function variable.

C.1.1 Model fitting programs

The optimisation was performed by a number programs written in *FORTRAN 77*, using the *g77* compiler. *FORTRAN* was chosen due to the large amount volume of optimisation routines available in the public domain. Unfortunately *FORTRAN* does not support complex data types (such as

record) thus making it less suited to data manipulation. Therefore, for convenience, particularly with manipulation of large sets of experimental data, the model fitting programs were linked to a common "front" end program (isofit) written in *Python* with the model fitting portion of the program being linked as a shared object library (isotherms.so).

C.1.2 Minimisation

The minimisation was performed using the *Port* libraries released by Gay (1990). For the purposes of the work presented here the minimisation routine chosen (dmnfb) was for the minimisation of a general unconstrained objective function using a finite-difference gradients and Secant Hessian approximations. The gradient calculations were performed internally by this routine. Simple boundary conditions could also be placed on the optimisation parameters.

C.2 Virial isotherm model parameters

Tables C.1 and C.2 present the virial isotherm model parameters found for the experimental data.

Table C.1: Virial isotherm model parameters for the adsorption of n-hexane

Experiment	Adsorbent	Temperature (K)	k′ ($mol \cdot kg^{-1} \cdot Pa^{-1}$)	A_0 ($kg \cdot mol^{-1}$)	A_1 ($kg^2 \cdot mol^{-2}$)	Residual error
MFI_1-9	MFI	348	1.289×10^{1}	9.42	−9.69	8.872×10^{-3}
MFI_1-10	MFI	348	1.184×10^{1}	8.88	−8.08	1.481×10^{-1}
MFI-AP_5	MFI-AP	349	2.410	8.07	−8.20	6.615×10^{-2}
MFI-APS15_4	MFI-APS_{15}	351	5.495×10^{-2}	1.80	3.43	5.606×10^{-1}
MFI_1-6	MFI	358	5.647	9.18	−9.22	2.228×10^{-2}
MFI_1-5	MFI	357	8.379×10^{-1}	6.09	−4.28	2.576×10^{-2}
MFI-AP_4	MFI-AP	358	1.520×10^{-1}	3.92	−0.23	5.194×10^{-2}
MFI-APS10_3	MFI-APS_{10}	358	1.658×10^{-1}	4.47	−0.85	5.419×10^{-2}
MFI-APS15_3	MFI-APS_{15}	361	1.266×10^{-2}	−0.73	11.11	1.202×10^{-1}
MFI_20	MFI	371	1.746×10^{-2}	−0.100	6.629	$1.656 \times 10^{E-03}$
MFI_1-7	MFI	374	2.326×10^{-2}	1.462	4.307	$2.193 \times 10^{E-02}$
MFI_1-2	MFI	373	1.690×10^{-2}	1.063	4.628	$3.863 \times 10^{E-02}$
MFI-P_1	MFI-P	374	1.658×10^{-2}	1.201	4.635	$4.123 \times 10^{E-02}$
MFI-AP_2	MFI-AP	374	1.537×10^{-2}	1.277	5.159	$3.676 \times 10^{E-02}$
MFI-APS10_2	MFI-APS_{10}	374	9.196×10^{-3}	0.229	8.113	$3.454 \times 10^{E-03}$
MFI-APS15_1	MFI-APS_{15}	377	8.951×10^{-3}	0.350	8.422	$1.520 \times 10^{E-02}$
MFI_1-8	MFI	393	5.496×10^{-3}	1.648	2.473	7.198×10^{-2}
MFI_1-3	MFI	393	6.231×10^{-3}	2.196	−0.630	5.823×10^{-2}
MFI_1-4	MFI	393	6.155×10^{-3}	2.161	−0.605	4.883×10^{-2}
MFI-AP_3	MFI-AP	394	3.419×10^{-3}	1.775	0.973	3.609×10^{-2}
MFI-APS10_1	MFI-APS_{10}	395	3.400×10^{-3}	1.551	2.569	1.003
MFI-APS15_2	MFI-APS_{15}	398	3.639×10^{-3}	2.468	−0.807	2.332×10^{-2}

Table C.2: Virial isotherm model parameters for the adsorption of 3 methyl pentane and 2,3 dimethyl butane

Experiment	Adsorbent	Temperature (K)	k′ ($mol \cdot kg^{-1} \cdot Pa^{-1}$)	A_0 ($kg \cdot mol^{-1}$)	A_1 ($kg^2 \cdot mol^{-2}$)	Residual error
3 Methyl pentane						
MFI-P_2	MFI-P	374	5.940×10^{-3}	1.878	2.233	9.025×10^{-2}
MFI-AP_1	MFI-AP	374	6.812×10^{-3}	1.592	3.545	8.372×10^{-2}
MFI-AP_6	MFI-AP	375	4.463×10^{-3}	1.487	3.836	7.182×10^{-2}
MFI-APS10_4	MFI-APS_{10}	376	4.407×10^{-3}	1.036	5.991	4.664×10^{-2}
MFI-APS15_6	MFI-APS_{15}	376	3.831×10^{-3}	1.396	4.911	5.106×10^{-2}
2,3 Dimethyl butane						
MFI-P_3	MFI-P	374	3.680×10^{-3}	2.293	−0.009	2.322×10^{-2}
MFI-AP_7	MFI-AP	374	2.097×10^{-3}	2.391	−1.203	4.868×10^{-2}
MFI-APS15_5	MFI-APS_{15}	377	2.069×10^{-3}	2.677	−0.787	3.406×10^{-2}

Appendix D

Experimental data

Due to the large volume of experimental data it is only available on the CD-ROM that accompanies this work. Tables D.1, and D.2 presents a list of the experimental work available on the CD-ROM. The experimental run name, which is also the file name, is the adsorbent name followed by an arbitrary run number. Each experimental data set consists of two file which are differentiated by the file extensions, a .dat file with the experimental data and a .inf file which contains all the experimental information pertaining to that data file, including model parameters. The experimental data can be found in the *data/isotherm* directory on the CD-ROM.

The CD-ROM contains a number of other items of interest apart from a complete copy of the experimental data and this thesis. The disc contains all the *Python* programs written to interpret the microbalance data and also contains the source tree for the microbalance control program.

Table D.1: n-Hexane experimental adsorption data list.

Experiment	Adsorbent	Temperature (K)	Comments
MFI_1-9	MFI	348	
MFI_1-10	MFI	348	
MFI_1-11a	MFI	349	q_s measurement
MFI-AP_5	MFI-AP	350	
MFI-AP_10d	MFI-AP	350	q_s measurement
MFI-APS15_4	MFI-APS_{15}	352	
MFI_1-5	MFI	357	
MFI_1-6	MFI	358	
MFI_1-11b	MFI	358	q_s measurement
MFI-AP_4	MFI-AP	358	
MFI-AP_10c	MFI-AP	359	q_s measurement
MFI-APS10_3	MFI-APS_{10}	358	
MFI-APS15_3	MFI-APS_{15}	361	
MFI_20	MFI	371	
MFI_1-2	MFI	373	
MFI_1-7	MFI	374	
MFI_1-11c	MFI	374	q_s measurement
MFI-P_1	MFI-P	374	
MFI-AP_10b	MFI-AP	375	q_s measurement
MFI-AP_2	MFI-AP	374	
MFI-APS10_2	MFI-APS_{10}	374	
MFI-APS15_1	MFI-APS_{15}	377	
MFI_1-3	MFI	393	
MFI_1-4	MFI	393	
MFI_1-8	MFI	393	
MFI-AP_3	MFI-AP	394	
MFI-AP_10a	MFI-AP	395	
MFI-APS10_1	MFI-APS_{10}	395	
MFI-APS15_2	MFI-APS_{15}	398	

Table D.2: 3 Methyl pentane and 2,3 dimethyl butane experimental adsorption data list.

Experiment	Adsorbent	Temperature (K)	Comments
3 Methyl pentane			
MFI-P_2	MFI-P	374	
MFI-AP_1	MFI-AP	374	
MFI-AP_6	MFI-AP	375	
MFI-AP_9	MFI-AP	374	
MFI-AP_9a	MFI-AP	375	q_s measurement
MFI-APS10_4	MFI-APS_{10}	376	
MFI-APS15_6	MFI-APS_{15}	376	
2,3 Dimethyl butane			
MFI-P_3	MFI-P	374	
MFI-AP_7	MFI-AP	374	
MFI-AP_8	MFI-AP	374	
MFI-AP_8a	MFI-AP	375	q_s measurement
MFI-APS15_5	MFI-APS_{15}	377	